AN INTEGRATED APPROACH TO THE DESIGN OF MOONPOOLS FOR SUBSEA OPERATIONS

A. H. Day

a thesis submitted for the degree of
Doctor of Philosophy

Division of Ship and Marine Technology
Department of Mechanical and Offshore Engineering
University of Strathclyde
Glasgow

April 1987

BRITISH LIBRARY HSTIRD

IMAGING SERVICES NORTH
Boston Spa, Wetherby
West Yorkshire, LS23 7BQ
www.bl.uk

BEST COPY AVAILABLE.

VARIABLE PRINT QUALITY

ABSTRACT

The use of moonpools for the launch and retrieval of diving bells and remotely operated vehicles from a mother ship is well established, and the advantages of the moonpool approach are well known. The use of moonpools in Floating Production Systems is also becoming more common, as a means of allowing the marine riser to enter the vessel. The moonpool offers protection from wind and current forces and reduces the effects of angular motions of the vessel. The only problem with the moonpool concept is that the water column inside a badly designed moonpool may suffer from large and apparently unpredictable vertical surges, making operations through the moonpool hazardous, and in extreme cases threatening the seaworthiness of the vessel. The work described here shows how a moonpool design may be optimised for a particular vessel in order that such problems may be avoided.

The dynamics of the problem are established, such that the water column oscillation and the forces on a subsea unit in the moonpool may be predicted. The effects of a variety of geometrical configurations are then studied, both mathematically and experimentally, in order to select configurations which allow large modifications of the moonpool response. A quantitative measure of moonpool performance is proposed, allowing individual designs to be ranked in terms of the long term expected downtime due to the moonpool. Finally, the understanding and results thus gained are integrated in order to produce a practical design procedure for a moonpool of any size, in any vessel, and in any operational area. A worked example basesd on a real design problem is presented in order to illustrate the practical application of the method.

AN INTEGRATED APPROACH TO THE DESIGN OF MOONPOOLS FOR SUBSEA OPERATIONS

1. INTRODUCTION

1.1 STATEMENT OF THE PROBLEM

As the exploration for offshore oil moves into deeper and more hostile waters, a vital requirement for the operation of offshore structures is safe and cost-effective subsea support. This support covers a wide range of tasks, encompassing the installation, inspection, repair and maintenance of fixed and floating structures, seabed equipment, and pipelines. One of the most serious limitations on these activities is the ability to launch and retrieve subsea units - typically manned diving bells or remotely operated vehicles - through the air/sea interface. This limitation arises because the environmental forces of wind, waves, and current are at their most severe at the air/sea interface. If the conventional 'over the side' method of launch/retrieval is employed, where the subsea unit is quite literally lowered from a crane over the side of the support vessel, then rapid variations in the magnitude and direction of the environmental forces can occur, causing large horizontal and vertical excursions of the unit. This in turn leads to a two risks. Firstly, the unit may collide with the mother vessel. If the unit were damaged in such a collision, then there could be serious financial consequences, in terms of both repairs to the unit and downtime incurred. In the case of pressurised diving bells the consequences of such a collision could be fatal for the occupants of the bell since any loss of integrity of the bell might lead to instant decompression. Secondly, large dynamic loadings in the hoist wire may result, with the possibility of a failure of the wire, resulting in the loss of the unit. The financial consequences of such a loss would be severe, as recovery of the unit could prove extremely expensive. In addition, if the unit in question were a diving bell, then the consequences in terms of loss of life might very well be disastrous.

One solution to the problem of launch and retrieval which has gained increasing popularity is the moonpool. A moonpool is a vertical tube, usually sited near the centre of the ship, through which the units may be launched. The concept was adapted from the wells used on drillships through which the drill string is lowered; the name apparantly came about because the early wells were circular in section, and if divers were working beneath the ship, the circle of light transmitted down the well looked like a full moon. There are several advantages of this approach relating to the launch and retrieval of subsea units. Firstly all the horizontal elements of the environmental loading on the unit are removed whilst the unit is in the moonpool. The wind effect is removed altogether, whilst the current and the horizontal component of the wave motion is removed for the initial launch period. Furthermore, the moonpool acts as a low pass filter to the vertical component of the wave motion, removing high frequency elements, and thus reducing the risks of slamming. Finally, if the moonpool is positioned near the centre of the vessel, the effects of the ship's angular motions - particularly roll and pitch - on the launch/retrieval operation are minimised.

An additional use of moonpools has come from the recent developments in floating production systems for marginal fields. Where such systems are based on conventional monohull ship forms, the marine riser must enter the vessel near the centre in order that the forces required to tension the riser can be supported. The obvious solution is thus to bring the marine riser into the vessel through a moonpool. Such moonpools will inevitably be larger than those used for the launch and retrieval of subsea vehicles, and due to the size of the vessels involved, will also have a greater draft. As with the case of launch and retrieval, an additional advantage of the use of the moonpool is to minimise the effects of the angular motions of the vessel during operation.

There is, however, one significant problem associated with the moonpool concept. The water column in the moonpool may, under certain conditions, undergo large and apparantly unpredictable vertical oscillations. In extreme cases, these oscillations may be as large as three or four times the external wave height. Such oscillations may lead to two distinct problems. Firstly, the deck area above the moonpool, used for submersible handling in the case of a diving support vessel, or riser handling in the case of a floating production vessel, may be flooded. This is undesirable for the safety of those working on equipment handling, and, in more general terms, for the safety of the vessel as a whole. Secondly, if the large oscillations occur during a launch/retrieval operation from a diving vessel, then the vertical forces on the unit may cause the hoist wire to go slack, then suffer a snatch load, with the risk of a failure.

The problems of large water column oscillation are not, however, inherent in the moonpool approach; they result from poor design of the moonpool from a hydrodynamic point of view. In many cases the moonpool on a vessel is designed with purely structural considerations in mind, with the result that the design is unsuited to the vessel in hydrodynamic terms. This study is aimed at providing the techniques required to design moonpools which are well suited to the ships in which they are to be installed and the sea areas in which those ships will work.

1.2 AIMS OF THE STUDY

(i) To acquire an understanding of the water column oscillation in the moonpool with or without the presence of a subsea unit.

(ii) To develop a technique to calculate the hydrodynamic loading on a subsea unit in the moonpool.

(iii) To model the ship/moonpool system mathematically, and examine the effects of variation of important geometric parameters on the system response.

(iv) To verify the conclusions reached and examine any deficiencies in the theoretical work by means of experimental studies.

(v) To devise a quantitative means of comparison of different moonpool designs, and to propose a practical procedure for the design of moonpools.

2. THE WATER COLUMN OSCILLATION IN A MOONPOOL

2.1 INTRODUCTION

Literature Review

The amount of research in the specific area of moonpool water column oscillation has been somewhat limited. Madsen [1980] studied the problem of a diving bell in a moonpool with the aim of predicting the forces on the hoist wire and the motions of the bell with various handling systems. His approach involved the formulation and solution of two simultaneous equations of motion; one for the bell and one for the water column. The water column oscillation equation allowed for non-linearities both in mass (due to the changing real mass of the water column with oscillation) and damping terms; the hydrodynamic coefficients for added mass and damping were obtained from empirical formulae due to Fukuda [1977], Massey [1975], and Prandtl [1965]. The excitation was considered to be due solely to the Froude-Krylov force - i.e. the wave force which would exist in the absence of the vessel. Solution was obtained by an initial value approach in the time domain. Results were presented in the form of time histories. A comparison was made with experimental data for a time history of about seven minutes duration; reasonable agreement appeared to be found. No water column oscillation statistics were calculated, either directly from the realisation or via response spectra. Whilst these statistics could be obtained from a sufficiently long realisation, the computer time required would be significant, and the rather crude approximations to both the excitation and the hydrodynamic coefficients could lead to serious inaccuracies for complex geometry moonpools and in certain sea states.

Spangeberg and Jacobsen [1983] extended Madsen's model for the water column oscillation without considering bell-moonpool interaction to include the influence of wave diffraction and ship heave in the excitation. However they retained the rather crude empirical approach to the calculation of the hydrodynamic coefficients. Few details of numerical results were given, the emphasis being placed on model test data in both frequency and time domains.

Aalbers [1984] offered a sophisticated model incorporating coupling between ship heave and water column oscillation using interaction coefficients obtained from both potential theory and model tests. The equation of motion for the water column oscillation allowed for non-linearities in both mass and damping terms; and an attempt was made to calculate the coefficients using potential theory. This did not prove successful, even for the simple moonpool geometries used, and the results presented used hydrodynamic coefficients obtained from model tests. The excitation for the water column oscillation was considered to consist of the Froude-Krylov force and the wave diffraction force; the influence of the ship heave being modelled through the interaction terms. The solution was again obtained in the time domain; however results were presented in the form of frequency domain transfer functions; the numerical method by which these were obtained not being described. Agreement with experimental data for the simple shapes tested appeared, on the whole, to be good.

In contrast Lee [1982] solved the problem using a mechanical oscillator model in the frequency domain. Non-linearities in the damping terms are allowed by the use of an iterative method of solution. Full coupling between ship heave and water column oscillation was assumed, with the cross-coupling coefficents as well as the added mass and damping coefficients obtained from an extensive set of experimental tests, involving the construction of models for both ship and

moonpool. Results were presented in the form of response amplitude operators; agreement with experimental data was generally rather poor. This seemed to be due partly to less than wholly reliable experimental results, as well as the inherent deficiencies in the method. The two major weaknesses with the fully coupled model as presented appear to be that the coupling coefficients had to be measured from experimental tests, but accurate measurements proved extremely difficult to achieve. In addition, the coefficients must be assumed independent of frequency in order to keep the amount of experimentation within reasonable limits. The errors introduced by these problems appear to be responsible for some rather counter intuitive 'valleys' in the theoretical prediction of the water column oscillation RAOs as well as being implicated in the generally poor agreement with experimental data.

Gran [1983] also solved the problem in the frequency domain, but the mathematical model and the method of solution employed are considerably simpler than those used by Lee. The damping is only represented by a linear term, obtained from experiments, whilst the added mass is estimated using an empirical equation. The effects of ship motions are neglected in the mathematical model. Experimental results for a moonpool fixed in space are presented both as RAOs where the agreement between prediction and experiment seems reasonable, and in the form of ratios of significant moonpool oscillation to external significant waveheight where the discrepancy between prediction and experiment is between 10 - 20%.

Selection of Approach

Despite the apparant problems with the frequency domain approaches described, the frequency domain approach has one major advantage over the time domain approach in that the amount of computation required to obtain the response spectra

for the water column oscillation is significantly smaller. For this study, then, it was decided to use a frequency domain approach somewhat similar to that of Lee, but to simplify the model in order to ease its use in practice as a design tool whilst attempting to improve the accuracies of the predictions made. The simplification made results from the application of an intuitive argument: that the ship heave will influence the water column oscillation, but that the reverse is not true to any significant extent. It is assumed that other modes of motion than heave do not affect the water column oscillation; furthermore that the only influence of the moonpool on the ship motions is geometric; i.e. through the reduction in displacement and waterplane area. Coupling between water column oscillation and ship heave was therefore neglected; coupling between ship heave and water column oscillation was only modelled through the excitation terms.

This simplification has the immediate advantage that only two sets of physical measurements are required in order to solve the equations of motion. Full details of the procedures established to carry out these measurements are given in Appendix 2.1.

The problem as a whole is thus formulated in two parts; the ship heave equation being solved as the first part, and the water column oscillation being solved as the second.

2.2 FORMULATION OF SHIP HEAVE PROBLEM

The global co-ordinate system for the solution of the ship heave / water column oscillation equations is shown in Figure 2.1. The co-ordinate system is space-fixed with the origin at the centre of the moonpool on the still water level. The ship is restrained in all modes of motion except heave; plane progressive waves of circular frequency ω and amplitude a

are incident upon the ship from a heading angle α. The resulting motion can be described with the equation:

$$m_s \ddot{Z}_s + r_s Z_s = Re\left[F_s e^{-i\omega t}\right] \qquad (2.1)$$

where m_s = mass of the ship
z_s = ship heave elevation
r_s = ship heave restoration
F_s = excitation force amplitude (generally complex)

It should be noted that the above equation assumes that viscous damping is negligable; the hydrodynamic forces acting on the ship due to the ship heave are included in the excitation term rather than in the usual form of 'added mass' and 'damping'.

It is assumed that the solution takes the form:

$$Z_s = Re\left[H_s e^{-i\omega t}\right] \qquad (2.2)$$

where H_s = ship heave amplitude (generally complex)

The excitation term takes the form:

$$F_s e^{-i\omega t} = \left[a\left(F_s^I + F_s^D\right) + H_s F_s^R\right] e^{-i\omega t} \qquad (2.3)$$

where a = wave amplitude
F_s^I = amplitude of force due to the wave in the absence of the ship for unit wave height.
F_s^D = amplitude of force due to wave diffraction around the ship for unit wave height.
F_s^R = amplitude of force which would result from forced heaving of the ship in otherwise still water.

and F_s^I, F_s^D, F_s^R are all, in general, complex. Substitution of (2.2) and (2.3) into (2.1) completes the solution.

2.3 FORMULATION OF WATER COLUMN OSCILLATION PROBLEM

It is assumed that the added mass of the water column is independent both of excitation frequency and oscillation amplitude, whilst the damping is considered to be independent of frequency, but linearly dependent on oscillation amplitude. The equation of motion for the water column oscillation can thus be written as:

$$m_m \ddot{z}_m + C_m \dot{z}_m + r_m z = Re\left[F_m e^{-i\omega t}\right] \qquad (2.4)$$

where

m_m = virtual mass of the water column

z_m = water column elevation in space-fixed co-ordinates

C_m = equivalent linear damping at the oscillation amplitude H_m (generally complex)

r_m = water column restoration

F_m = water column excitation amplitude (generally complex)

Before a solution is obtained for this equation, it is worth examining some of the terms in more detail.

(i) Virtual mass

The virtual mass consists of the sum of the real and hydrodynamic (or added) mass of the water column. In the more complex moonpool geometries the actual mass of the water column may be somewhat difficult to calculate; in order to standardise the procedure it is assumed that the mass is equal to the cross sectional area of the moonpool at the still water level multiplied by the ship draft. This assumption is used in the calculation of the added mass from the experimental data as well as in the solution of the equation of motion, and thus the virtual mass will be correctly ascertained from the data even if the individual masses (real and hydrodynamic) are slightly in error. The virtual mass is thus expressed

as:

$$m_m = \rho A_m T (1 + a_m) \tag{2.5}$$

where

ρ = mass density of water

A_m = cross section area of the moonpool at still water level.

T = ship draft

a_m = water column added mass

(ii) Damping

The equivalent linear damping C_m is expressed in the usual form of a critical damping ratio. Following Lee, this is expressed as the sum of two terms; one which is constant, and one which is proportional to the relative oscillation between the water column and the ship. The term C_m is thus written as:

$$C_m = 2 m_m \omega_n \left[\xi_{r_I} + \frac{1}{T} |H_m - H_s| \xi_{r_G} \right] \tag{2.6}$$

where

ξ_{r_I} = damping ratio for zero relative oscillation amplitude

ξ_{r_G} = damping ratio gradient with relative oscillation

ω_n = undamped natural frequency of the water column oscillation

and ω_n is obtained from the solution of the undamped equation of motion as:

$$\omega_n = \sqrt{g / T (1 + a_m)} \tag{2.7}$$

The choice of this formulation is justified by the excellent agreement with experimental results obtained; an example is given in Figure A2.1.6.

(iii) Restoration

The water column restoration is expressed quite simply in terms of the cross sectional area of the moonpool at the still water level:

$$r_m = \rho g A_m \tag{2.8}$$

(iv) Excitation

The excitation term takes the form:

$$F_m = \left[a\left(F_m^I + F_m^D\right) + H_s F_m^H\right] e^{-i\omega t} \tag{2.9}$$

where F_m^I , F_m^D , F_m^H are the amplitudes of the forces acting on the water column corresponding to the forces F_s^I , F_s^D , F_s^H acting on the ship.

It is assumed that the solution takes the general form:

$$Z_m = Re\left[H_m e^{-i\omega t}\right] \tag{2.10}$$

Using (2.4 - 2.10) an implicit solution for the moonpool oscillation is obtained.

2.4 NUMERICAL SOLUTION

The oscillation of the water column is thus calculated in two stages. The solution of the equation of motion for the ship heave must first be calculated. The mass and restoration terms for the ship heave may be obtained knowing the operating draft and the underwater form of the vessel. The Froude-Krylov force is obtained directly from first order (Airy) wave theory. The bulk of the computational effort lies in the calculation of the force amplitudes F_s^D and F_s^H .

These are obtained using a two-dimensional source distribution method due to Frank [1967] in conjunction with a strip theory approach. Although more sophisticated models have since become available in recent years, it is felt that the extra accuracy obtained would not justify the resulting vast increase in computer time required, from the point of view of an engineering solution; particularly as the approach used is known to be at its best for the case of a stationary ship undergoing heave.

Having calculated the values of all coefficients and obtained a solution for the complex heave amplitude H at each frequency of interest, it is then possible to calculate the solution for the water column oscillation amplitude. As mentioned previously, the coefficients a_m, ξ_I, ξ_c are obtained from experimental measurements (Appendix 2.1). The moonpool cross sectional area, A_m, and draft, T, are known from the moonpool geometry. The moonpool excitation force amplitudes F_m^o and F_m^H are obtained from the same source distribution method as the corresponding ship excitation terms.

It would then be possible to use an iterative approach to obtain results in the form of transfer functions from wave height to water column oscillation amplitude. However, whilst this form is eminently suitable for linear systems such as the ship heave, it is not suitable for non-linear systems such as the water column oscillation, as the magnitude of the function at any given frequency depends upon the amplitude of the input (in this case the wave height) at that frequency. Furthermore, in order to produce estimates of the statistics of the random process such as significant oscillation amplitudes or long term exceedance probabilities, the information about the water column oscillation amplitude is more useful in the form of a power (or variance) spectrum.

It is well known that the reponse spectrum for a linear system may be related to the input spectrum via the system response amplitude operator (RAO) - ie the magnitude of the transfer function - using the expression (eg Jenkins & Watts [1968]):

$$S_{RR}(\omega) = S_{II}(\omega) . M^2(\omega) \qquad (2.11)$$

where

$S_{RR}(\omega)$ = response spectral ordinate
$M(\omega)$ = response amplitude operator
$S_{II}(\omega)$ = input spectral ordinate

The ship heave response spectrum may thus be obtained directly from this expression, but a more subtle approach is required to obtain the water column oscillation response spectrum due to the non-linearity of the transfer function with wave amplitude. Lee [1982] suggests that the problem might be solved by calculating the amplitude of discrete components of the input spectrum associated with predetermined frequency bands; however the results gained from such an analysis would be sensitive to the number of components chosen; as the number increased, then the amplitude of the components would diminish, and the damping term calculated would reduce towards the value for zero oscillation amplitude. In order to avoid this problem, the magnitude of the damping term is calculated on the basis of an assumed significant oscillation amplitude, and the response spectrum calculated on the basis of this assumption. This spectrum is used to calculate the significant moonpool oscillation amplitude and the value thus obtained is then used to provide a new estimate for the damping term. The procedure is repeated until convergence of the estimated and calculated damping is achieved. The non-linear problem is thus solved as an equivalent linear system, with the value adopted for the equivalent linear damping depending upon the total energy in the system.

It should be noted that the transfer function between the wave and the water column oscillation in the moonpool results from several separate physical effects. There is a linear transfer function between wave amplitude and ship heave amplitude, related to the ship form as a whole. There are separate linear transfer functions from the ship heave amplitude to the ship heave water column excitation term F_m^H, and from the wave amplitude to the wave diffraction water column excitation term F_m^D, both of which are implicitly assumed (by the use of the strip theory approach) to relate to the ship underwater form in the region of the moonpool. There is a linear transfer function between wave amplitude and the Froude-Krylov water column excitation term F_m^I. Finally there is a non-linear transfer function between the total water column excitation force amplitude and the water column oscillation amplitude. The system is, then, modelled in the form of a mechanical oscillator, but the mechanism is more complex than might be thought at first sight. The relationship between the input wave and the moonpool oscillation is illustrated in the form of a block diagram in Figure 2.2.

2.5 EXPERIMENTAL VERIFICATION

In order to examine the accuracy of the proposed method, a series of experimental studies were carried out. The aim of these studies was to demonstrate that the procedure described to calculate the moonpool response spectrum (and hence the water column oscillation random process statistics) produces results which are accurate enough to be used for engineering design purposes.

The method was tested for three different moonpools; for each moonpool two sets of tests were performed. The first series produced the hydrodynamic coefficients for the moonpool using the procedure set out in Appendix 2.1. The second series

produced the moonpool response spectra for a three given input wave spectra with the moonpools mounted in a ship model, the ship being fixed in the wave tank such that all modes of motion except heave were restrained. Three random realisations were generated using the 'coloured noise' method described in Chapter 3 from JONSWAP wave spectra. The realisations were then converted from wave elevation to voltage values and used as the input for the wavemakers, so that unidirectional random seas could be run in the tank. Measurements were taken of the water surface elevation realisation near the ship and inside the moonpool (relative to the ship).

For each moonpool the wave height and water column oscillation power spectra were calculated numerically for the three realisations. The wave height power spectra resulting from this sequence of measurements were then used as the input for the theoretical calculation procedure in conjunction with the moonpool hydrodynamic coefficients, and the predicted water column oscillation power spectra thus calculated were compared to those measured. The moonpools used are shown in Figure 2.3; the ship model with moonpool mounted is shown in Figures 2.4 - 2.5.

2.6 RESULTS AND DISCUSSION

Hydrodynamic Coefficients

The results for the hydrodynamic coefficients for the three moonpools are shown in Appendix 2.2. It can be seen that in all three cases the added mass of the moonpools is relatively small, and that the major contribution to the damping comes from the non-linear component ξ_{ϵ}.

Prediction of Significant Water Column Oscillation

The significant oscillation in the moonpool is shown in Appendix 2.3 for both measured and predicted values. The agreement is quite good, with the worst error being less than 15% and the mean error over the nine tests being 7.5%. The errors are mostly on the side of safety (from the point of view of design) with the predicted significant oscillations being larger than those measured in seven out of the nine cases studied. The possible reasons for these discrepancies are discussed later.

Prediction of Water Column Oscillation Response Spectra

Plots of the measured wave spectrum, the predicted oscillation spectrum and the measured oscillation spectrum are shown in Figures 2.6 - 2.14. In each case the solid line represents the input wave spectrum, the dashed line represents the predicted moonpool response spectrum, and the triangular symbols represent the measured moonpool response spectrum. It can be seen that in all cases the input wave spectra are not very smooth, with two peaks in all the runs of realisation 1 and 2, and three peaks in all the runs of realisation 3. There are two distinct phenomena causing these problems, both related to the experimental equipment. Firstly, the beam of the vessel, as compared to the width of the tank was quite large (of the order of 20%). This led to a parasitic cross wave in the tank between the tank walls and the side of the vessel; this is shown quite clearly in all the input wave spectra as a peak at about 1.35 Hz. Secondly, the calculation of the realisations took no account of variation in the transfer function of the wavemakers, assuming that the response in the tank (in terms of wave height / voltage) was constant. In practice the tank was found to suffer from a 'dead' spot at about 0.65 Hz; this is clearly shown in the wave spectra for the three runs of realisation 3 (Figures 2.8, 2.11 & 2.14) as a dip in the wave

spectrum at this frequency. As a result, the moonpool response spectra also exhibit multiple peaks in some cases, with peaks occurring both at input spectrum peak values and at the natural frequency of the water column oscillation. In all cases, the shape of the predicted moonpool response spectrum is similar to that measured.

Sources of Experimental Error

There are several possible sources of error with the experimental equipment and procedures used. The calibration of the wave probes used to measure the water surface elevation both inside the moonpool and external to the ship could not be carried out to an accuracy greater than about 5%, given the small amplitude of the waves (and water column oscillation). In real terms this implies an accuracy of about 1 - 2mm in the values measured for the water surface elevations. In addition, the diffraction of the waves around the ship would be significantly affected by the close proximity of the tank walls, and the cross waves caused by this effect will also have influenced the results obtained, particularly in the case of realisation 1, where the energy present in these waves can be seen from the spectra to be about 25% of the total. The proximity of the tank bottom would also affect both the diffraction of the waves around the ship and the flow in and out of the moonpool. Finally, the spectral analysis techniques used to obtain the power spectra from the realisations will tend to smooth out sharp peaks in the measured spectra due to the phenomenon of spectral leakage. It is to be expected, then, that the results for the realisation with the smallest significant waveheight (realisation 1) would exhibit the largest errors; this is, in fact, found to be the case. If the results for this realisation were to be neglected, then the worst error would be less than 10%, and the average error would drop to just over 5%.

Effect of Moonpool Configuration on Prediction Error

It should be noted that the moonpools used provide a more exacting test for the method than those which might be used in practice. As will be seen later (Chapter 6), one effect of the introduction of even a small baffle is to increase the linear component of the damping as a proportion of the non-linear component, and thus make the system as a whole less strongly non-linear. Since the approximate method used to estimate the equivalent linear damping for the system will provide the greatest errors when the non-linear component of the damping is most dominant, such alterations to the moonpool geometry will tend to lead to more, rather than less, accurate predictions.

Summary

In summary, the results suggest that the mathematical model used to predict the water column oscillation suitable for the purposes of engineering design. However the measurement of the moonpool hydrodynamic coefficients should ideally be carried out in a wave tank where the blockage caused by the presence of the ship is much less than was the case with these measurements, and at a larger scale in order to ensure similarity between the flow in the model moonpool and the full scale moonpool, in order to achieve good agreement between model and full scale coefficients.

Having established a model which may be used to predict the water column oscillation in a moonpool, it is now required to develop a method of predicting the forces on a subsea unit in a moonpool. The following chapter describes such a model.

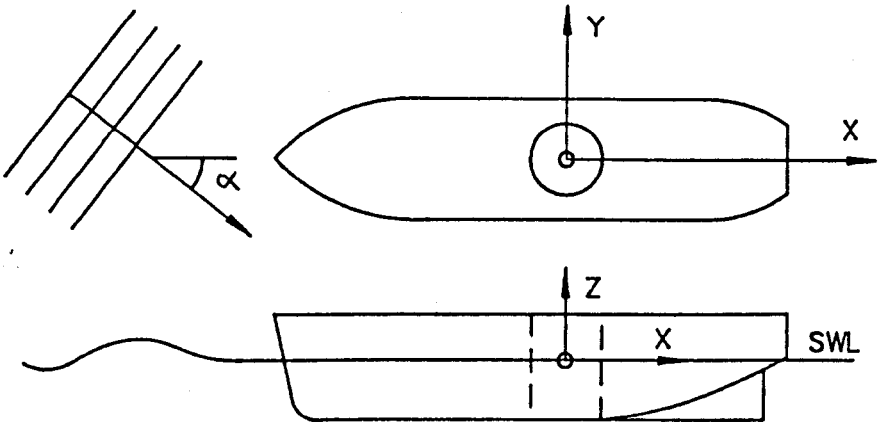

Figure 2.1

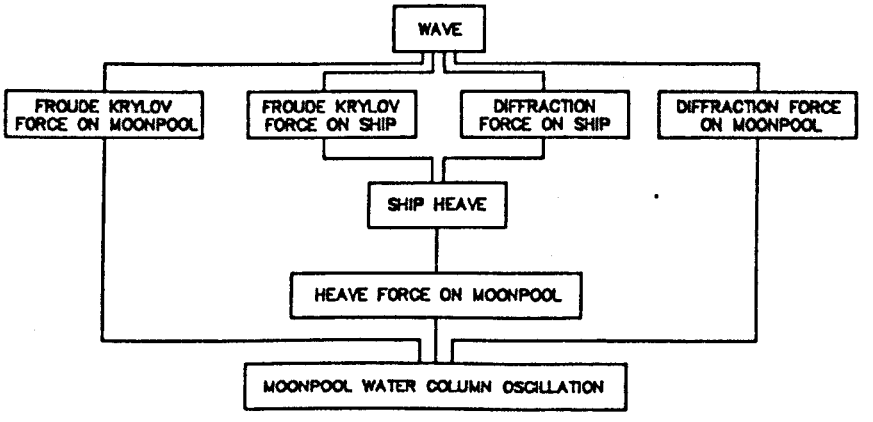

Figure 2.2

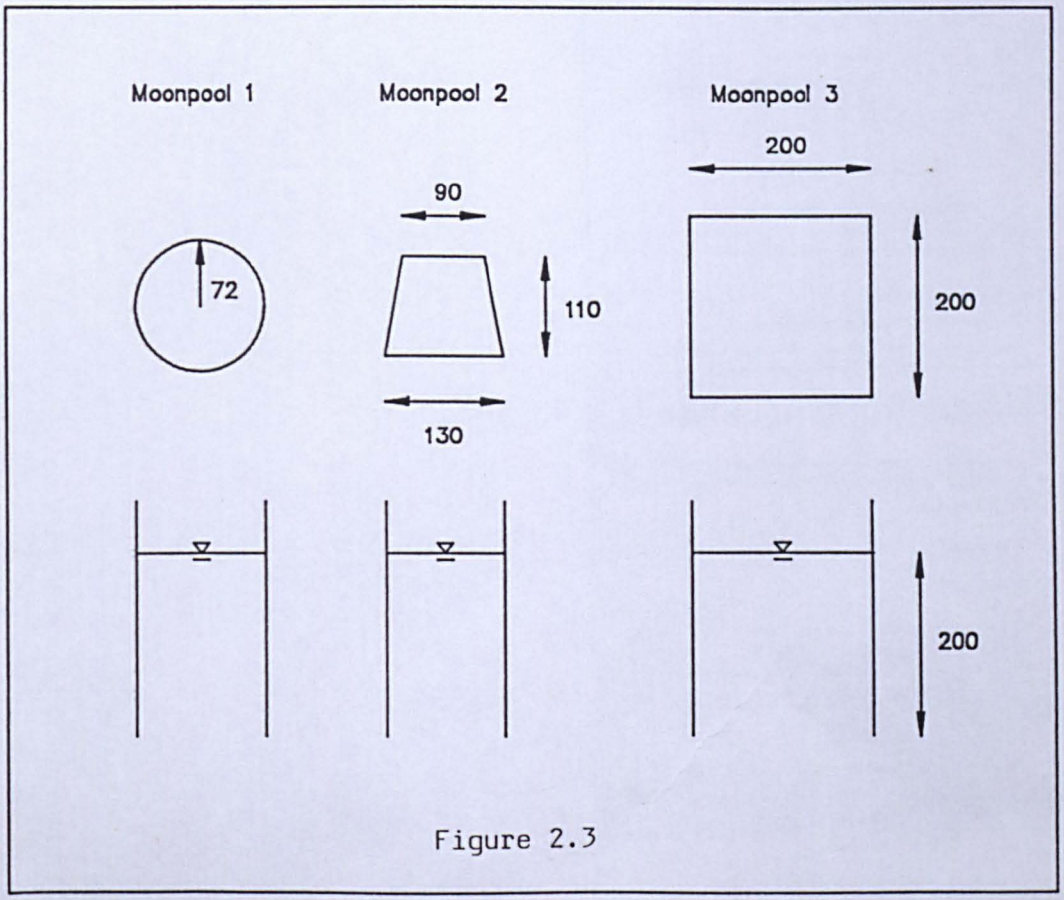

Figure 2.3

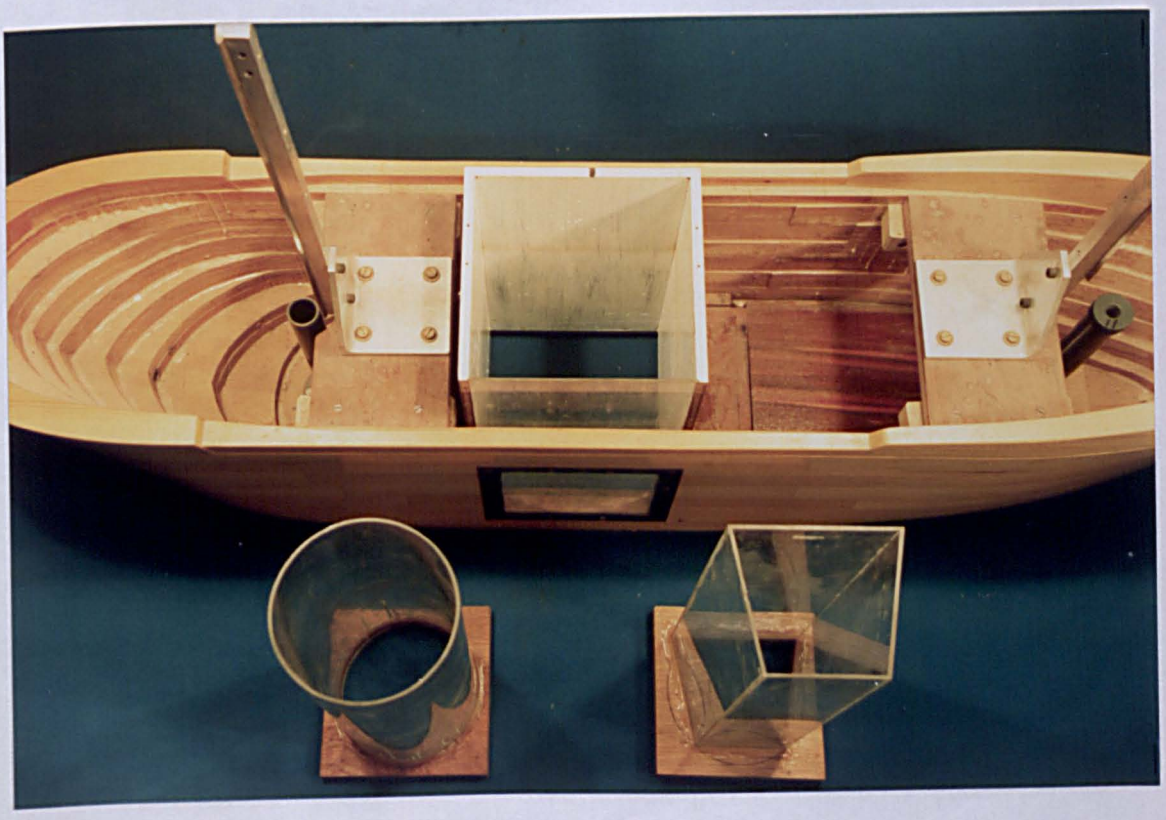

Figure 2.4

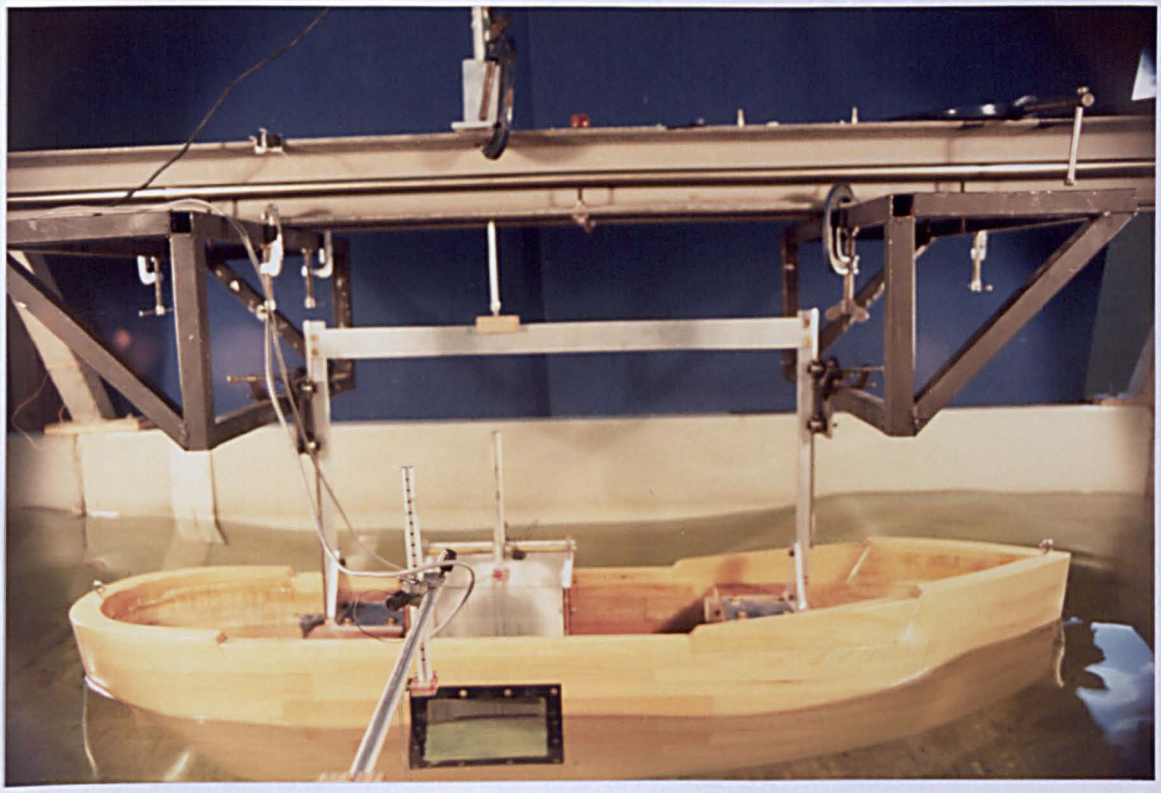

Figure 2.5

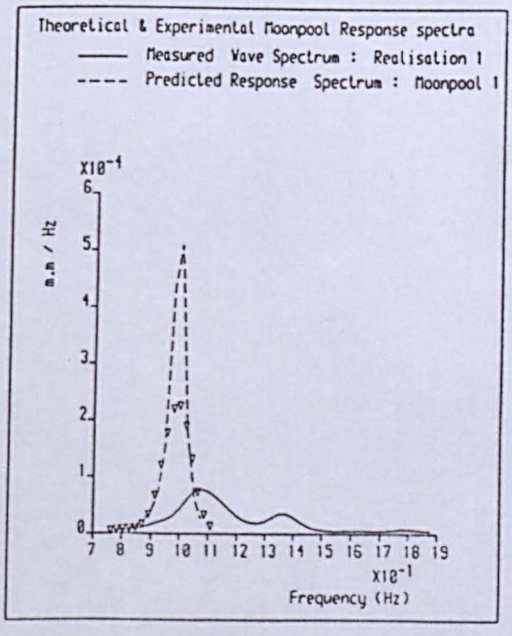

Figure 2.6

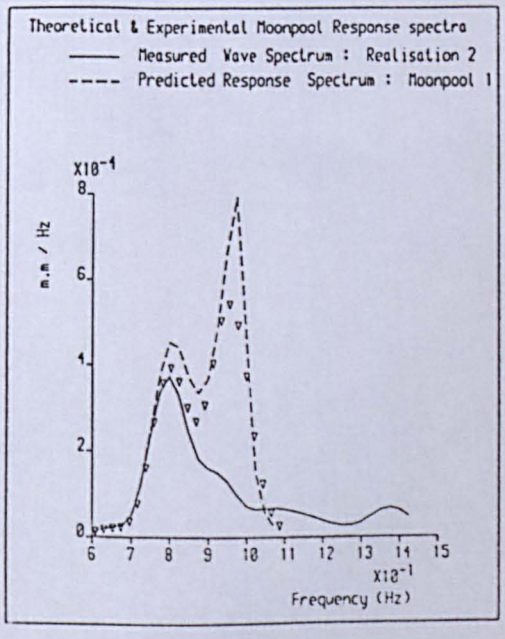

Figure 2.7

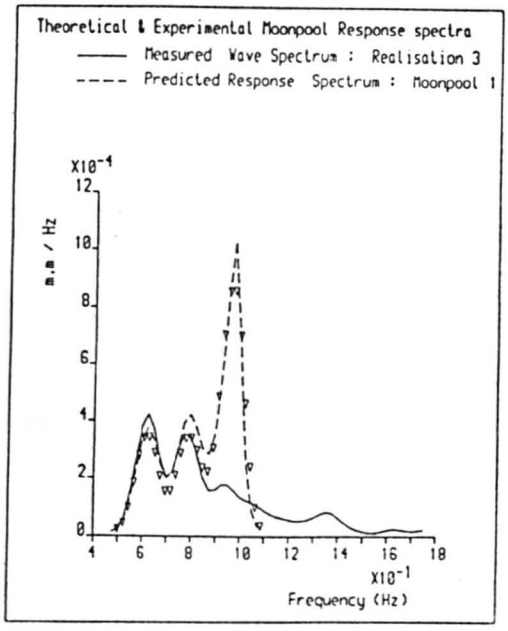

Figure 2.8

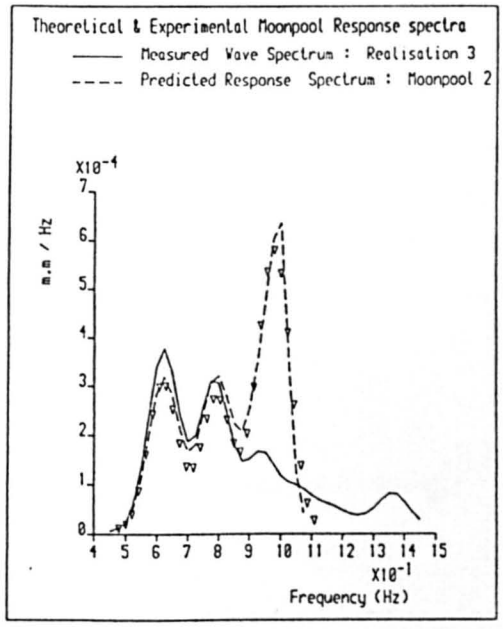

Figure 2.9

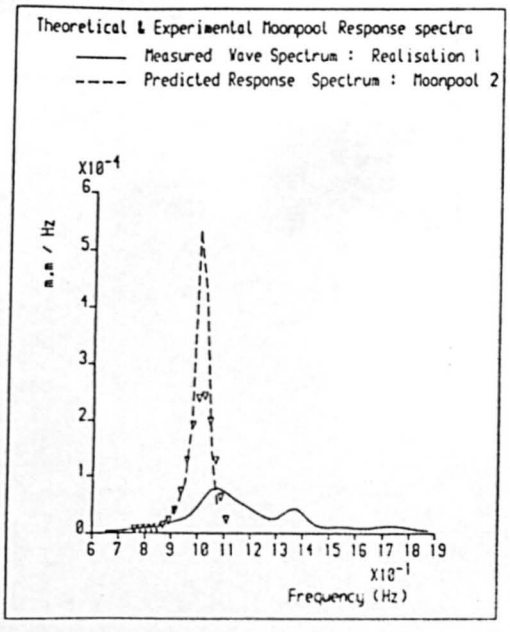

Figure 2.10

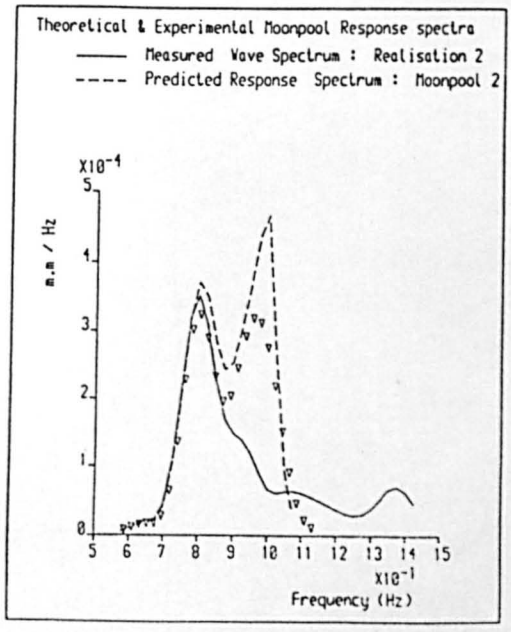

Figure 2.11

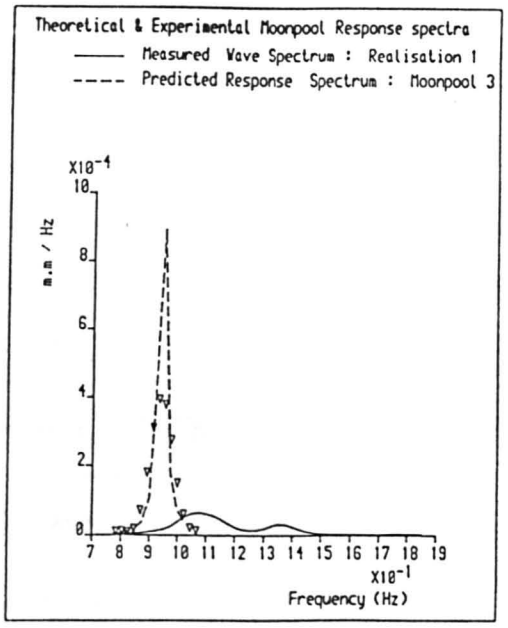

Figure 2.12

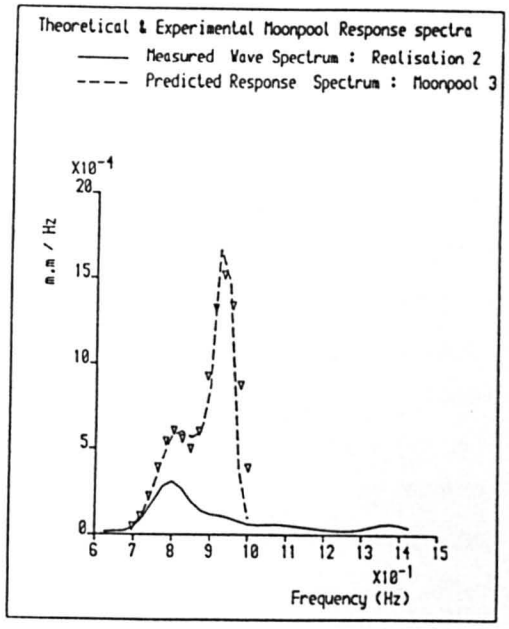

Figure 2.13

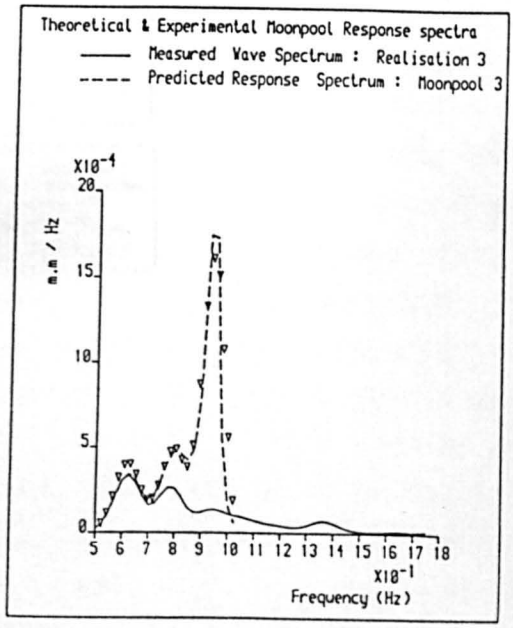

Figure 2.14

3. THE HYDRODYNAMIC FORCES ON A SUBSEA UNIT IN A MOONPOOL

3.1 INTRODUCTION

Having obtained the response spectrum for the moonpool water column oscillation, the next step required in the procedure is the calculation of the hydrodynamic forces on the subsea unit in the moonpool. This is a complex problem, for two major reasons. Firstly, the relationship between the forces on the unit and the water surface elevation is non-linear; this non-linearity prevents the direct use of spectral techniques. Secondly, the presence of the subsea unit in the moonpool will affect the water column oscillation whilst the presence of the moonpool around the subsea unit will affect the flow around the unit in some way.

Literature Review: Forces on a Diving Bell in a Moonpool

Madsen [1980] calculated the force on a diving bell fully submerged in a moonpool using a deterministic initial value time domain approach involving the solution of a system of differential equations based on the bell motion and the water column oscillation. The hydrodynamic forces on the bell were calculated using Morison's equation (Morison et al [1950]); the inertial and drag coefficients for the four bells tested in various sized moonpools were measured in small scale (1:20) experiments; the Reynolds numbers attained during the tests are not made clear. The effect of the moonpool on the flow around the bell is accounted for using experimentally derived empirical relations between the blockage coefficient (ie the ratio of the bell projected area to the moonpool cross section area) and the hydrodynamic coefficients. Results for the hydrodynamic coefficients are compared with the full scale measurements carried out by Mellem [1979a]; the agreement obtained is rather poor. Results for the force on the bell are presented in the form of time histories, for both a regular and a random wave input. Some comparison is

made with experimental results; good agreement appears to be obtained; however the comparison is only presented for about one cycle of oscillation. No attempt is made to predict a power spectrum for the force or to obtain any statistics for the force random process. Whilst the force random process statistics could be obtained from a suffiently long force realisation, it is felt that the method proposed is computationally too complex to be of practical use in this regard, and an alternative must be used if these statistics are to be calculated.

Gran [1983] adopts a frequency domain approach using Morison's equation. The influence of the bell on the moonpool is allowed for by using an empirical equation for the linearised damping ratio. Results are presented firstly in the form of an RAO calculated using Morison's equation, and secondly in the form of Root Mean Square (RMS) forces on the bell calculated from the RMS wave elevation. The RAO presented appears to give reasonable agreement with measurement, but the RMS forces predicted are too large by a factor varying between just over 2.0 to about 4.5. A discussion on the calculation of drag coefficients for a diving bell in a moonpool is presented, which suggests that the empirical equations obtained by Madsen seriously underestimate the drag coefficient at high blockage ratios. An alternative equation is proposed which assumes high blockage ratios, but produces significant overestimates of the drag coefficient for low blockage ratios. Comparison of the drag coefficient obtained from the proposed equation with full scale measurements carried out by Mellem [1979b] in a case where the blockage ratio was quite high (0.55) indicate that even the alternative equation underestimates the drag coefficient on the bell - in this case by a factor as great as 1.7.

Since neither of the works discussed provide a successful solution to the problem of calculating the random hydrodynamic forces on a subsea unit in a moonpool, an alternative approach is desirable. In recent years much work has been devoted to the study of random hydrodynamic forces on fixed objects, with the goal usually being the estimation of wave loading on fixed structures such as steel jackets or subsea pipelines. The problem of calculating the hydrodynamic forces on a subsea unit in a moonpool is in many ways similar to this type of calculation. Whilst the moonpool problem is, in one sense, simpler in that the water motion in a moonpool can reasonably be considered to be one dimensional, it is, in another sense, more complex in that the oscillation spectrum is not known in functional form, and in that the unit is only restrained in one direction in the moonpool. If, however, the assumption is made that the unit is fixed in the moonpool, then the problem is simplified significantly. The statistics for the hydrodynamic force on the unit may be calculated with relative ease, either directly from a time domain simulation, or from a force power spectrum. The resulting values may then be compared with the weight of the unit in water in order to ascertain the probability of a slack wire situation.

Borgman [1967a, 1967b] uses a linearised version of Morison's equation to calculate the force spectral density on a circular pile from the wave elevation spectral density. Whilst the derivation itself is somewhat complex, the resulting equations are relatively straightforward to use, and the force random process statistics may be obtained from the spectrum. The weakness of the method lies in the linearisation of the velocity dependent term in Morison's equation. Few results are given; however those shown suggest good agreement with experimental data. Borgman defends the

linearisation process by suggesting that greater errors may be introduced by inaccurate values of the inertial and drag coefficients required by Morison's equation.

The force random process statistics may also be calculated from a time domain simulation. If the oscillation spectrum is known, then a realisation of the water surface elevation (and any other required wave information such as velocity or acceleration) may be calculated, and the force may be calculated deterministically at each time step by a strightforward application of Morison's equation in the full non-linear form. If the realisation is long enough such that the sample statistics can be considered to represent the process adequately, then the force random process statistics may be obtained from the realisation. Alternatively a force spectrum may be calculated from the realisation. In general terms, the weaknesses of the time domain approach lie in the generation of the water surface realisation in that the the water surface elevation spectrum may not be adequately represented by the realisation and that a large number of calculations are required in order to obtain the final information, making the process costly in both computer storage and time. The choice of method for the generation of the realisation is therefore of great importance.

Literature Review: Generation of Random Process Realisations

One method commonly used in the past to generate realisations (eg Borgman [1969]) involves the summation of a finite number of Fourier components of fixed amplitudes determined from the power spectrum and random phases. Tucker et al [1984] point out a major error implicit in this approach, and discuss its effect on the wave group statistics of the realisations generated. An alternative method is therefore desirable.

Spanos and Hansen [1981] use linear prediction theory to generate realisations based on the Pierson-Moskwitz spectrum using an all pole recursive digital filter. The method is computationally efficient, but the results show that the power spectra of the generated realisations suffer from significant fluctuations whose bandwidth is related to the order of the filter selected. Cuong, Troesch and Birdsall [1982] give a method involving the inverse fourier transform of 'coloured' noise to generate realisations based on the JONSWAP spectrum. Whilst not as efficient computationally as the linear prediction method, the periodogram generated from the realisation shows good agreement with the target spectrum. Finally, Spanos [1983] uses an autoregressive moving-average (ARMA) approach to generate realisations based on the Pierson-Moskwitz spectrum; no results are presented comparing power spectra generated from the realisations with the target spectra. The method involves the fitting of an empirical curve to the target spectrum in order that the ARMA coefficients may be obtained. The method is complex, and the determination of the coefficients expensive in computer time.

Selection of Approach

For this study, two approaches were adopted, with a common set of assumptions. The first approach uses the method proposed by Cuong et al to generate realisations of the moonpool oscillation in conjunction with Morison's equation to obtain the force random process statistics. The second uses Borgman's frequency domain solution of Morison's equation.

3.2 FORMULATION OF THE PROBLEM

The co-ordinate system for the solution of the force on the subsea unit is shown in Figure 3.1. The system is space fixed with the origin at the centre of the moonpool on the still water level. All displacements, velocities, accelerations, and forces are defined as positive in the direction z-positive (ie upwards).

The assumptions made in order to set up the mathematical model are as follows:

Hydrodynamic Force Equation

It is assumed that Morison's equation can be used to calculate the forces on a subsea unit in a moonpool; whilst the equation was originally devised for the calculation of wave forces on vertical piles, it has since been extensively used to calculate in line forces on a wide variety of objects in oscillatory flow with good agreement with experimental and full scale results.

Motion of Subsea Unit

The subsea unit is assumed to be fixed in space. In practice the unit will usually be free to move laterally to some extent before it hits the moonpool walls; it will, of course, also be free to move vertically upwards if the upwards hydrodynamic forces are greater than the weight of the unit in water. For this study, lateral movement is ignored, as the water column oscillation is considered to be purely vertical. The restriction on vertical movement can be thought of in physical terms as an artificial increase in the weight of the unit such that the hoist wire tension will always be greater than zero. The results thus obtained for the upwards hydrodynamic force can then be compared with the actual weight of the unit in water, and the actual tension in

the hoist wire estimated. When the tension reduces to zero, then a slack wire situation will result. For the purposes of moonpool design, the prediction of this event is of prime importance; whilst the behaviour of the subsea unit subsequent to the slack wire cannot be modelled by this approach, the designer of a moonpool needs primarily to know how likely the slack wire situation is, rather than the exact consequences of its occurrance. This assumption allows the hydrodynamic force on the unit to be calculated from one equation, removing the need to set up and solve an equation of motion for the unit simultaneously with the equation of motion for the water column, and simplifying the solution significantly as a result. The effect of a constant launch (or retrieval) velocity can easily be included as an alteration of the static weight in water of the unit; the calculation here only concerns the random hydrodynamic forces.

Submergence of Subsea Unit

The subsea unit is assumed to remain fully submerged at all times. This assumption bypasses the initial phase of the launch retrieval operation whilst the unit is passing through the air/water interface. The effects of slamming are thus ignored, as are the effects of the inertial and drag forces whilst the unit is partly submerged. It is felt that the hydrodynamic forces occurring during this short period will not, in general, lead to a slack wire situation for several reasons. The static hoist wire tension will be greater than for a fully submerged unit, as the buoyancy forces will not have taken full effect. Furthermore, the likelihood of slamming will be small; the water column oscillation will tend to have a minimal high frequency content due to the filtering effect of the moonpool; in addition the water surface in the moonpool will not usually be particularly flat, and the appendages usually present on the underside of subsea units will tend to break up the water before it hits

the bottom of the unit proper. The forces on the unit as it passes through the interface are highly non-linear and the appropriate values for the hydrodynamic coefficients extremely hard to determine. Finally, the hydrodynamic properties of the moonpool - in particular the restoring force - will change dramatically if the subsea unit breaks the free surface inside the moonpool.

Subsea Unit - Water Column Interaction

It is assumed that the effect of the subsea unit upon the water column oscillation can be accounted for with an appropriate choice of moonpool hydrodynamic coefficients. These coefficients are obtained using the procedure described in Appendix 2.1, with the unit submerged inside the moonpool.

Water Column - Subsea Unit Interaction

It is assumed that the velocity and acceleration of the fluid flow around the unit can be calculated from the motions of the free surface of the water column, and that the effects of local acceleration of the flow around the unit due to the blockage can be accounted for by an appropriate choice of inertial and drag coefficients. These coefficients are obtained using an experimental procedure described in Appendix 3.1.

3.3 SOLUTION IN THE TIME DOMAIN

The time domain solution involves the generation of water column oscillation realisations from the water column oscillation response spectrum, which may be used to calculate fluid velocity and acceleration realisations. These may then be used to effect a solution of Morison's equation on a step by step basis, to produce a force realisation. The force spectrum may be obtained using a Fourier transform of this

realisation; alternatively, the force statistics such as the significant force on the subsea unit may be obtained directly from the realisation, whilst a statistical distribution may be fitted directly to the values of the peak to peak forces obtained such that force exceedances may be estimated.

Generation of Water Surface Elevation Realisation

The method chosen for the generation of the random water column oscillation realisation is based on the methods suggested by Cuong et al [loc.cit] and Tucker et al [loc.cit]. This method was chosen because it was found that the power spectrum reconstructed from the realisation was much closer to the target spectrum than for other methods tested. This is illustrated in Figure 3.2a and 3.2b. These figures show power spectra reconstructed from water surface elevation time histories generated firstly by the method chosen (Figure 3.2a) and secondly, for comparison, the linear prediction method (Figure 3.2b). The target spectrum in each case was Pierson Moskwitz in form with significant wave height of 4.0m and mean zero crossing period of 7.0s. Both spectra were found by averaging three individual spectra each obtained from time histories of equal length (8192 points). The same computer routines were used in each case to calculate the autocovariance function and hence the power spectrum. Smoothing of both spectra was carried out using a Tukey lag window on the autocovariance function. For the time histories used to generate Figure 3.2a the frequency range 0 -> 0.5Hz was represented by 2048 points, and the series was padded with 6144 zeros. The inverse fourier transform from the frequency to time domain was carried out using a standard fast fourier transform subroutine. Figure 3.2b shows the power spectrum obtained from time histories generated using the linear prediction method, with a filter order of 40. It can be seen that the method adopted produces a significantly better fit to the target spectrum. A full description of the method is given in Appendix 3.2.

The resulting time series of water surface elevation is then used to calculate the fluid velocity and acceleration past the subsea unit using the difference equations:

$$\dot{z}_i = (z_{i+1} - z_i)/\Delta t$$
$$\ddot{z}_i = (z_{i+1} - 2z_i + z_{i-1})/\Delta t^2 \qquad (3.1)$$

The velocity and acceleration time series could, in fact, be calculated separately by obtaining the velocity and acceleration power spectra and then using the technique described twice with the same series of random numbers. The oscillation amplitudes implicit at each frequency would thus be the same, and an appropriate adjustment could be made to the phase at each frequency. This approach could be employed if it was felt that any error was introduced at the high frequency end of the spectrum by the differencing technique described above; however in the cases studied here the zero padding led to a time increment small enough that all relevant frequencies were present in the realisation; the difference equations were therefore used on the grounds of computational efficiency.

Calculation of Hydrodynamic Force Realisation

Having obtained the fluid velocity and acceleration at each time step, the random hydrodynamic force realisation for the unit is calculated using Morison's equation:

$$F_i^{RH} = \rho V_b (1+C_m)\ddot{z}_{m_i} + \tfrac{1}{2}\rho A_b C_d \dot{z}_{m_i}|\dot{z}_{m_i}| \qquad (3.2)$$

where V_b is the displaced volume of the unit
A_b is the projected area of the unit
C_m is the inertial coefficient of the unit
C_d is the drag coefficient of the unit

The inertial coefficient is defined here as being the ratio of the added mass of the unit to its displacement.

The selection of appropriate values for the force coefficients (inertial and drag) and the experimental technique used to obtain these values is discussed in Appendix 3.1. Time histories generated in this manner can be used to calculate the hydrodynamic force power spectrum; however, there seems little point in such a calculation as the force random process statistics may be obtained by fitting statistical distributions directly to the force realisation data.

A slack wire situation will occur if the upwards hydrodynamic force is greater than the net force downwards; ie if:

$$F_i^{RH} > m_b g - \rho g V_b + \tfrac{1}{2} \rho A_b C_d v |v| \qquad (3.3)$$

where v is the velocity of the subsea unit. The first term on the right hand side is the weight of the unit; the second term is the buoyancy of the unit, and the final term is the steady hydrodynamic force due to the velocity v.

A time domain solution thus retains the non-linearity inherent in Morison's equation; however, in order that the statistics of the force realisation adequately represent the statistics of the force random process, it is necessary that enough data is calculated. If the statistics are to be obtained directly from the realisation, it is not important whether the volume of data is increased by increasing the length of the realisations or by increasing the number of realisations; however, if it is required to calculate a force power spectrum, then a better spectral estimate will result if the data is segmented by restricting the length of the realisations, and calculating more of them (see, for example, Schwartz and Shaw [1975]). A check on the quantity of data used can be carried out by calculating the force statistics for a given data set, then increasing the size of the data set and recalculating. If the statistics do not change significantly with the increase in size of the data set, then

the set can be assumed to be representative of the process as a whole.

3.4 THE FREQUENCY DOMAIN APPROACH

The method used to solve the problem in the frequency domain is that suggested by Borgman [loc.cit.]. The method is derived by the use of Morison's equation in the calculation of an analytic force covariance function. This function is approximated as a series expansion, and linearised by calculation of only the first term of the series. A linearised force spectral density may thus be obtained by applying a Fourier transform to the linearised covariance function, resulting in the expression for the force spectral density:

$$S_{FF}(\omega) = \left[\rho V_b (1+C_m)\right]^2 S_{AA}(\omega) + \left[\tfrac{1}{2}\rho A_b C_d\right]^2 \frac{8 m_{0_v}}{\pi} S_{vv} \qquad (3.4)$$

where

S_{FF} is the force spectral density

S_{AA} is the water column acceleration spectral density

S_{vv} is the water column velocity spectral density

m_{0_v} is the zeroth moment of the water column velocity spectrum:

$$m_{0_v} = \int_0^\infty S_{vv}(\omega)\, d\omega$$

Since the water column oscillation is assumed to be simple harmonic, the water column acceleration and velocity spectra may be obtained in terms of the water column elevation spectrum as:

$$S_{vv}(\omega) = \omega^2 S_{EE}(\omega)$$

$$S_{AA}(\omega) = \omega^4 S_{EE}(\omega) \qquad (3.5)$$

leading to an expression for the force spectral density in terms of the water column oscillation spectral density:

$$S_{FF}(\omega) = \rho^2\omega^2\left[V_b^2(1+C_m)^2\omega^2 + 2A_b^2C_d^2M_{0_v}/\pi\right]S_{\zeta\zeta}(\omega) \quad (3.6)$$

As with the time domain model, the experimental technique used to obtain appropriate values for the inertial and drag coefficients used is discussed in Appendix 3.1. The force spectrum thus obtained may be used to calculate the statistics of the force random process.

3.5 EXPERIMENTAL VERIFICATION

In order to examine the accuracy of the two methods adopted, a series of experimental studies was carried out, with the aim of demonstrating that both the water column oscillation spectra obtained with the subsea unit in the moonpool and the subsea unit force spectra (and hence the force random process statistics) obtained are accurate enough for the purposes of engineering design.

In order to establish that the response spectra are accurate enough for engineering design purposes, two series of tests must be carried out:

(i) A set of tests to measure the moonpool water column response with a subsea unit present. The results from these tests may be compared with predictions made using the method set out in Chapter 2.

(ii) A set of tests to measure the force on the subsea unit in the moonpool

In all cases the moonpools were mounted in a ship model; due to the complexity of the equipment used to measure the force on the subsea unit, the ship model was restrained in the tank such that all modes of motion were restrained. Three

moonpools were used for the tests with a single subsea unit; the time required to construct the relatively complex shapes of realistic units precluded the construction of more than one model. In all cases the subsea unit was placed at the moonpool exit, such that the bottom of the unit was flush with the bottom of the ship.

The first series of tests involved obtaining the hydrodynamic coefficients for the moonpools with the subsea units using the procedure set out in Appendix 2.1. The three random realisations used previously (see section 2.5) were run in the tank, and the water surface elevation measured both inside the moonpool and external to the ship. In each case the wave spectra and the water column oscillation response spectra were calculated numerically. As in section 2.5 the wave spectra obtained were then used as the input for the theoretical calculation procedure (with the moonpool hydrodynamic coefficients), and the water column oscillation spectra thus predicted were compared to those measured.

The second series of tests required the inertial and drag coefficients for the subsea unit in each of the moonpools; these were obtained using the procedure set out in Appendix 3.1. The three random realisations were then rerun; the water surface elevation inside the moonpool and the force on the subsea unit were measured. The water column oscillation spectrum and the force spectrum were then calculated numerically; the water column oscillation spectrum was then used as the input for the two methods set out in sections 3.3 and 3.4. The force spectra thus predicted were then compared with those measured.

The moonpools used are shown in Figure 3.3; moonpools 1 and 3 were chosen as identical to moonpools 1 and 3 of chapter 2 in order that comparisons could be made between the water column oscillation with and without the subsea unit. The ship model with moonpool mounted is shown in Figures 3.4 - 3.5.

3.6 RESULTS AND DISCUSSION

Since two distinct sets of tests were carried out, the presentation and discussion of the results is carried out in separate sections.

3.6.1 RESULTS AND DISCUSSIONS: WATER COLUMN OSCILLATION

Moonpool Hydrodynamic Coefficients

The blockage coefficients and the hydrodynamic coefficients for the three moonpools with the subsea unit are shown in Appendix 3.3. It can be seen that the added masses for the moonpools are relatively high (in comparison with the empty moonpools of chapter 2). This is particularly noticeable for the moonpool 1, which had the highest blockage ratio (0.695), where the added mass rose from 0.27 (see Appendix 2.2) to 1.2 due to the presence of the unit. The added mass for moonpool 3, which had a relatively small blockage ratio (0.283) rose from 0.4 to 0.8. A similar trend can be seen in the damping coefficients, where both the damping ratio intercept and the damping ratio gradients increase significantly between the empty moonpool and the moonpool with the subsea unit. Again the increase is greatest for moonpool 1, with the damping ratio intercept increasing from 0.0113 to 0.0369, and the damping ratio gradient increasing from 0.1846 to 0.8643.

Prediction of Significant Water Column Oscillation

The significant oscillation in the moonpool from the random wave tests is shown in Appendix 3.4 for both measured and predicted values. The agreement is fair, with the worst error being less than 30% and the mean error being less than 11%. The predictions are all high for moonpool 1, but all low for the other two moonpools. Possible reasons for these discrepancies are examined later. It is interesting to note

that the significant water column response in the moonpools is not reduced by as much as might be expected due to the presence of the bell for the larger waveheights; whilst the damping of the system is substatially increased by the presence of the bell, the reduction in the frequency of peak system response due to the increased added mass and damping brings the natural response frequency of the system nearer to the peak energy frequency of the wave spectra, largely cancelling out the benefits gained from the reduction in the maximum magnitude of the moonpool transfer function. The effect of the shifts in peak response frequency will be discussed in more detail in Chapters 4 - 6.

Prediction of Water Column Oscillation Response Spectra

Plots of the measured wave spectrum, the predicted oscillation spectrum and the measured oscillation spectrum are shown in Figures 3.6 - 3.14. In each case the solid line represents the wave spectrum, the dashed line represents the predicted water column oscillation spectrum and the triangles represent the measured water column oscillation spectrum. As in the results presented in Chapter 2, the wave spectra are not very smooth, with multiple peaks exhibited in all cases. The reasons for these peaks are discussed in section 2.6. In all cases, the shape of the predicted oscillation spectrum is similar to that measured.

Sources of Experimental Error

There are several possible sources of error with the experimental equipment and procedures used. Many of these are exactly as discussed in section 2.6; however it is worth pointing out that the problems due to cross waves was exacerbated in these tests by the fact that the ship could not be placed centrally between the tank walls due to the force measurement rig. As a result, the cross waves occurred at several frequencies, with peaks being noticeable in the

wave spectra at about 1.1Hz, 1.35 Hz, and 1.65Hz. A further effect of this asymmetry was that the amplitude of the cross waves was different from one side of the ship to the other, being noticeably greater on the side of the ship closer to the tank wall. Since the wave elevation was measured on the other side of the ship, the wave spectra obtained may well be unrepresentatively small.

An additional problem found with these tests was that the resistance wave probes used to measure the water surface elevation proved to be sensitive to the proximity of solid objects; this became particularly noticeable for the cases where the blockage was high (moonpools 1 and 2), as the probe had to be placed in a very confined space between the bell and the moonpool wall. The sensitivity of the probes to this small space meant that calibration could be carried out less accurately than in open water, and that the output was not as linear as would be desired.

Finally, it was observed that the free surface inside the moonpool was far from being flat due to the presence of the bell in the centre of the moonpool. Since the wave probes had to be positioned near the walls of the moonpool (rather than in the centre as in the tests described in Chapter 2), it is likely that the measured oscillation in the moonpool was greater than the mean oscillation across the whole free surface.

These three effects may help to explain the underprediction of the significant oscillation in these tests as compared to the tests described in Chapter 2. It is possible that an error of calibration was made in the case of the test of moonpool 1 with realisation 1; even considering all the possible sources of experimental error, the result for this test is worse by a factor of two than all the other tests. If this result were neglected, the mean error would fall to less than 9%.

Sources of Error in Mathematical Model

In addition to the errors due to experimental equipment, it is likely that some of the error is caused by the inability of the mathematical model to cope with the highly complex dynamic system of the moonpool with the subsea unit present, for a variety of reasons.

Firstly, the modelling of the damping ratio as being the sum of a constant and a term proportional to the oscillation amplitude may not be sufficient when the blockage ratio is high; it would be interesting to try a quadratic model to see if any advantage were gained. Secondly, the modelling of the system as a simple mechanical oscillator breaks down when the bell breaks the free surface, as the restoration force on the water column then becomes dependent upon the area of the free surface, which will vary through the oscillation cycle.

In addition, the water surface in the moonpool can no longer be reasonably assumed to be flat; this will cause additional variation in the restoration, as well as affecting the measured surface elevation. Since the draft of the ship in all the tests was 20cm, and the length of the subsea unit was 17cm, any oscillation of height greater than 6cm would start to uncover the unit. This affected both the single frequency tests used to determine the moonpool added mass (see Appendix 2.1) and the random wave tests. The significant water column oscillation was greater than 6cm in three out of the nine tests, implying that the unit was breaking the free surface for a substantial proportion of the time in these tests. The error caused by this phenomenon will be dependant on the blockage ratio, as the restoration of the system and the slope of the free surface will vary more at higher blockage. It is not surprising then to see that, of these three cases, the worst error is found for moonpool 1, which has the highest blockage ratio.

Summary

In summary then, the results suggest that, whilst the mathematical model as presented is less successful for the case of a moonpool with a subsea unit than for an empty moonpool, the significant oscillations and response spectra predicted are accurate enough for the purposes of engineering design. It is possible that the accuracy of the hydrodynamic coefficients could be improved both by running the single frequency tests for the added mass at a smaller wave height and using a more sophisticated model to represent the non-linearity of the damping.

3.6.2 RESULTS AND DISCUSSIONS: FORCE ON THE SUBSEA UNIT

Force Coefficients for Subsea Unit

The results obtained for the force coefficients for the bell in each of the three moonpools, together with the Reynolds numbers and Keulegan Carpenter numbers for which these values were achieved are shown in Appendix 3.5. In each case three tests were carried out, at different frequencies, and the largest values taken. It can be seen that the inertial coefficient falls with the blockage ratio, whilst the drag coefficient falls then rises as the blockage ratio falls. The first effect is as would be expected; the second effect is probably related to the Reynolds number and Keulegan Carpenter Numbers attained rather than the blockage ratio. It should be pointed out that the Reynolds number given is calculated on the basis of the nominal flow velocity rather than the actual flow velocity; the effect of this assumption is discussed in Appendix 3.1.

Prediction of Significant Force on Subsea Unit

The significant forces on the bell, both measured and predicted, and the errors in both the prediction methods adopted are given in Appendix 3.6. It can be seen that the agreement is on the whole very good for both approaches, with the worst error being less than 15%, and the average errors being just under 6% for the frequency domain approach, and just under 5.5% for the time domain approach. As with the previous random wave results, the errors are worst for the smallest realisation, though the results for Moonpool 3 in the large realisation are also less good. Reasons for these discrepancies are examined later.

Prediction of Force Response Spectra

Plots of the measured and predicted force spectra are shown in Figures 3.15 - 3.23. In each case the solid line represents the force spectra predicted by the frequency domain method, the dashed line the force spectra predicted by the time domain method, and the triangles represent the measured force spectra. In all but one case, the shape of the predicted force spectra are similar to those measured.

Sources of Experimental Error

There are several sources of error with the experimental equipment and procedures used. All the reservations about the measurement of the water column oscillation in the moonpool mentioned in the previous section apply again. In addition, the uncovering of the bell in the larger oscillations will cause the force on the bell to be reduced, in addition to altering the dynamics of the ship/moonpool system. This probably explains the over prediction of the force for moonpool 3 in realisation 3 (Figure 3.23).

Sources of Error in Mathematical Model

Both prediction methods show a tendency to over predict the size of the high frequency components of the force; this tendency has been partly alleviated by the imposition of a 'cut-off' at 1.5Hz. This was felt to be sufficiently far enough above the dominant frequencies of the water column oscillation that all data above the cut-off frequency could be regarded as spurious. Even with this approach, however, a certain amount of over prediction is shown, particularly in the case of moonpool 1 and realisation 1 (Figure 3.15). In general the time domain approach does show a slightly better fit to the experimental data than the frequency domain approach, though at a significant extra cost in computing time.

Application of Procedure to Full Scale Prediction

It must be stressed that the experiments were in no way intended to provide an accurate representation of any real system; the sole aim was the verification of the mathematical models presented. The good agreement obtained was certainly due in part to the fact that the tests used to find the force coefficients for the bell in the moonpool and the random wave tests were carried out at the same scale. The method used to obtain the force coefficients would not be directly suitable for the case where a prediction of full scale forces was required; an alternative technique is suggested in Appendix 3.1. A further effect of the small scale of the random wave tests is to increase the dependance of the force coefficients on the Reynolds number, whilst reducing the dependance on the Keulegan Carpenter number. In practice, it is felt that the choice between the two methods will be strongly influenced by their ability to deal with the variation of the force coefficients with Keulegan Carpenter number; however this problem is outside the scope of this study.

Summary

In summary, it has been shown that both the frequency domain and the time domain models proposed may be used to predict the forces on a subsea unit in a moonpool to a level of accuracy appropriate to engineering design. Some modifications to both the experimental procedures adopted will, however, be necessary in order for the method to be used with confidence, and further extensions to the mathematical model to deal with the variation of the force coefficients with frequency may be desirable.

Mathematical models have thus been proposed with which the response of the moonpool to environmental forces - in terms of both the water column oscillation and the force on a subsea unit inside the moonpool - may be calculated with a sufficient degree of confidence. However the analysis of the response is only one part of the design process as a whole. Before a systematic design process may be adopted it is necessary for the designer to understand the relationship between the performance of the system and the system parameters. In the case of the moonpool, the area of particular interest is the variation of the moonpool response with the moonpool geometry. A study of these variations is presented in the following chapters.

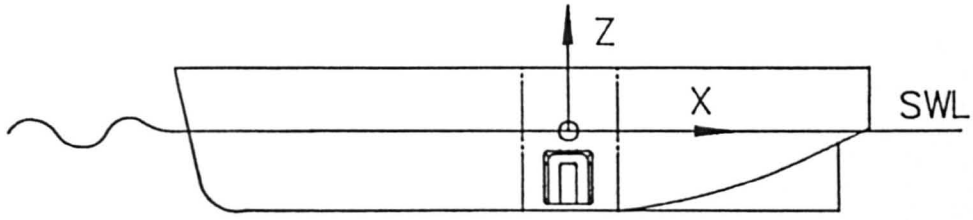

Figure 3.1

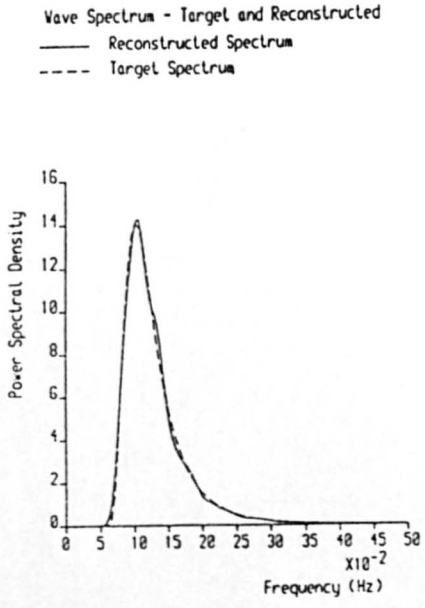

Figure 3.2a

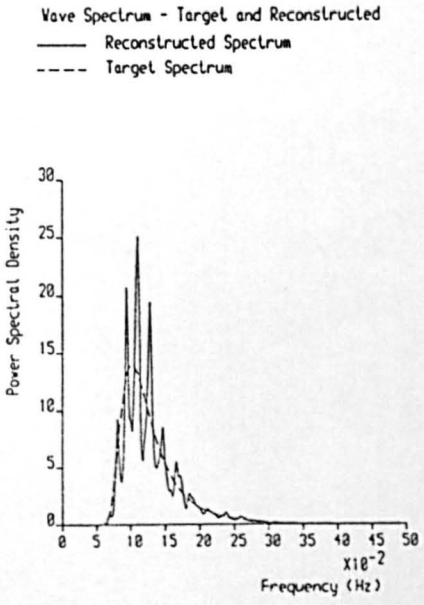

Figure 3.2b

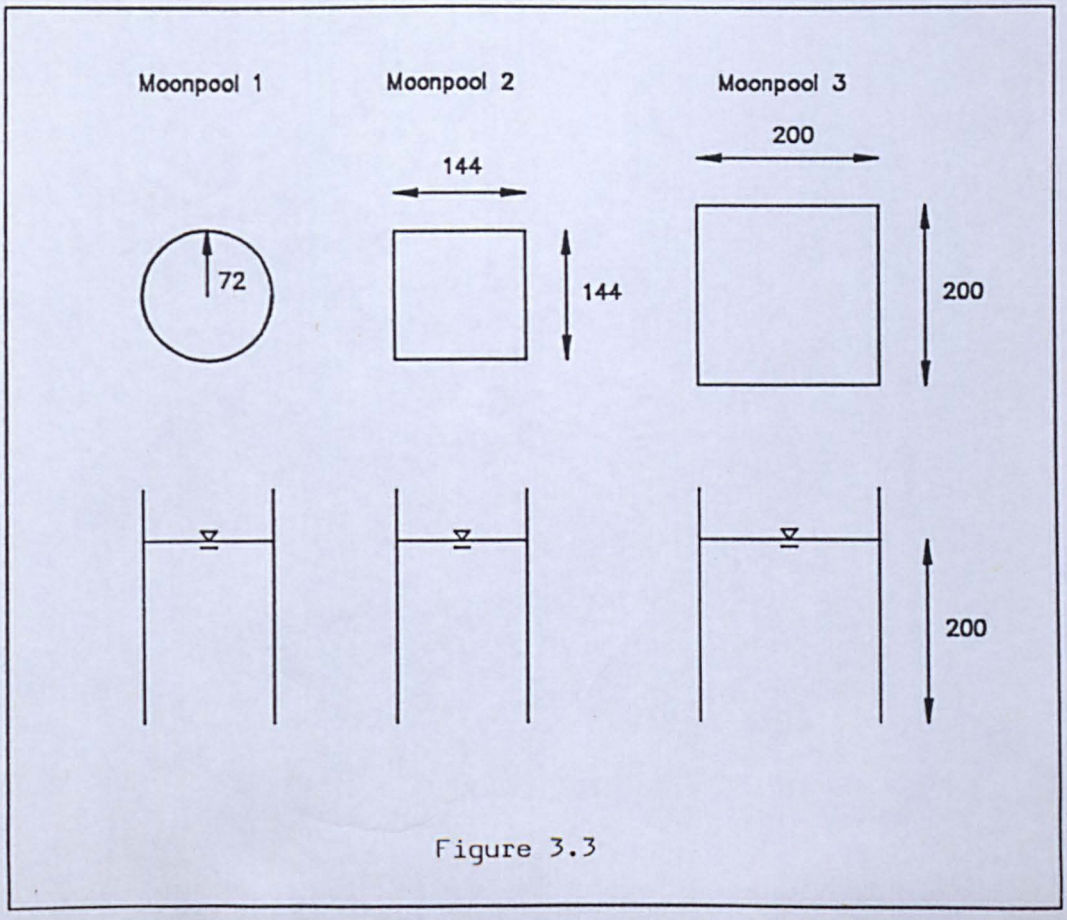

Figure 3.3

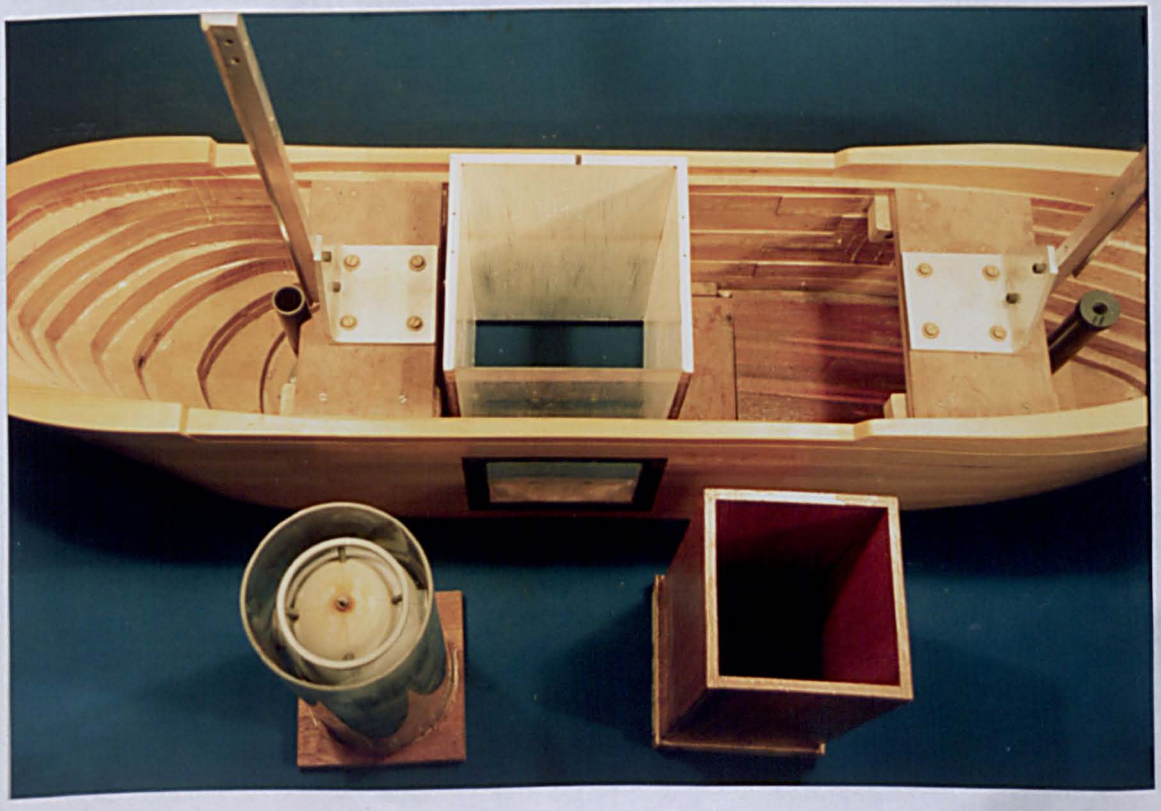

Figure 3.4

Figure 3.5a

Figure 3.5b

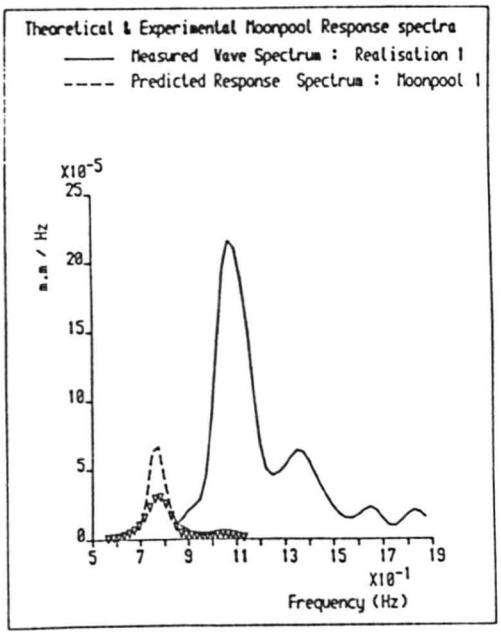

Figure 3.6

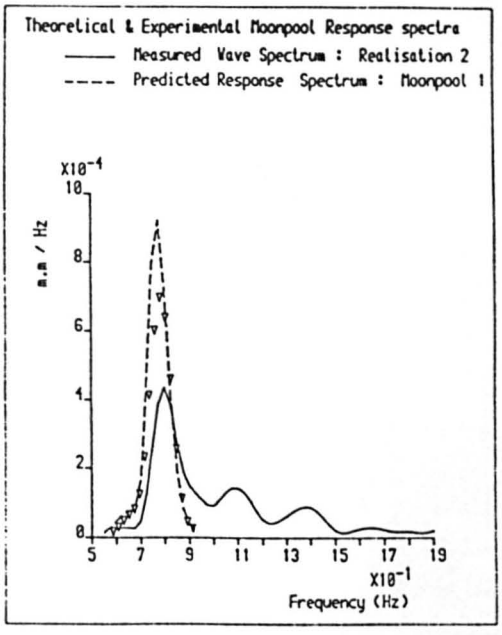

Figure 3.7

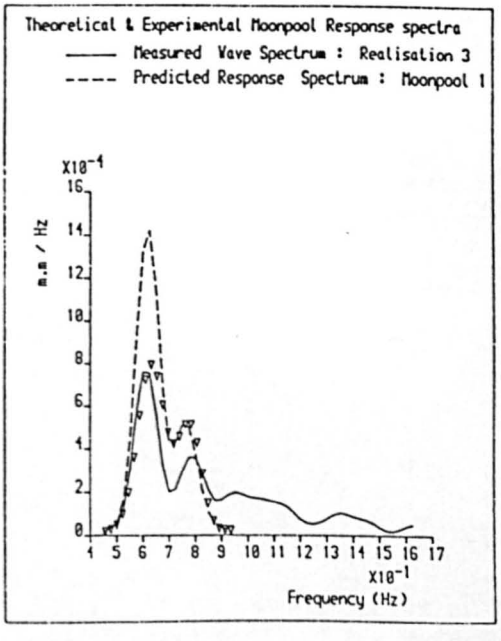

Figure 3.8

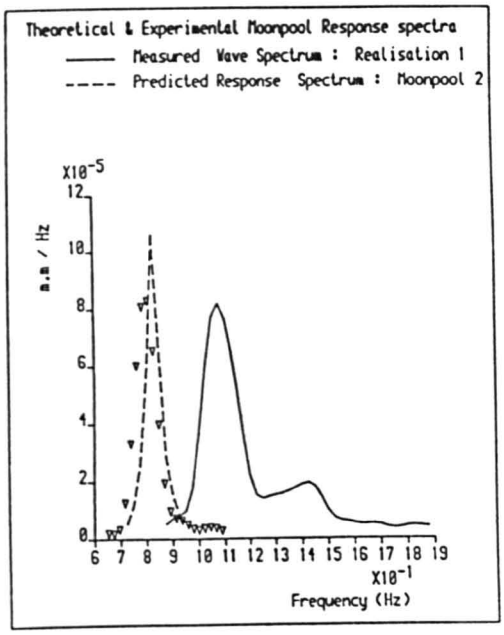

Figure 3.9

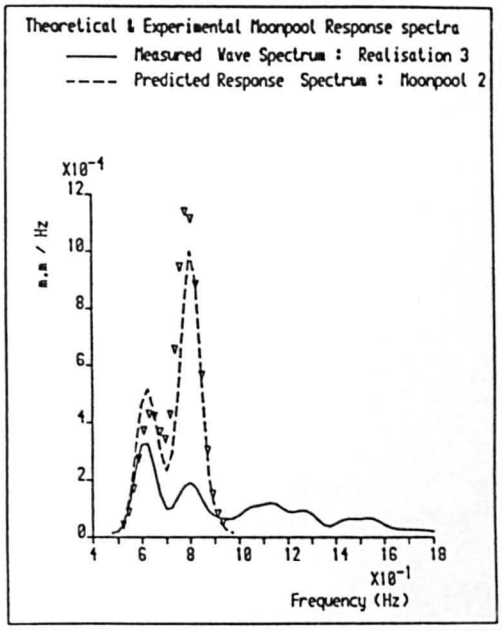

Figure 3.10

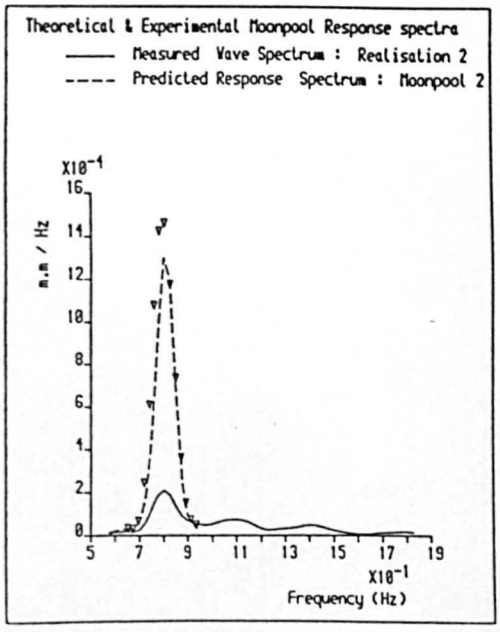

Figure 3.11

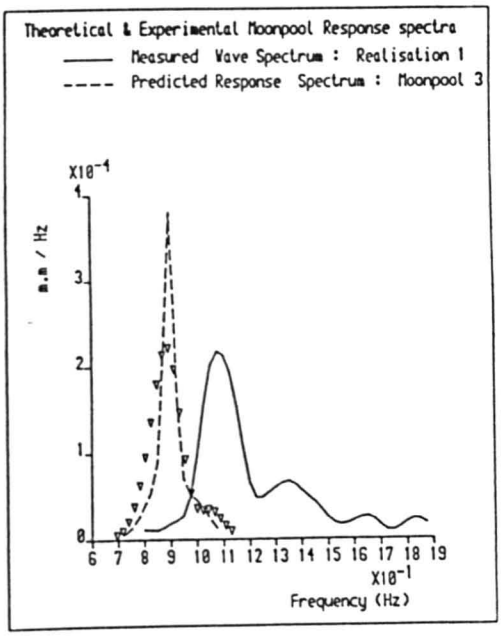

Figure 3.12

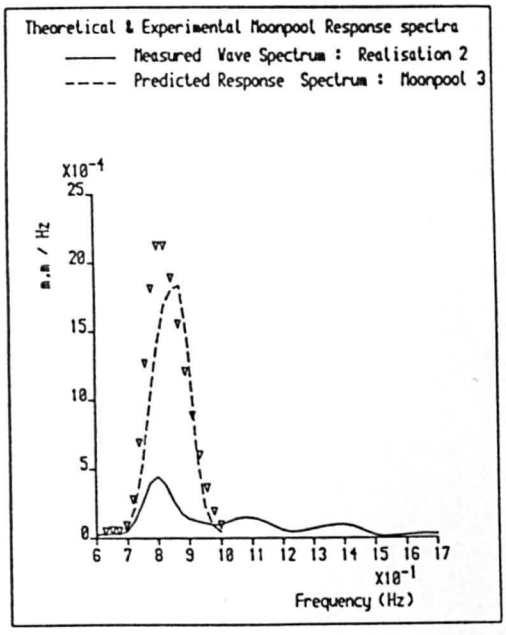

Figure 3.13

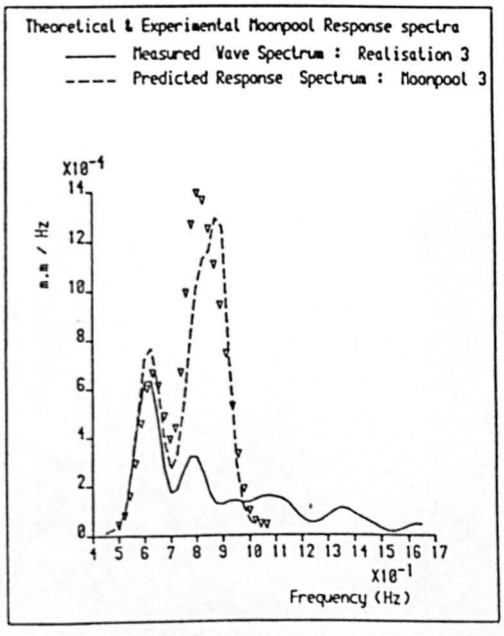

Figure 3.14

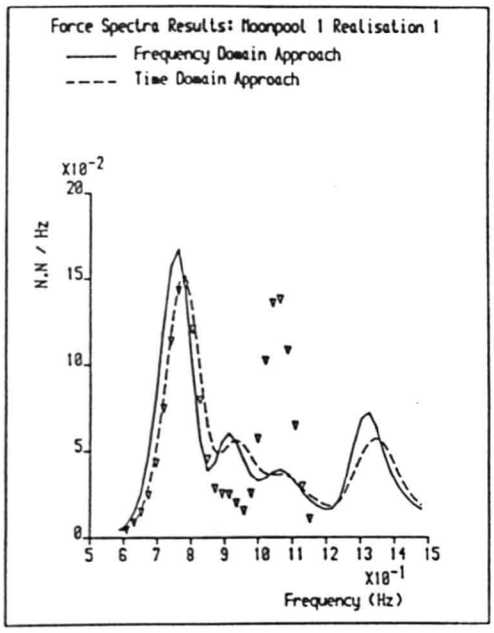

Figure 3.15

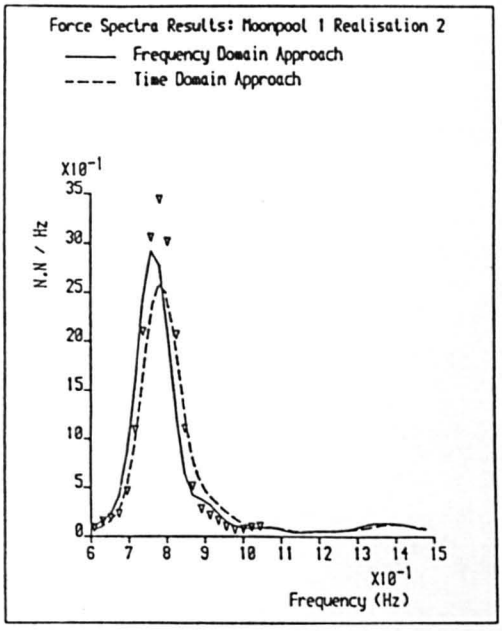

Figure 3.16

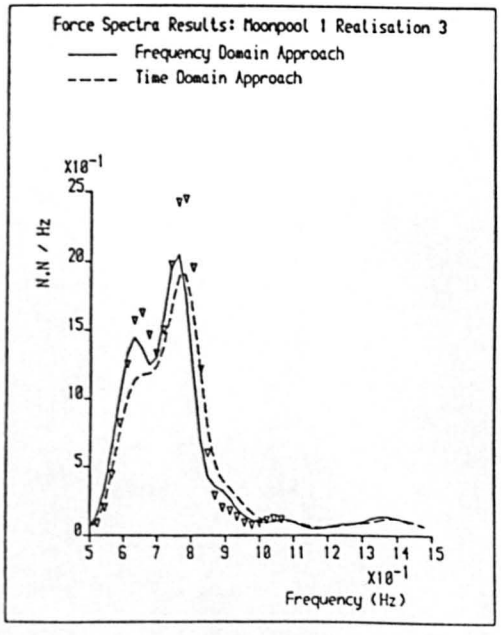

Figure 3.17

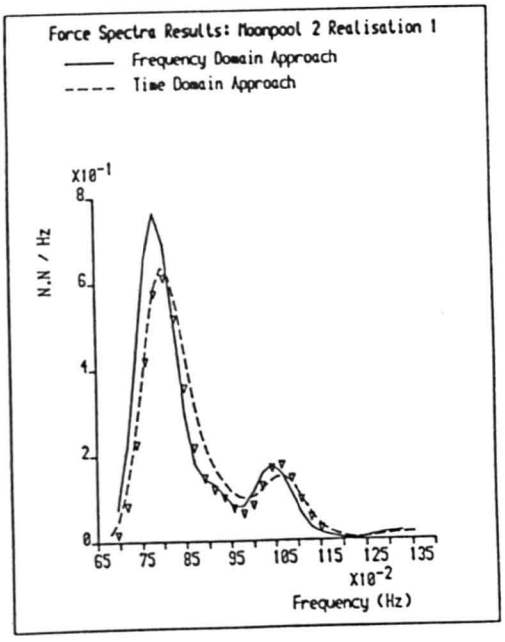

Figure 3.18

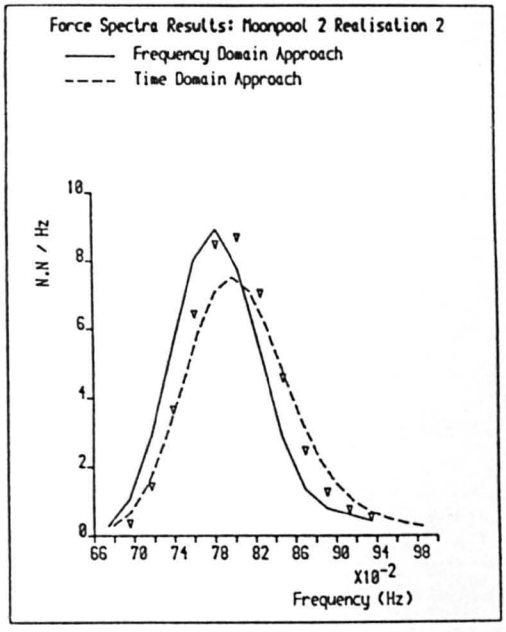

Figure 3.19

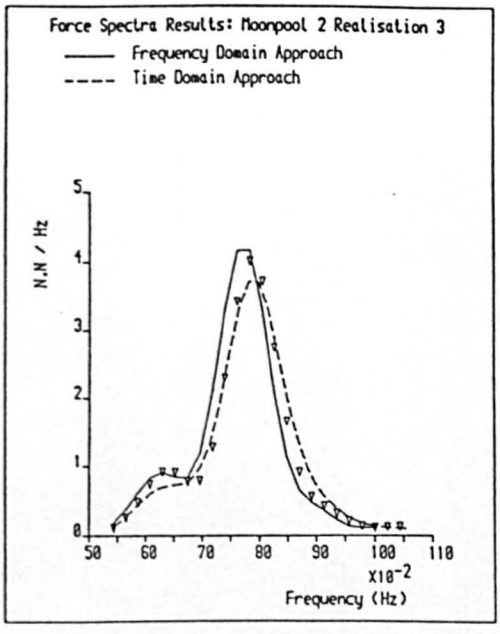

Figure 3.20

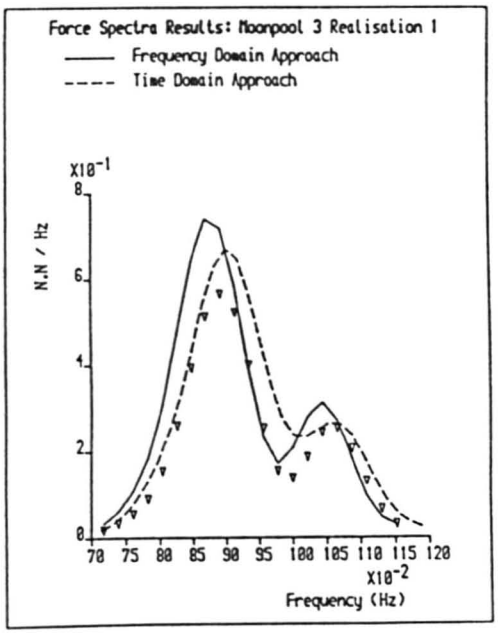

Figure 3.21

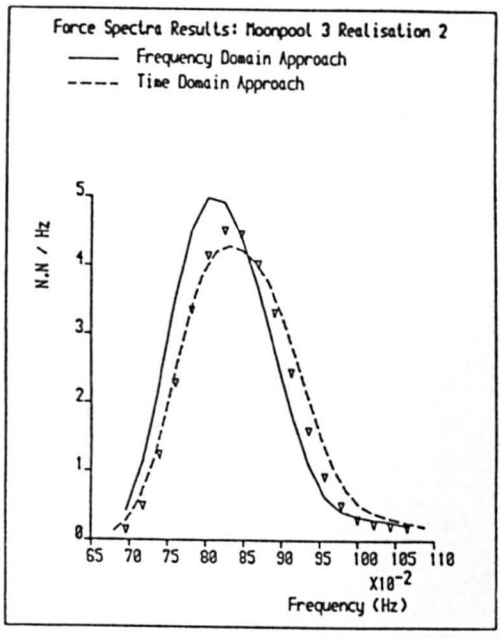

Figure 3.22

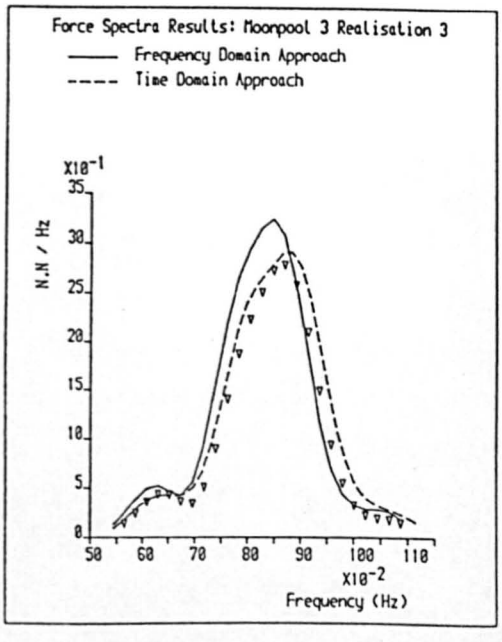

Figure 3.23

4. A POTENTIAL FLOW MODEL OF THE SHIP/MOONPOOL SYSTEM

4.1 INTRODUCTION

The Prerequisites for a Moonpool Design Procedure

The work outlined in the previous chapters presents an approach whereby the response spectra for both the water column oscillation and the hydrodynamic forces on a subsea unit may be calculated. The approach is not, however, entirely based on calculation, either analytical or numerical, and involves the measurement of certain hydrodynamic coefficients using laboratory tests. This level of understanding of the ship/moonpool/subsea unit system is sufficient to allow the development of a design assessment procedure; however it is not sufficient to allow the development of a systematic design procedure. In order to develop such a procedure for the design of moonpools it is also necessary to have an understanding of the problems which the designer is trying to surmount, a strategy which may be used to surmount these problems, and a means of implementing the strategy.

The moonpools considered up to now have been 'smooth'; that is to say they have a constant cross sectional area from from the waterplane to the exit. The response amplitude operators (RAOs) of such moonpools resemble those of a lightly damped mechanical oscillator, with a large response at the natural frequency falling away to zero at higher frequencies and tending towards unity at lower frequencies. If the peak of the RAO of the water column oscillation falls close to the peak energy of the wave spectrum, then the water column response spectrum will exhibit a large peak value, and the significant oscillation will tend to be large. This is illustrated in Figure 4.1a. In practical terms, such a moonpool will incur large amounts of downtime, and the vessel on which it is installed will now be as cost effective as it

could. The problem facing the moonpool designer is thus to reduce the response of the moonpool such that the downtime incurred is reduced. The quantification of this downtime is discussed in detail in Chapter 7.

Moonpool Design Strategies

There are two basic strategies which might be used to approach the design problem as stated. Firstly the designer may try to modify the moonpool such that the magnitude of the peak response of the water column oscillation RAO is reduced; this approach is illustrated in Figure 4.1b. Alternatively the designer may attempt to modify the moonpool such that the frequency at which the peak occurs is shifted away from the predominant frequencies of the waves. In terms of the mechanical oscillator analogy, the first approach requires that the system damping be increased, whilst the second approach requires that the system added mass be changed. In practice, of course, an increase in the system damping will tend to lead to a reduction in the natural frequency, and any change in the moonpool geometry which will affect the added mass will also affect the system damping; however the broad distinction remains.

The first strategy is suited to the case where an existing moonpool is to be improved; in such a case, any alterations to the moonpool geometry will be necessarily minor since it is unlikely that much space will be available around the moonpool in order to make significant changes to the geometry. Horizontal stiffeners or baffles may be added to the moonpool interior in order to increase the viscous damping of the system due to eddy shedding. When the problem can be tackled from the design stage, this method appears crude, taking account neither of the geometrical requirements of the moonpool (ie working cross section area and draft) nor of the operational areas of the vessel. The second strategy, on the other hand, does take account of these factors, in

that the geometry of the moonpool will influence its natural frequency, whilst the predominant frequency of the waves will be governed by the operational area of the vessel. If the designer can modify the moonpool such that the natural frequency of the system is shifted away from the predominant wave frequencies, then the moonpool performance will be improved.

In order to implement this strategy the designer needs to have an understanding of the way in which changes in the moonpool geometry affect the characteristics of the moonpool (in terms of both the water column oscillation and, by inference, the forces on a subsea unit in the moonpool). In particular the relationship between the moonpool geometry and the added mass of the water column must be understood. It is therefore necessary to construct a model with which the relationship between basic geometric parameters in a variety of moonpool configurations and the natural frequency of the water column oscillation may be established. The process by which the form of this model was decided is described in the following section.

4.2 SELECTION OF APPROACH

In order to gain an understanding of the way in which changes in the moonpool geometry affect the natural frequency of the moonpool, it is necessary to carry out a study relating the natural frequency to basic geometric parameters. In order to carry out such a study, a model of the ship/moonpool system is required. Such a model may take several forms; for example the model may be physical, numerical or analytical; or it may comprise elements of each form. The model set out in Chapter 2 has elements of all of these forms - the measurement of the hydrodynamic coefficients uses a physical model, the calculation of the pressure on the base of the moonpool uses a numerical model, whilst the calculation of

the water column oscillation uses an analytical model.

In this case, the model chosen must indicate the relationship between the natural frequency and the basic geometrical parameters of the moonpool. A further requirement is that a wide range of values of these parameters must be studied. This requirement rules out any element of experimental study, at least at the initial stages, since the time taken to build models would be prohibitive for a large study. The approach set out in Chapter 2 is thus of no use for this initial study. The problem could be solved using a numerical method; for example a time domain numerical solution of the Navier-Stokes equations for the moonpool using one of the algorithms currently available could be used to obtain water column oscillation time histories from which the moonpool natural frequency could be deduced. The drawbacks of such an approach are, however, similar to those of the experimental approach, since the methods available are time consuming to program and require large amounts of computer storage and CPU time to run. The use of purely physical or numerical models is thus ruled out.

In contrast, an analytic solution to the problem, once derived, could be solved quickly and relatively easily for each variation in parameters. The use of an analytical model does, however, impose some restrictions upon the solution.

Since it is not possible to produce an analytical solution of the full Navier-Stokes equations for realistic geometries, the effects of viscosity must be neglected. This has the effect that the damping of the model will be unrealistically low, since the only non-viscous damping present in the ship/moonpool situation is that caused by the radiation of waves from the moonpool. As a result, any transfer functions calculated using such an approach will have very large magnitudes. Furthermore, an analytic potential flow solution of the moonpool problem will require the use of conformal

mapping techniques; and as such, will be restricted to two dimensions. These problems are not, however, prohibitive; if qualitative trends can be established for various configurations using the analytic model subject to these restrictions, then the most promising configurations may be studied experimentally to examine the effects of viscosity and the actual 3D geometry.

It was thus decided that a 2D potential flow model would be used to establish qualitative trends for the natural frequency of water column oscillation. A short series of experimental tests would then be carried out in order to confirm the trends and examine the effects of the assumptions made.

If the ship/moonpool system is to be simplified to 2D, then the possible six degrees of freedom of motion are reduced to three: heave, roll and sway. It has been argued earlier (Chapter 2) that since the moonpool will generally be close to the centre of the ship the effects of angular motions will be negligable, and since the water column oscillation is in the vertical plane, excitation in the horizontal plane will have little effect. The effects of sway and roll may therefore be disregarded immediately. The system is thus reduced to a duct between two thick heaving barriers. This simplification is shown in Figure 4.2a-b.

Literature Review

The phenomenon of the interaction of water waves with surface piercing vertical barriers has attracted considerable interest over the years, for a variety of reasons. The reflection and transmission coefficients obtained from studies of this phenomenon have been used to suggest possibilities for floating breakwater development, whilst the oscillation of the water column in the duct between the barriers has been studied as being relevant to the design of

both wave energy devices and moonpools.

Newman [1974] solved the double barrier problem using the assumptions of negligable barrier thickness and a small duct width / barrier draft ratio, using a method similar to Tuck [1974]. Evans [1978] extended the method to deal with the case of a float connected to a spring-dashpot system at the free surface, and also produced a three dimensional solution for a narrow tube. Lee [1982] extended Newman's method to deal with the case of barriers of significant thickness, and showed how the oscillation would be affected by heaving of the barriers. The results showed that the oscillation displays a distinct peak response phenomenon, that the key parameter controlling this response is the ratio of duct width to barrier draft, and that the fixed barriers case offers a good first approximation to the heaving barriers case.

Selected Solution Approach

In order to simplify the problem further then, the heave of the barriers may be neglected, and the ship/moonpool system modelled as a duct between two thick barriers completely space-fixed. This simplification is shown in Figures 4.2b-c.

In order to solve the simplified geometry, the fluid domain is first divided into inner and outer regions. The inner region, comprising the flow within and near to the lower exit of the duct is solved using a conformal mapping technique. The outer region, in which the two barriers are considered as a continuous ship section and the mass flow from the duct is represented by a source singularity, is solved using a source distribution method. The two solutions are then matched asymptotically to allow calculation of the water column response. Only the inner solution, therefore, need be modified in order to accommodate different duct configurations.

4.3. FORMULATION OF THE PROBLEM

A cartesian coordinate system is chosen with its origin in the still water level on the centreline of the duct. The y coordinate is defined as positive vertically downwards. The width of the duct is 2b and the draft of the barriers is a. The coordinate system and the definition of parameters are shown in Figure 4.3.

It is assumed that the water depth is infinite; plane progressive waves of frequency $\omega / 2\pi$ are normally incident from $x = +\infty$ upon the two dimensional space-fixed ship hull. The usual assumptions of linearised irrotational flow are made, and the time-dependent velocity potential is expressed as:

$$\Phi(x,y;t) = \mathrm{Re}\left[\phi(x,y)e^{-i\omega t}\right] \qquad (4.1)$$

The time-independent part $\phi(x,y)$ satisfies the governing equation:

$$\nabla^2\phi = 0 \text{ for } y > 0 \text{ external to the body boundary}$$

and the following boundary conditions:

$$\text{(i)} \quad K\phi + \frac{\partial\phi}{\partial y} = 0 \text{ on } y = 0$$

$$\text{(ii)} \quad \frac{\partial\phi}{\partial n} = 0 \text{ on the body boundary}$$

$$\text{(iii)} \quad \phi \to 0 \text{ as } y \to \infty$$

$$\text{(iv)} \quad \phi(x,y) \sim e^{-Ky}\left(e^{-iKx} + Re^{iKx}\right), \; x \to \infty$$

$$\phi(x,y) \sim Te^{-Ky-iKx}, \; x \to -\infty$$

A solution of this boundary value problem is sought under the further assumptions on the geometry of the problem:

$$\varepsilon = b/a \ll 1 \; ; \; Ka = O[1]$$

These imply that the width of the duct is small relative to the draft of the barriers, a, and the wave-length $\Lambda = 2\pi / K$.

The flow field is now divided into two regions to be considered separately:

(i) the outer region - defined as: (Kx,Ky) = O[1]
(ii) the inner region - defined as: x/b = O[1], 0 < y < a

4.4 SOLUTION OF THE INNER REGION

The inner region is solved using the Schwarz-Christoffel transform, which is particularly suited to dealing with boundaries consisting of straight lines and sharp corners. The method of solution of the transform integral depends on the complexity of the integrand; which depends in turn on the complexity of the geometry. There are two distinct cases to be considered; firstly where a solution of the transform integral is available in closed form, and secondly where the solution of the integral is not available in closed form. Examples of both types of solution will be given here; the full range of solutions obtained is given in Appendices 4.1-4.5.

4.4.1 CLOSED FORM INNER SOLUTION

Two geometries were considered for which the inner region solutions were available in a closed form. The first geometry considered was the smooth duct, as modelled by Lee [1982]. Whilst the method used to obtain the solution differs slightly from that of Lee, the results obtained are largely similar. A complete solution for the smooth duct is given in Appendix 4.1. The simplest modification to the smooth duct geometry is the incorporation of a thin baffle at

the exit. The solution for this geometry is outlined here in order to illustrate the method; a complete solution is given in Appendix 4.2. The two geometries examined are illustrated in Figure 4.4.

The symmetry of the region about x = 0 is used to simplify the required solution region to the right half of the duct, shown in Figure 4.5a. The flow field is transformed onto the upper half plane using the Schwarz-Christoffel transform, with the solid boundaries of the z-plane forming the real axis of the ζ-plane (Figure 4.5b). The transform relation takes the form (see, for example, Lamb [1962]):

$$z = \mathbb{K} \int_0^{\zeta} t\,(t-k)^{-1/2}\,(t-1)^{-1}\,dt + \mathbb{L} \tag{4.1}$$

where $\mathbb{K}$ and $\mathbb{L}$ are complex constants. The expression describes a line integral in the ζ-plane; the path of integration in this case being along the real axis and around the singular points as shown by the dotted line in Figure 4.5b. A complete solution for the flow in the z-plane is obtained by evaluation of the integral in (4.1), and applying the boundary conditions:

$$z = b-p \quad @ \quad \zeta = 0 \tag{4.2}$$

$$z = b \quad @ \quad \zeta = k \tag{4.3}$$

$$Re[z] = 0 \quad @ \quad \zeta > 1 \tag{4.4}$$

The flow in the ζ-plane is represented using a source/sink singularity placed at $\zeta = 1$. The complex potential in the ζ-plane is thus given as:

$$W = k_1 \ln(\zeta - 1) + k_2 \tag{4.5}$$

yielding:

$$\zeta = 1 + e^{\alpha w + \beta} \tag{4.6}$$

A complete solution for the inner region is thus obtained as:

$$z = \frac{-ib(1-k)^{1/2}}{\pi}\left[2\sqrt{1-k} + e^{\alpha w+\beta} + \frac{1}{(1-k)}\ln\frac{\sqrt{1-k+e^{\alpha w+\beta}} - \sqrt{1-k}}{\sqrt{1-k+e^{\alpha w+\beta}} + \sqrt{1-k}}\right] \tag{4.7}$$

subject to the geometrical constraint:

$$p/b = 2\left[\tan^{-1}\frac{k}{\sqrt{1-k}} - \sqrt{k(1-k)}\right]/\pi \tag{4.8}$$

This expression may be used to obtain a plot of the streamlines and potential lines for the inner region. Figure 4.6 shows one such plot for the case where $\varepsilon = 0.1$, and $p/b = 0.5$. The constants α and β must be found before proceeding with the solution. β is found using the asymptotic potential as $\zeta \to 1$ in conjunction with the free surface condition:

$$\beta = \frac{\pi}{b}\left[\frac{1}{k} - a\right] - 2\left[(1-k) - \ln 2\sqrt{1-k}\right] \tag{4.9}$$

α is found by matching the asymtotic expansion of the inner region potential in the overlap domain with the corresponding expansion of the outer solution. This asymptote is found as:

$$\Phi = \frac{2}{\alpha}\ln\frac{r}{2a} + \frac{2}{\alpha}\ln\frac{\pi C_m a}{b} - \frac{\beta}{\alpha} \tag{4.10}$$

where $C_m = (1-k)^{-1/2}$.

The solution is now ready for matching; full details of the procedure outlined here are given in Appendix 4.2.

4.4.2 IMPLICIT INNER SOLUTION

In the two cases mentioned in the previous section the inner solution was found explicitly from the Schwarz-Christoffel transform, and the required asymptotes of the inner region potential were found from this explicit solution. In the case of more complicated modification to the duct exit geometry, the inner solution will, however, not always be available in closed form, and an implicit approach is required. The complexity of the solution is a function of the number of 'corners' in the geometry of the configuration which become mapped onto known points in the transform plane. The smooth duct has two such 'corners', at $z = (b,0)$ and at $z = (0,\infty)$; the boundary conditions relating to these corners allow the solution of the two unknown complex constants K and L (see (4.1)). The introduction of a thin baffle at the exit introduces an extra corner at $z = (b-p,0)$; this is reflected in the geometrical constraint applied to the solution (4.8). In general, for each additional 'corner' introduced to the solution, an additional geometrical constraint will also be introduced; and since the solution will only be available in an implicit form, the constraint will also be in an implicit form.

The simultaneous solution of a series of such constraints is only possible by an iterative technique; this becomes very expensive in terms of computer time if a large number of constraints apply. In practical terms, it is only feasible to attempt solutions which have a limited number of additional 'corners'; the largest number attempted here being three. This restriction forms the first criterion which was used to decide the alternative configurations chosen for solution here.

Two other criteria were also applied to the selection of alternative configurations: that they should have the potential to offer significant shifts in peak response frequency, and that they should be practical from the point of view of design and construction in three dimensions for a real ship. Three configurations satisfying these criteria were ultimately chosen; a baffle internal to the duct (for which the exit baffle previously considered is a limiting case), a flow expansion at the duct exit, and a flow constriction at the duct exit. The geometry and the parameters to be varied for each configuration are shown in Figure 4.7. The solutions obtained for these configurations are detailed in Appendices 4.3-4.5; the solution for the internal baffle is outlined here in order to illustrate the method.

The formulation of the problem is as described in section 4.3. The solution again uses a Schwarz-Christoffel transform to map the degenerate polygon formed by the boundaries of the inner region onto a half-plane. The symmetry of the region about x = 0 is used to simplify the problem to the right half of the region (Figure 4.8a). This region is transformed onto an upper half plane (Figure 4.8b).

The transform is described by the expression:

$$Z = \mathbb{K} \int_0^{\zeta} F(t)\,dt + \mathbb{L} \qquad (4.11)$$

where $F(t) = t^{1/2}(t-k)^{-1/2}(t-\lambda)\,(t-\mu)^{-1/2}(t-1)^{-1}$, and $\mathbb{K}$ and $\mathbb{L}$ are complex constants. This expression describes a line integral along the boundary and around the singular points as shown in the dotted line in Figure 4.8b. In order to find $\mathbb{K}$, $\mathbb{L}$, k, λ and μ and hence solve the problem the following boundary conditions are applied:

$$Z = b \quad @ \quad \zeta = 0 \qquad (4.12)$$

$$Z = b + iq \quad @ \quad \zeta = k \qquad (4.13)$$

$$z = b - p + iq \quad @ \quad \zeta = \lambda \tag{4.14}$$

$$z = b + iq \quad @ \quad \zeta = \mu \tag{4.15}$$

$$Re[z] = 0 \quad @ \quad \zeta > 1 \tag{4.16}$$

The solution of this boundary value problem leads to the complete solution for the inner region:

$$z = \frac{-ib}{\pi C_m} \int_0^{\zeta} F(t)\,dt + b \tag{4.17}$$

subject to the geometrical constraints:

$$p/b = \frac{i}{\pi C_m} \int_k^{\lambda} F(t)\,dt \tag{4.18}$$

$$q/b = \frac{-1}{\pi C_m} \int_0^{k} F(t)\,dt \tag{4.19}$$

and

$$\int_k^{\mu} F(t)\,dt = 0 \tag{4.20}$$

where $C_m = (1-k)^{-1/2}(1-\lambda)\,(1-\mu)^{-1/2}$

The coefficients k, λ and μ are found for a given baffle geometry by means of an iterative solution of Equations (4.18 - 4.20).

As in the case of the closed form inner solution, the flow in the transform plane is modelled using a source/sink singularity placed at $\zeta = 1$. ζ is thus given by equation (4.6); this expression is used as the upper limit of the integral of Equation (4.17). This integral, however, cannot, in general, be evaluated in closed form; thus, in order to obtain the streamlines and potential lines, Equation (4.1.7) must be evaluated numerically. The function F(t) is decomposed into real and imaginary functions before the complex line integral is evaluated. Figure 4.9 shows a typical plot obtained by this method for the internal baffle for $\varepsilon = 0.1$, p/b = 0.5 and q/b = 0.9.

The constants α and β are, however, still unknown. β may be evaluated using the asymptote of this solution near the free surface (i.e as $\zeta \to 1$).

As $\zeta \to 1$ Equation (4.17) may be rewritten in the form:

$$z = \frac{-ib}{\pi}\int_0^{\zeta}(t-1)^{-1}dt - \frac{ib}{\pi C_m}\int_0^{1}(t-1)^{-1}\left[\frac{t^{1/2}(t-\lambda)}{(t-k)^{1/2}(t-\mu)^{1/2}} - C_m\right]dt + O[\zeta-1] + b \qquad (4.21)$$

Denoting the second integral as N, and neglecting the order term the asymptotic potential at the free surface is obtained, and substitution of the free surface condition yields:

$$\beta = \frac{\pi}{b}\left[\frac{1}{K} - a\right] - N/C_m \qquad (4.22)$$

The integral N is evaluated numerically.

In order to evaluate α, the inner and outer solutions must be matched in the overlap domain. The matching is carried out using the asymptotic expansion of (4.17) as $|\zeta| \to \infty$.

As $|\zeta| \to \infty$, Equation (4.17) may be rewritten in the form:

$$z = \frac{-ib}{\pi C_m}\int_0^{\zeta} t^{-1/2}dt - \frac{ib}{\pi C_m}\int_0^{\zeta} F(t) - t^{1/2}\,dt + b \qquad (4.23)$$

The second integral in this expression is bounded as $|\zeta| \to \infty$, and may thus be neglected. The asymptotic potential in the overlap domain is thus given as:

$$\phi = \frac{2}{\alpha}\ln\frac{r}{2a} + \frac{2}{\alpha}\ln\frac{\pi C_m a}{b} - \frac{\beta}{\alpha} \qquad (4.24)$$

and the solution is now ready for matching. This equation can be seen to take the same form as that obtained for the exit baffle (Equation (4.10)). Full details of the solution outlined here are given in Appendix 4.3.

4.5 SOLUTION OF THE OUTER REGION

In the outer region, as $\varepsilon \to 0$, the two barriers are effectively collapsed into one, representing a ship section with a solid boundary. The mass flux in and out of the duct is then represented by a source/sink singularity placed at $y = a$, $x = 0$. This is shown in Figure 4.10a.

The time-independent part of the velocity potential is given as:

$$\phi(x,y) = \Phi_I + \Phi_D + m\Phi_S \quad (4.25)$$

where Φ_I is the potential of the incident wave
Φ_D is the potential of the diffracted wave
m is the outer region source strength
Φ_S is the potential due to the source

The incident wave potential is given in the form:

$$\Phi_I = e^{-ky} e^{-ikx} \quad (4.26)$$

and the three potentials of equation (4.25) (Φ_I, Φ_D, Φ_S) should satisfy the free surface condition and the governing Laplace equation. In addition, Φ_D and Φ_S should also satisfy the radiation condition. The following body boundary conditions also apply:

(i) Diffraction Potential (Φ_D)
The diffraction potential satisfies the body boundary condition

$$\frac{\partial \Phi_D}{\partial n} = -\frac{\partial \Phi_I}{\partial n} \quad (4.27)$$

on the body surface, where n is the normal vector positive outwards from the body.

(ii) Source Potential (ϕ_s)

The potential of a source of unit strength satisfying the free surface condition, the governing Laplace equation and the radiation condition can be expressed in the form (Wehausen and Laitone [1960]):

$$G(x,y;a) = \frac{1}{4\pi}\ln\frac{x^2+(y-a)^2}{x^2+(y+a)^2} - \frac{1}{\pi}\int_0^\infty \frac{e^{-p(y+a)}}{p-K}\cos px\,dp - ie^{K(y+a)} \qquad (4.28)$$

An additional term is required here to take account of the presence of the barriers; the potential ϕ_s must also satisfy the body boundary condition $\partial\phi_s/\partial n = 0$ on the contour S_B shown in Figure 4.10b. Following Lee [1982]:

$$\phi_S = G + \phi_{SD} \qquad (4.29)$$

where G is the Green's function given in Equation (4.28), and ϕ_{SD} is the potential due to the diffraction of the flow from the source around the body obtained from the solution of a boundary value problem.

Finally, in order to enable matching of the inner and outer solutions, the total potential in the region of r = 0 is found as:

$$\begin{aligned}\lim_{r\to 0}\phi(x,y;a) &= \lim_{r\to 0}(\phi_I+\phi_D) + m\lim_{r\to 0}G + m\lim_{r\to 0}\phi_{SD} \\ &= \lim_{r\to 0}(\phi_I+\phi_D) + \frac{m}{2\pi}\ln\frac{r}{2a} + m\lim_{r\to 0}\phi_{SD} - \\ &\quad - \frac{m}{\pi}\int_0^\infty \frac{e^{-2pa}}{p-K}dp - ime^{-2Ka} + O\left[(r/a)^{1/2}\right] \qquad (4.30)\end{aligned}$$

A computer program using Frank's close fit source distribution method ([1967)] was written to solve the boundary value problems for ϕ_D and ϕ_{SD}. The next stage in the procedure is to match the inner limit of the outer solution with the outer limit of the inner solution such that the water column oscillation may be calculated.

4.6 CALCULATION OF WATER COLUMN RESPONSE

In order to complete the solution the inner and outer regions must be matched, to establish a relationship between the singularity strength related terms m (in the outer solution) and α (in the inner solution). In each case the inner region asymptote has the same form (equations (4.10) and (4.24)). The outer region overlap asymptote is given in equation (4.30). Matching the O[ln(r/2a)] terms in (4.30) with (4.10) gives the identity

$$\frac{2}{\alpha} = \frac{m}{2\pi} \tag{4.31}$$

Similarly, matching the O[1] terms:

$$m = \lim_{r\to 0}(\Phi_I + \Phi_D) \Big/ \left[\frac{1}{2\pi}\ln\frac{\pi a C_m}{b} + \frac{1}{\pi}\int_0^\infty \frac{e^{-2pa}}{p-K}dp - \frac{1}{4b}\left[\frac{1}{K}-a\right] + \right.$$
$$\left. + \frac{1}{2\pi}\frac{Re[N]}{C_m} - \lim_{r\to 0}\Phi_{SD} + ie^{-2Ka}\right] \tag{4.32}$$

The external wave amplitude is calculated from the linearised free surface condition for the external wave field:

$$A_I = \frac{K}{\omega}\left|\Phi(x,0)\right|_{x>B/2} \tag{4.33}$$

Assuming that, to this order of approximation, the water surface in the duct is flat, then the amplitude of oscillation of the water column in the duct is given as:

$$A_{WC} = \frac{K}{\omega}\left|\Phi(0,0)\right| \tag{4.34}$$

As the incident wave potential at y = 0 is of unit amplitude, the RAO is thus:

$$H = \left|\Phi(0,0)\right|$$
$$= |m|/4Kb \tag{4.35}$$

and the solution is complete. A computer program was written to evaluate the RAOs given by (4.35) over a range of 1000 frequencies. This was felt to be sufficient to enable the determination of the peak response frequency with a reasonable degree of accuracy.

4.7 NUMERICAL STUDY

4.7.1 NUMERICAL STUDY: SMOOTH DUCT

Scope of Study

An initial study was carried out using the solution for the smooth moonpool in order to alllow a comparison with published results, and to assess the influence of the shape of the barriers themselves.

The barrier shapes used are shown in Figure 4.11; these shapes are identical to those used by Lee. Figure 4.12(a-c) shows the RAOs plotted against the non dimensional wavenumber Ka for a smooth duct with the duct width / barrier draft ratio, ε , varying between 0.05 and 0.20 for each of the barrier shapes examined.

Discussion of Results

The magnitude of the RAOs calculated are in all cases very large. This is to be expected, however, since the mathematical model includes no allowance for the effects of viscous damping; in practice, the viscous damping, in the form of eddy shedding from sharp corners will provide the major part of the system damping. Attention should therefore be concentrated on the frequencies at which the peak response occurs.

It will be seen that the results for the smooth duct are somewhat different from those given by Lee; the difference being far greater than that which would be caused by his incorrect formulation of the expression used to calculate the inner region constant β (see Appendix 4.1). On examination of his computer program used to evaluate the outer solution diffraction term ϕ_D, an error was discovered in the method used to solve the body boundary condition; this was found to be the source of the discrepancy. However, the results show that, whilst the numerical results given by Lee for the RAOs of the smooth duct are incorrect, the conclusions drawn from his study remain valid. The major conclusion was that the key parameter controlling the response of the water column is the duct width / barrier draft, ε .

The geometry of the barriers appears in this case to have little effect on the magnitude of the frequency shift, suggesting that the use of three different barriers is unnecessary, and that appropriate inferences may be drawn from just one barrier shape. Subsequent results served to confirm this observation, and for all other calculations the results are presented only for barrier (b).

4.7.2 NUMERICAL STUDY: MODIFIED DUCTS

Scope of Study

A parametric study of the variation in response with duct exit geometry was carried out for each of the three basic modifications to the smooth configuration by systematically varying the dimensions of the exit geometry, p and q. Since the exit baffle is a limiting case of the internal baffle, the results for both baffle geometries are presented together.

About 1250 combinations of p and q were studied in the cases of the baffle and the flow constriction, and about 2500 in the case of the flow expansion. The difference in the number of cases studied arose because it was felt that a reduction in the duct width of more than 50% would not be considered in practice, whilst an expansion of the duct of 100% might well be considered reasonable. This difference arises because of the location of the extra space required for each configuration over and above the minimum working area. In the case of the flow expansion, the extra space is required at the moonpool exit, and will probably come largely within the double bottom, where space will not, in general be at a premium. In the case of either the baffle or the flow constriction, however, the extra space will be required higher up in the moonpool, and will come within the tween decks, where space will be much tighter. The amount of extra space allowed for the moonpool geometry is thus likely to be less for these configurations. In each case barrier (b) from the previous section (see Figure 4.12) is used; the duct width / barrier draft ratio was kept constant at 0.1.

The RAOs for each configuration were calculated over a range of the non dimensional wavenumber Ka from 0.6 - 1.0; 1000 steps were used. In each case, the wavenumber at peak response (PRWN) was recorded. Typical RAOs are shown in Figure 4.13, in order to demonstrate the scale and direction of the shifts in the peak response wavenumber.

In order to illustrate the effect of these configurations on the response of the system, a comparison was made between the peak response wavenumber for the modified exit geometry duct and the smooth duct. The percentage shift in the peak response wavenumber due to the modification can then be ascertained. Figures 4.14 - 4.19 show the variation in this shift plotted against geometrical variations in the three configurations. The shift is plotted as positive (ie towards higher wavenumbers) in each case; the actual direction of the

shift in each case is indicated by Figure 4.13. The slight irregularities in the plots are due to the discretisation of the wavenumber variation. A discussion of the results presented here is now given.

Discussion of Results

The direction of the frequency shift effected by the baffle is given by Figure 4.13, whilst figures 4.14 and 4.15 show the effect on peak response wavenumber of baffles of varying sizes (p) and in varying positions (q). The general trends observed from these plots are as follows:

(i) The presence of an baffle is shown to reduce the peak response wavenumber of the system. The reduction is, however, small; for the cases examined here the reduction is less than 5%.

(ii) Both the shift and the rate of change of shift increase with baffle size.

(iii) For a given baffle size the reduction does not depend strongly on baffle position; however baffles nearer the duct exit produce the larger shifts in peak response wavenumber.

The direction of the frequency shift effected by the flow expansion is given by Figure 4.13, whilst Figures 4.16 and 4.17 show the effect on peak response wavenumber of flow expansions at the exit of varying width (p) and height (q). The general trends observed are:

(i) The presence of a flow expansion at the exit is shown to increase the peak response wavenumber of the system. The shifts are in general slightly greater than those attainable from the baffle.

(ii) The shift increases with expansion width; however the rate of change of shift decreases.

(iii) The shift is approximately linear with the expansion height. For a given expansion volume, then, a deep narrow expansion effects a greater increase in peak response wavenumber than one which is shallow and wide.

The direction of the frequency shift effected by the flow constriction is given by Figure 4.13, whilst Figures 4.18 and 4.19 show the effect on peak response wavenumber of flow contractions at the exit of varying width (p) and height (q). General trends observed are:

(i) As would be expected from the results for the thin baffles, the presence of a flow contraction at the exit is shown to cause a reduction in the peak response wavenumber of the system. The shift is relatively large compared to the other configurations examined, approaching 15% for the larger constrictions studied.

(ii) For a given height of constriction the shift and the rate of change of shift increase with expansion width.

(iii) For a given contraction width the shift has a minimum value equal to that given by an baffle at the exit, and increases approximately linearly with height. For a given constriction volume, then, a shallow wide constriction effects a larger frequency shift than one which is deep and narrow.

Summary

Considering all the configurations together, it has been shown that the shifts in peak response wavenumber are in general small; though the flow expansion and contraction are undoubtably more effective than the baffle. The results suggest that an attempt to effect a significant shift in peak response wavenumber in a practical two dimensional system

using this approach would require drastic variations in the duct exit geometry. This does not, however, necessarily imply that the shifts effected by the corresponding three dimensional configurations will be as small. In order to investigate the performance of the two more promising configurations (ie the flow expansion and the flow constriction) in the three dimensional case, an experimental study was carried out. This is described in the following chapter.

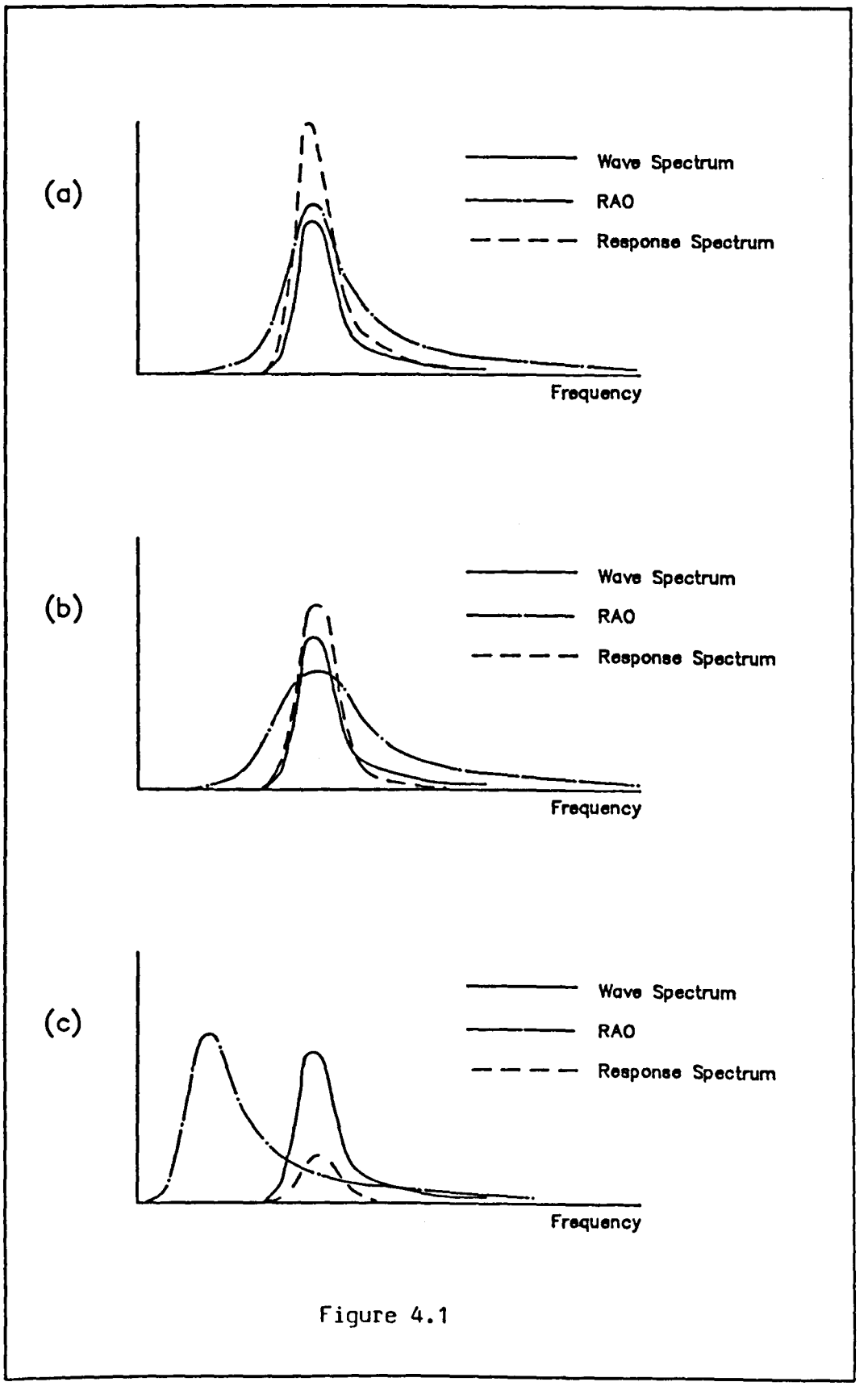
(a)
Wave Spectrum
RAO
Response Spectrum
Frequency
(b)
Wave Spectrum
RAO
Response Spectrum
Frequency
(c)
Wave Spectrum
RAO
Response Spectrum
Frequency

Figure 4.1

(a) 3D Ship/Moonpool System – Beam Seas – 6 DOF motion

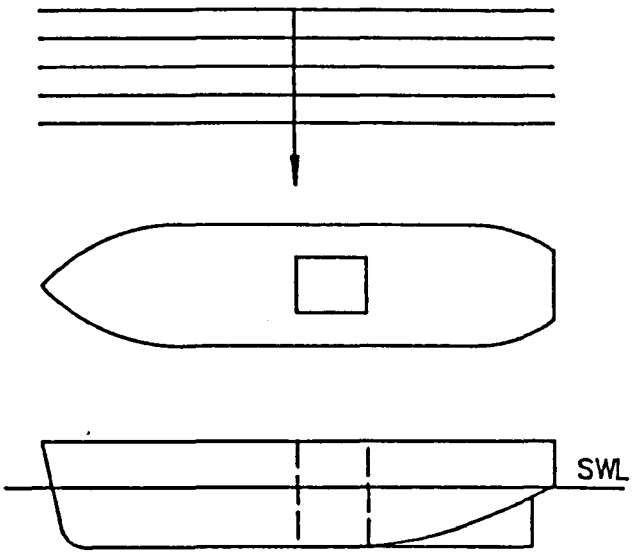

(b) 2D Ship/Moonpool System – Beam Seas – 3 DOF motion

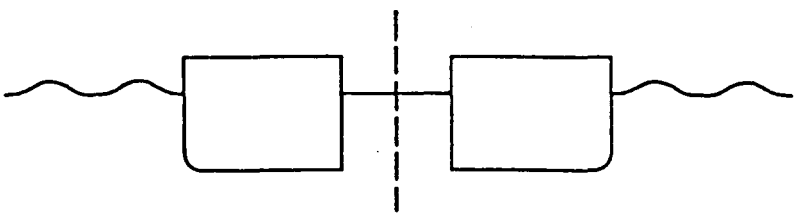

(c) 2D Double Barrier Problem – Beam Seas – Space Fixed

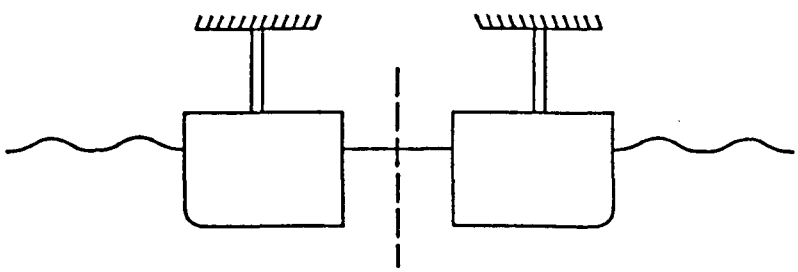

Figure 4.2

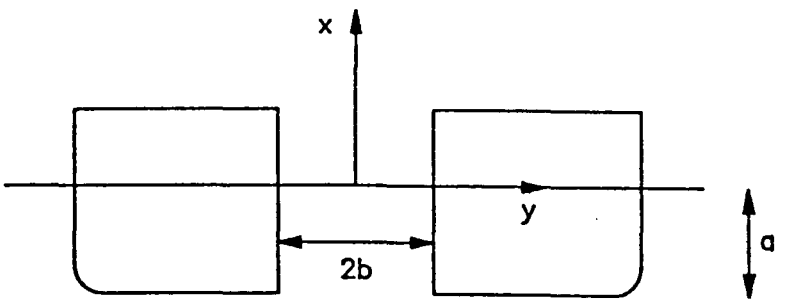

Figure 4.3

(a) Smooth Duct

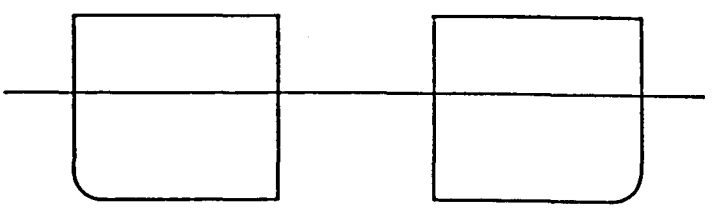

(b) Duct with Exit Baffle

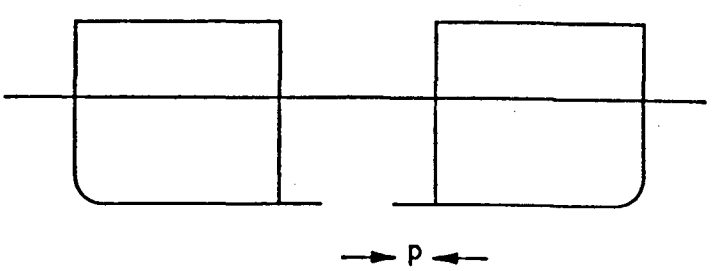

Figure 4.4

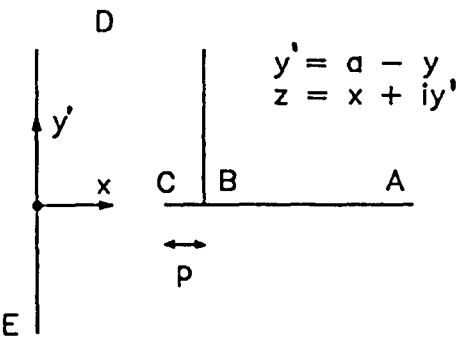

Figure 4.5a

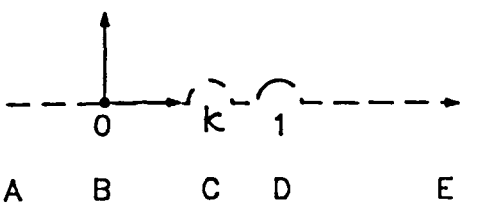

Figure 4.5b

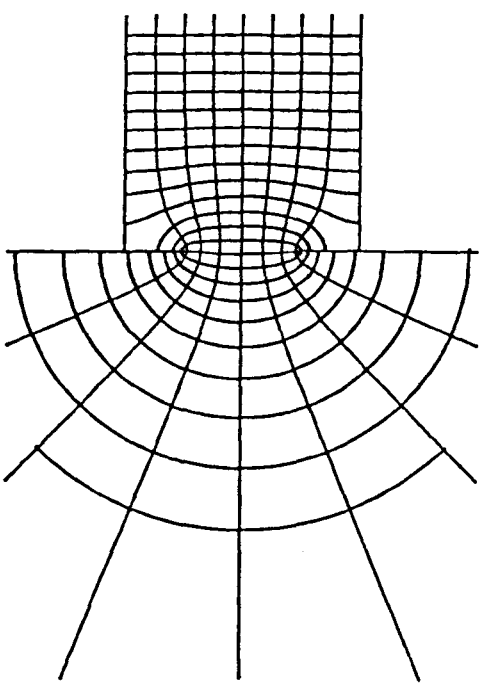

Figure 4.6

(a) Internal Baffle

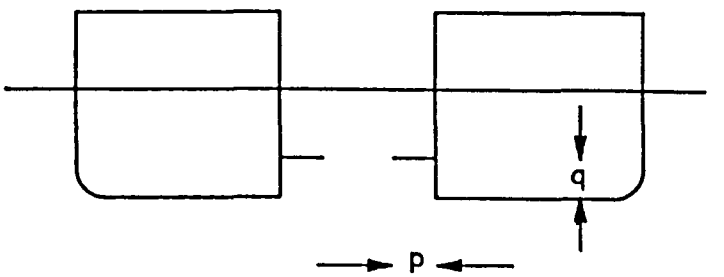

(b) Flow Expansion

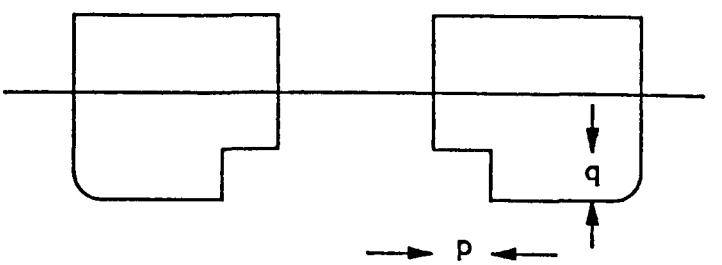

(c) Flow Constriction

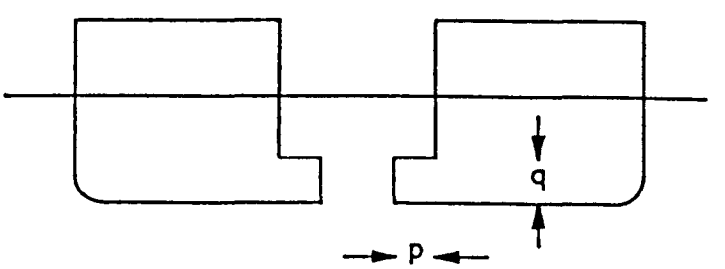

Figure 4.7

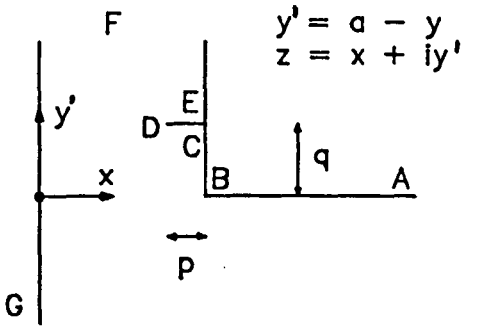

Figure 4.8a

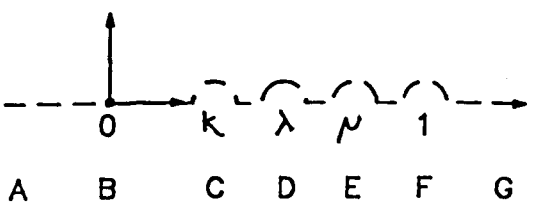

Figure 4.8b

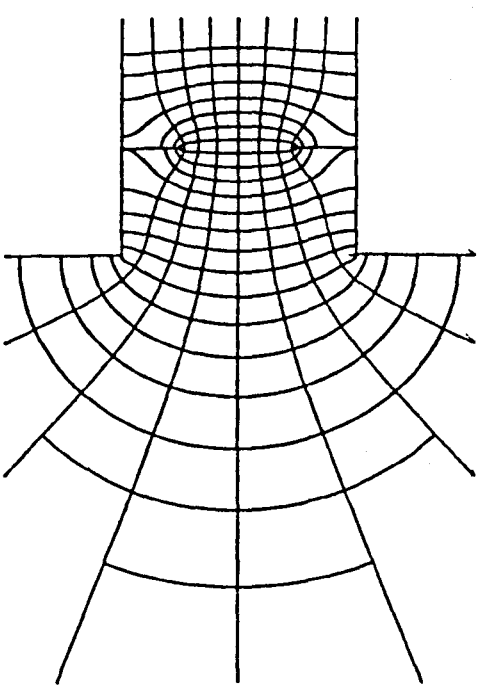

Figure 4.9

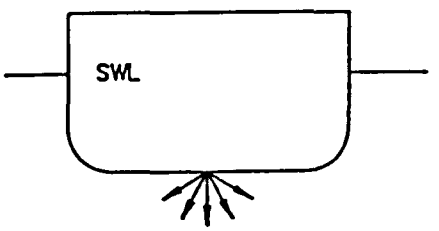

Figure 4.10a

Figure 4.10b

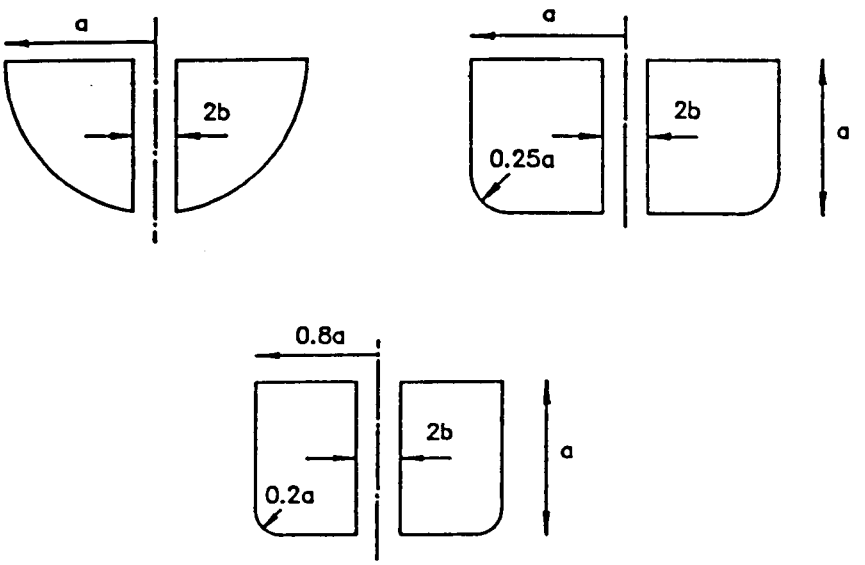

Figure 4.11

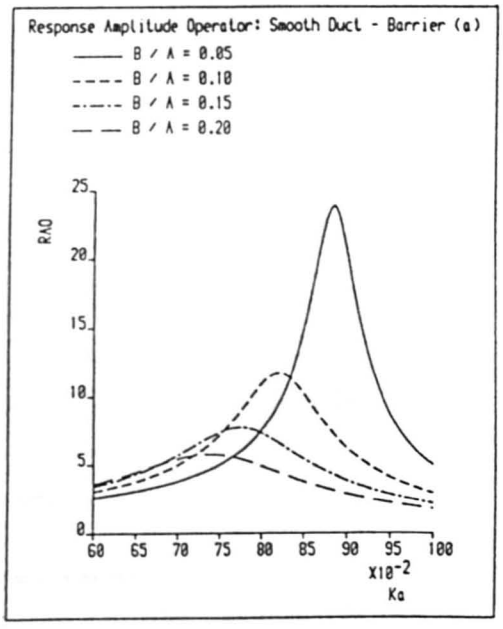

Figure 4.12a

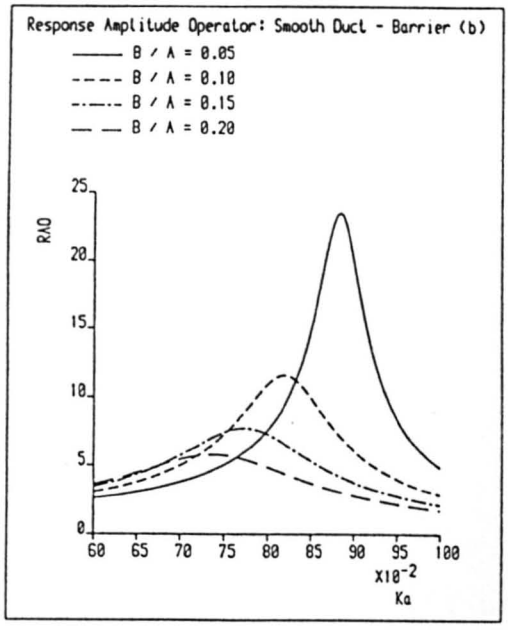

Figure 4.12b

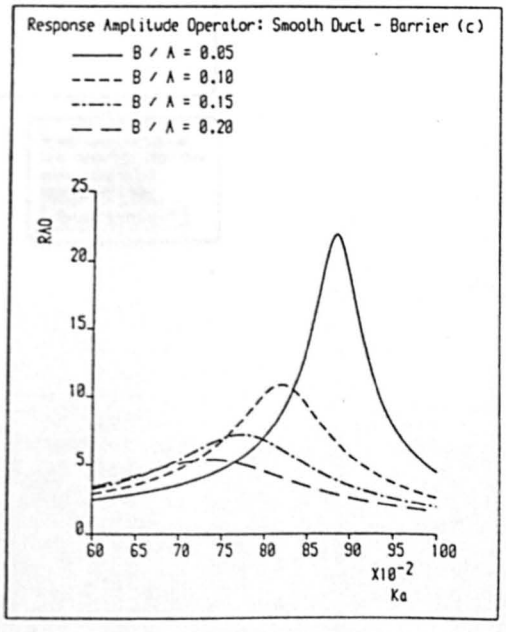

Figure 4.12c

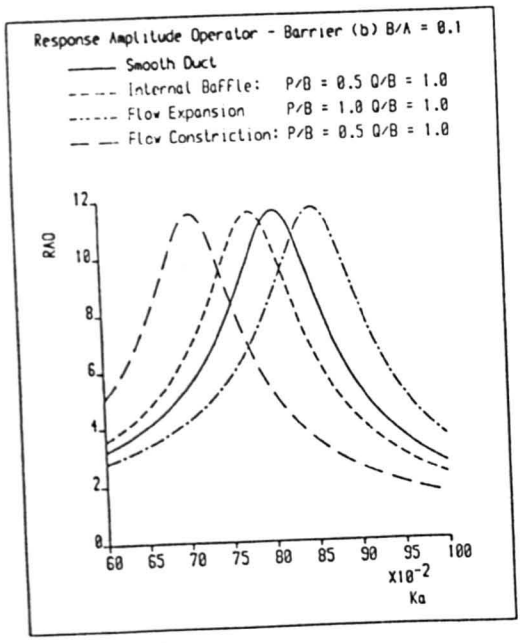

Figure 4.13

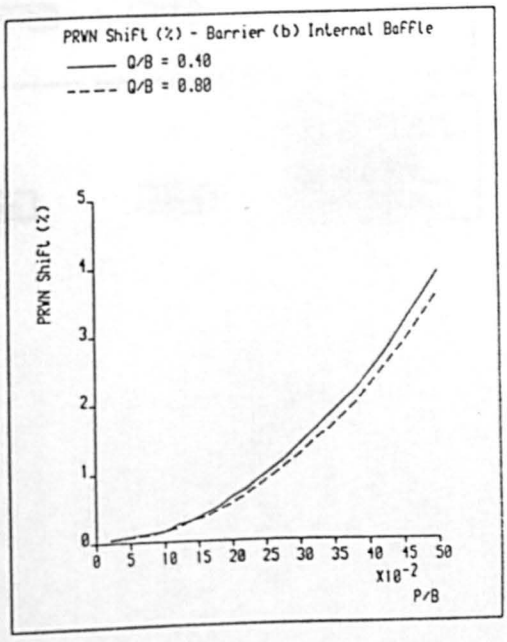

Figure 4.14

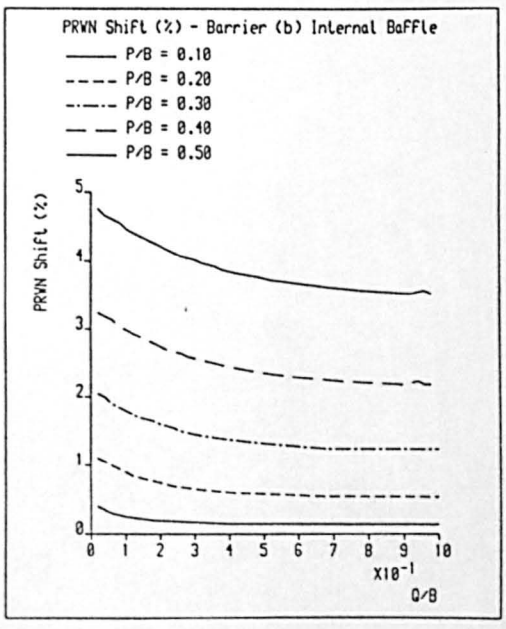

Figure 4.15

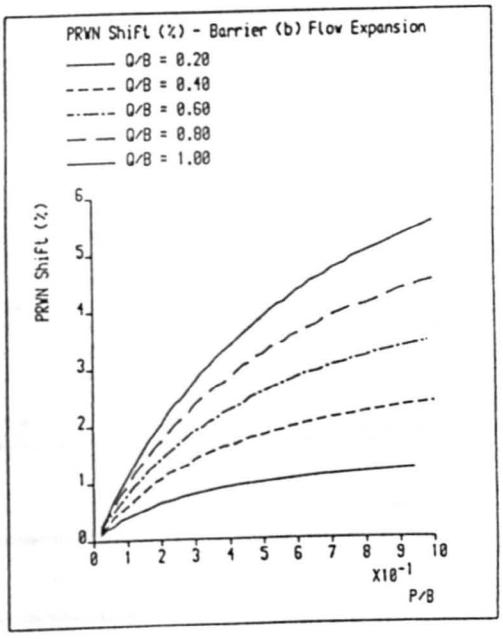

Figure 4.16

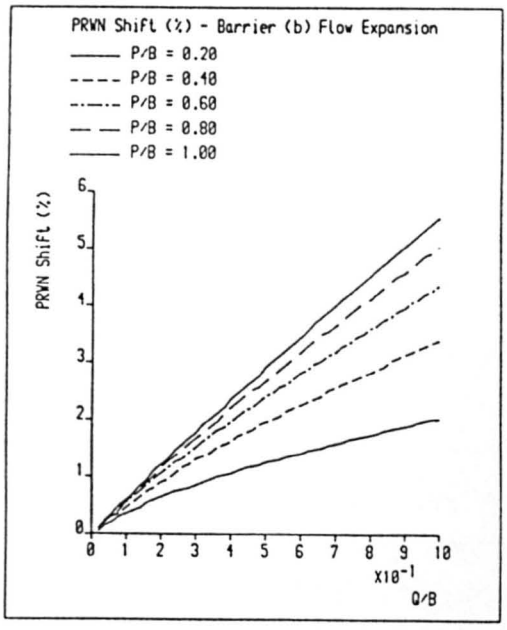

Figure 4.17

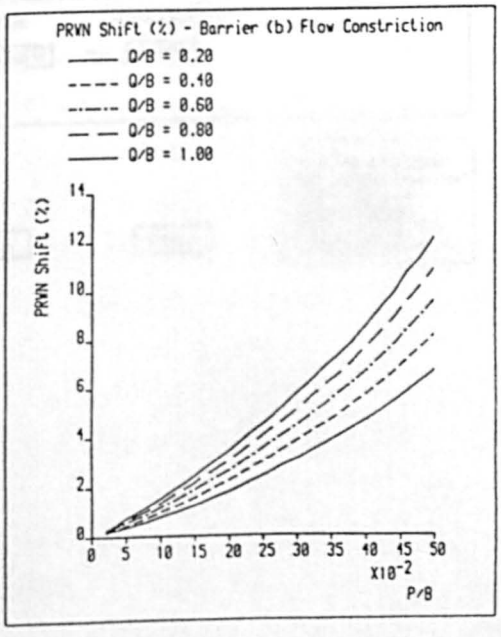

Figure 4.18

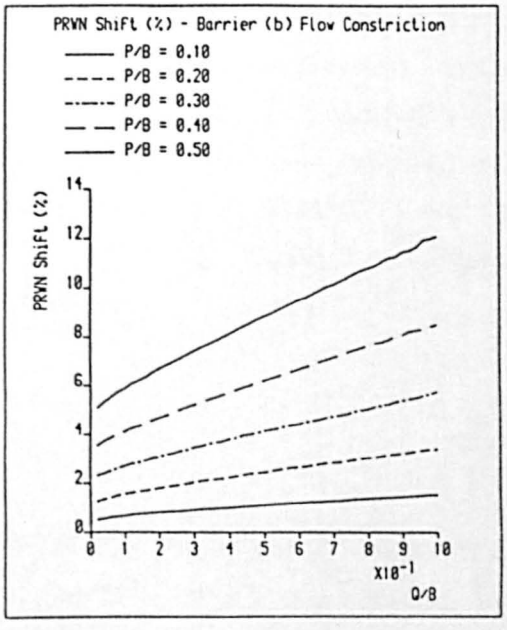

Figure 4.19

5. EXPERIMENTAL STUDIES ON MOONPOOL EXIT GEOMETRY

5.1 INTRODUCTION

The work outlined in the previous chapters describes how a theoretical method may be used to predict the shift in natural frequency of the oscillation of a 2D water column between two barriers effected by the alteration of the duct exit geometry. Two of the exit configurations studied - the flow expansion and the flow constriction were shown to have the potential to effect significant shifts in natural frequency, with the shifts being towards higher and lower frequencies respectively. The use of these configurations thus suggest possibilities for improvement of the moonpool performance from that offered by the smooth moonpool. In addition, the viscous damping associated with these configurations, which was not modelled by the theoretical approach, should, intuitively be greater than that for the smooth moonpool, as more sharp corners are present to cause flow separation, and vortex shedding. Finally, the simple geometry of the configurations would not present any difficulties in construction if they were to be incorporated into a real moonpool design. To this end, a series of experimental tests were carried out in order that a parametric study could be made of the water column oscillation for varying exit geometries.

5.2 EXPERIMENTAL STUDY

A moonpool with a series of inserts was constructed for the tests. The moonpool had a maximum cross section of 200 x 200mm and a draft of 200mm. The inserts allowed for a variation in the exit geometry of both configurations of $p/b = 0.0 \rightarrow 0.48$ and $q/b = 0.0 \rightarrow 1.5$. In the case of the variation of p for the flow constriction, and both p and q for the flow expansion, the reduction of the variables to

zero corresponds to a smooth moonpool. However, in the case of the flow constriction, the reduction of q to zero corresponds to a thin baffle at the exit, as examined theoretically in Chapter 4. The geometry of the flow constriction configuration tested is shown in Figure 5.1a; that of the flow expansion configuration is shown in Figure 5.1b. The tests carried out comprised simply of obtaining the hydrodynamic coefficients for each of the combinations using the procedure set out in Appendix 2.1.

The tests of the flow constriction configurations proved to be extremely successful in that the results obtained fitted in well with the mathematical model (see Appendix 2.1) in all cases, and that very few spurious data points were obtained. The tests using the flow expansion configurations, however, were not so successful; with $q/b > 0.4$ and $p/b > 0.24$ such that the cross section at the still water level was reduced to 116 x 116mm, the water column oscillation was influenced more by surface tension effects than was desirable; meniscuses of several millimetres were noticed on both the moonpool walls and the wave probes. Since the restoration forces are much smaller for these configurations than for the flow constriction configurations, the increased surface tension has a more detrimental effect. In addition, the greater depth expansions exhibited resonance at frequencies for which the problem of side waves in the tank became severe. As a result of these problems, the table of results is incomplete for the flow expansion.

5.3 RESULTS AND DISCUSSIONS

The results obtained for the hydrodynamic coefficients are set out in Appendices 5.1 and 5.2. The general trends observed are as follows:

(i) Added mass

For the flow constriction the added mass increases with increases in both p/b and q/b.

For the flow expansion the reverse is true; the added mass reduces with increases in both p/b and q/b.

(ii) Damping Ratio Intercept

For the flow constriction the damping ratio intercept is largest for q/b = 0.0; ie a thin baffle at the exit; for this case the damping ratio intercept increases with increases in p/b. A slight trend is apparent for q/b = 0 for the damping ratio intercept to reduce with increases in q/b and to increase with increases in p/b.

For the flow expansion there are no obvious trends in the relationships between p/b, q/b, and the damping ratio intercept.

(iii) Damping Ratio Gradient

For the flow constriction the damping ratio gradient increases with increases in p/b, and increases then reduces with increases in q/b, with the value of q/b for which the maximum occurs reducing as p/b increases.

For the flow expansion there are no obvious trends in the relationship between the damping ratio gradient and p/b; a similar trend to that observed for the flow constriction occurs in the relationship between the damping ratio gradient and q/b.

In order to provide a qualitative comparison with the results obtained in the two preceding chapters, a measure of the shift of the peak response wavenumber is required. This shift is, however, not as easily defined as in the case of the double barrier problem, since the non-linearity of the damping results in a dependancy between the peak response wavenumber and the amplitude of the excitation - ie the waveheight. In order to compare the moonpools directly the undamped peak response wavenumber was calculated for each configuration, using (2.7):

$$\omega_n = \sqrt{g/T(1+a_M)}$$

and thus:

$$PRWN = 1/(1+a_m) \qquad (5.1)$$

These values were then compared with the values obtained for the smooth moonpool, and the percentage shift in PRWN calculated. The results obtained are plotted in Figures 5.2 - 5.5. It can be seen that the general trends established in Chapters 4 and 5 are followed, in that the peak response wavenumber is reduced in the case of the flow expansion, and increased in the case of the flow constriction. The magnitude of the shifts is, however, much greater, with the maximum shift produced by the flow constriction about 70%, and that produced by the flow expansion about 50%, with the trends suggesting that larger shifts would have produced by the larger flow expansions, had these been studied. The increases do, however, appear to be more linearly related to the exit geometry than in the theoretical study.

This comparison is, however, somewhat simplistic. The effect of the damping, not included in this calculation, will be to reduce both the magnitude of the peak response and the frequency (and wavenumber) at which it occurs. As a consequence, the percentage shifts for the flow constriction will be greater than those suggested by Figures 5.2 - 5.3, and those for the flow expansion will be lesser. In addition, the performance of the moonpool in terms of water column oscillation amplitude at resonance will also be significantly affected by the magnitude of the damping. Comparisons between the moonpools could be made for individual input wave spectra but there is no guarantee that a moonpool which has a good response (in terms of water column oscillation) in one sea state will necessarily perform well in another. In order to select a moonpool for a given ship, then, a quantitative means of comparison between different moonpools must be developed. The development of such a technique is described in the following chapter.

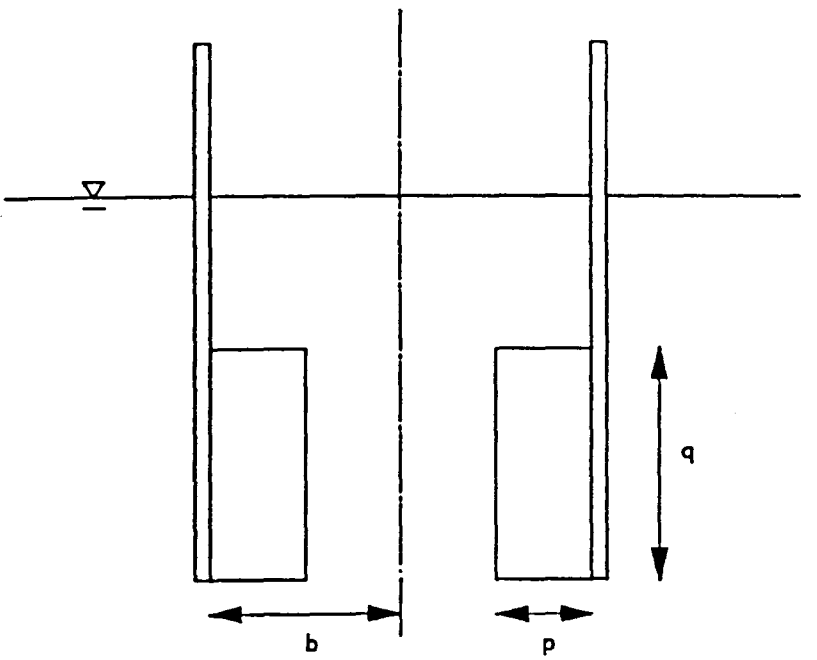

Figure 5.1a

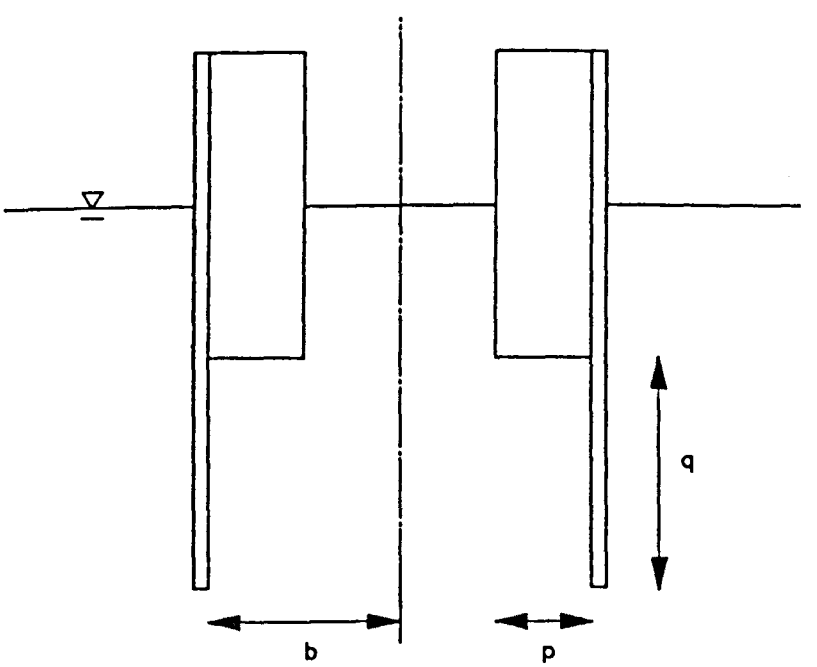

Figure 5.1b

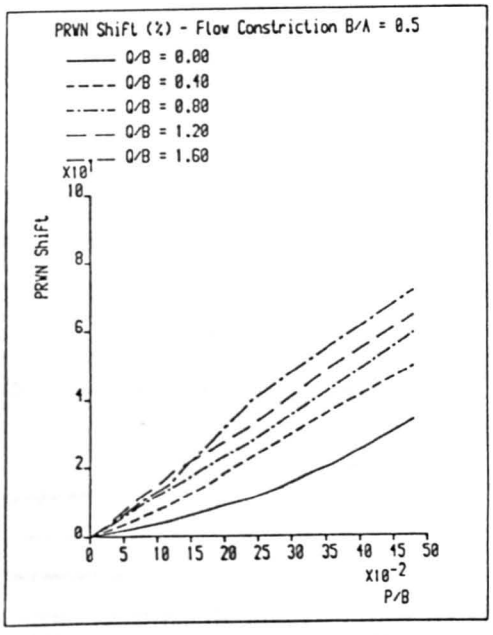

Figure 5.2

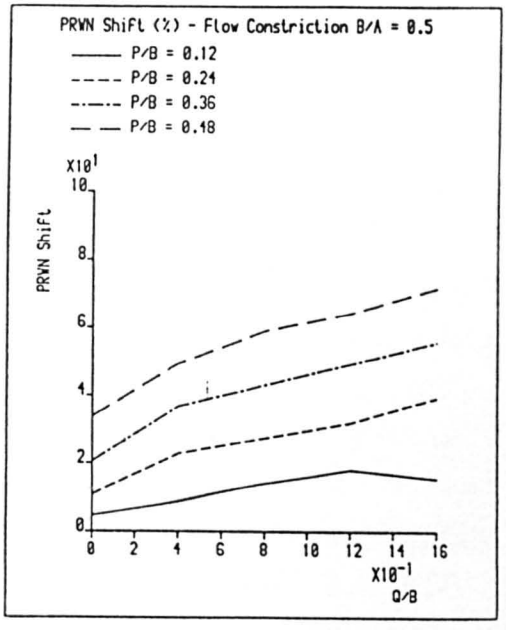

Figure 5.3

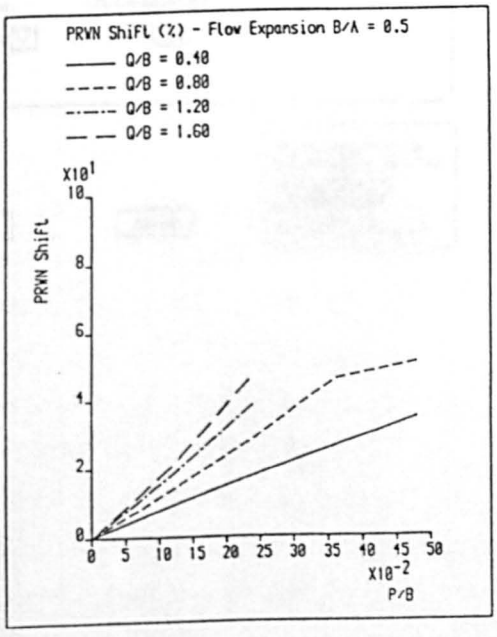

Figure 5.4

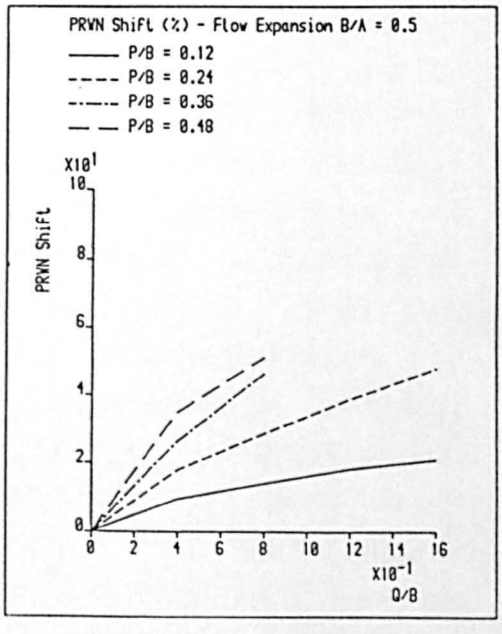

Figure 5.5

6. THE PRACTICAL ASSESSMENT OF MOONPOOL PERFORMANCE

6.1 INTRODUCTION

Having shown in the previous chapter that the water column oscillation in the moonpool may be dramatically altered by the alteration of the exit geometry, the question arises as to how a moonpool configuration should be chosen for a given ship. In most cases constraints upon structural integrity and space will restrict the number of practical configurations, but a wide variety of possibilities will still exist. In order to select the most suitable configuration, it must be possible to rank the possible designs on the basis of performance. A suitable basis must therefore be chosen by which the moonpool performance may be assessed.

One of the criteria which will inevitably be considered in the evaluation of any design is the long term downtime of the system. In the case of the moonpool, this downtime may be due to poor structural design, faulty construction, accidental damage, or simply the inability of the vessel to work due to bad weather. The downtime due to this last cause provides a means of comparison of the performance of different moonpool designs; if one design can be shown to cause less downtime in the long term than another, then the first design can be said to have a superior performance. If a series of moonpool designs is under consideration, then the designs may be ranked in terms of the expected annual downtime caused by each; the design with the smallest value will be the design which performs best. In order to obtain such a ranking a formal calculation must be carried out to determine the expected annual downtime for each moonpool; a procedure established for this purpose is described in the following sections.

6.2 THE CALCULATION OF VESSEL DOWNTIME

For a general comparison between significantly different designs, perhaps at an early stage in the vessel design process, the amount of vessel downtime due to the moonpool might be assumed to be the amount of time for which the moonpool itself is not operable; that is to say the amount of time for which the launch/retrieval operation through the moonpool is not possible. If comparisons are to be made between relatively similar moonpools, at an advanced stage of the design process, then this assumption is inadequate, and the ability of the vessel to work with regard to other factors - station keeping, roll motion etc. - must be considered. A more sophisticated indicator is required. A logical extension to the indicator proposed above is to compare the moonpools on the basis of the vessel downtime caused solely by the moonpool; that is to say the amount of time for which the vessel is unable to work, but could work if the moonpool were better.

In general the two indicators proposed above will lead to similar rankings, but differences may occur in some cases. The kind of differences possible is illustrated in Figures 6.1-6.3, which show graphical representations of the sea states for which the moonpools are operable. Figure 6.1 shows the operable sea states for two hypothetical moonpools, A and B. It is clear that moonpool B can work in more sea states than moonpool A, and the diagram thus suggests that B is the more suitable moonpool. Since no other constraints on working are considered, this diagram is analogous to the application of the first performance indicator suggested. Figure 6.2 shows the same two moonpools; however an additional constraint of vessel operability (apart from the moonpool) is imposed. The area of the diagram hatched with dashes is therefore not considered in the comparison of the moonpools. It can be seen that moonpool B is still more suitable, but the difference is more marked; on the basis of

this comparison moonpool A offers no advantage whatsoever over moonpool B. This comparison is analogous to the application of the second performance indicator suggested. Figure 6.3 shows the same two moonpools again, with a different pattern of vessel operability imposed. This time it is seen that moonpool B is better than moonpool A.

Whilst a discrepancy between the two indicators as extreme as that illustrated in Figure 6.1 and 6.3 is rather unlikely as the pattern of vessel operability shown in figure 6.3 is somewhat artificial, the discrepancy of the type illustrated in Figures 6.1 and 6.2 is almost inevitable. This is not to say that the first indicator is of little use; in many cases, the information required to determine the vessel operability - in terms of station keeping, roll motion, etc. - will not be available at an early stage of the design process, so this indicator will have to be used. However, given that all such data is available, then the second indicator will give a more accurate representation of the relative merits of the moonpools under consideration.

The qualitative comparison illustrated here is not, however, in itself, enough to enable a quantitative comparison of the relative performance of the moonpools, as the different sea states within the diagrams do not have equal probabilities of occurrance. These probabilities must also be taken into account with either indicator, in order to assess the relative importance of the ability to operate in a given sea state. The technique of operability analysis has been used in various forms, and with varying degrees of sophistication, to assess performance in terms of expected downtime (see for example Goren & Springett [1974], Rawstron & Blight [1978], or Hutchison [1981]). In this context it enables a formal calculation to be carried out to rank the moonpools in terms of expected annual downtime for those sea areas for which long term wave statistics exist.

The procedure for a moonpool performance assessment based on the first indicator considers the percentage of time for which the moonpool is operable in a given sea state, and multiplies that percentage by the probability of occurrance of the sea state. The sea states are defined in terms of significant wave height / mean zero crossing period pairs. If all likely sea states are considered, and the results for each sea state are summed, then the result will be one number indicating the expected percentage downtime for the moonpool if the vessel were to work continuously in the given operational area over a number of years. The procedure can be summarised in the form of a flow diagram; this is shown in Figure 6.4. A moonpool performance assessment based on the second indicator requires a slightly more complex procedure; the sea states are only considered if the vessel (excepting the moonpool) could operate in the sea state. The result of the procedure will be a number indicating the expected percentage downtime for the moonpool if the vessel were to work over a number of years in all sea states for which the vessel (excepting the moonpool) could be operated. This is illustrated in the form of a flow diagram in Figure 6.5.

The procedures mentioned above only deal with a single heading angle; in practice, whilst vessels will always work in head seas where possible, there will always be cases when other headings must be adopted. In the case of a diving support vessel, this may occur when the vessel is forced to work alongside a fixed structure; in the case of a floating production vessel an oblique heading may be adopted when the wind (and hence the local wind sea) is not in the same direction as the swell. The variation in heading angles may be dealt with by assigning a probability to each angle, calculating the moonpool downtime at each angle using either of the procedures set out above, then using the probabilities to obtain a weighted sum of the downtime values for each angle.

There are, however, still some details to be resolved before these procedures may be used to assess the moonpool performance. An appropriate limit criterion (or criteria) for the moonpool must be chosen. The method of calculation of the operability of the system (either the moonpool alone or the vessel excepting the moonpool) must be determined; finally the method of calculation of the cumulative probability must also be decided. These questions are addressed in the following sections.

6.3 SELECTION OF MOONPOOL OPERABILITY LIMIT CRITERIA

In order to carry out the procedures described in the previous section, a limit criterion (or criteria) must be established in order to enable the calculation of the operability of the moonpool. The selection of this criterion is inevitably somewhat subjective, depending, as it does, on the perceived risks to the operation in question.

In the case of a launch/retrieval operation, the decision as to whether or not the operation will proceed will be taken by the diving superintendant. Having taken advice from the ship's master on the station keeping (particularly if the ship is working close to a fixed platform) the decision will be made on the basis of observation of the water column oscillation in the moonpool allied to the experience of the individual concerned. Discussions with diving superintendents suggest that a variety of factors influence the decision as to whether or not the dive takes place; however, the greatest risk to the safety of the operation is generally considered to be the possibility of a 'snatch' load of the hoist wire. This occurs when an upwards motion of the water column in the moonpool causes hydrodynamic forces large enough to lift the unit and thus cause a slack wire situation. The following downwards motion of the water column then accelerates the unit downwards until the hoist

wire becomes tight once more. Very large transient loadings can then occur on the hoist wire, with the possibility that the wire will fail, causing the loss of the unit. An appropriate criterion for the moonpool operability can thus be expressed in terms of the probability of the hoist wire tension being reduced to zero during the period of the launch/retrieval operation.

In the case of other operations carried out through moonpools - for example production in the case of floating production systems, or drilling in the case of drillships - then alternative criteria must be adopted. Depending upon the precise nature of the operation, different factors may become important; several criteria may be needed to represent a series of important risks. For some operations the operability of the moonpool may never be called into question, as other criteria will always cause the operation to be halted before the moonpool operability limit is reached. One risk, however, which is common to most operations is the possibility that the water column oscillation in the moonpool may become large enough that the equipment handling area, usually the lowest space in the vessel open to the moonpool, becomes flooded. A suitable criterion for the moonpool operability in this respect is thus the probability of the water column oscillation becoming large enough to reach this level inside the moonpool. This criterion has a significant advantage in simplicity over the force criterion as it is dependant only on the ship-moonpool system, whereas the force criterion is dependant on the whole ship-moonpool-subsea unit system, and will thus have different values for different subsea units. It is therefore more easily used at an early stage in design when details of subsea units may not be available, and could thus be used to provide an early comparison between moonpools intended for launch/retrieval as a precursor to a more detailed study at a later stage in the design process.

The limit criteria for the vessel excepting the moonpool with regard to the operation to be performed must also be determined by an evaluation of the risks to the operation posed by the aspect of the vessel's performance under consideration. This is, however, outside the scope of this work.

Having decided on the physical nature of the limitations on operability of the moonpool, the probabilities of exceedance of these limits must now be calculated and a moonpool performance index established. This is dealt with in the next section.

6.4 A MOONPOOL PERFORMANCE INDEX

Having established suitable limit criteria for the moonpool operability and for the various aspects of the vessels performance which also have the potential to restrict the operation in question, the operability of the vessel with regard to the various criteria must be determined. The concept of 'operability' must therefore be defined. It is unrealistic to define an operable condition as one in which the limit criterion will never be exceeded; it is easily shown that there is a finite mathematical probability of any gaussian process exceeding any given value, even if physical limitations would prevent such an occurrance in practice. The operability must therefore be defined in terms of the probabilities of exceedance of the limit criteria.

These probabilities may be calculated in several ways, depending on the nature of the process involved. If the process is adequately represented by a calculated power spectrum, then the probability may be calculated using results from spectral theory. If, however, this is not the case, and it is felt that a calculated power spectrum does not adequately represent the process - and in particular the

extremes of the process - then an alternative method must be employed.

Spectral Approach: Performance Indicator I

The flooding criterion falls into the first category. The water column oscillation power spectrum as calculated in Chapter 2 was shown to predict the behaviour of the physical model with accuracy, despite the non-linearities in the system. The calculated spectral model can thus represent the physical reality with a reasonable degree of verisimilitude. Assuming that the spectral bandwidth of the process is small the exceedance probability can be calculated using the expression (eg Bishop & Price [1979])

$$p(h > H_L) = e^{-(H_L/8m_0)^2} \qquad (6.1)$$

where

h is the process double amplitude

H_L is the limit criterion double amplitude

m_0 is the zeroth moment of the process power spectrum (ie the water surface elevation power spectrum here)

Thus if the probability were to be 0.01 then if the vessel worked continuously for 100 days in the same environment at the same heading angle, the criterion would be exceeded on average for one day in total. Considering the set of N sea states selected as being representative of the operational area, then the net probability of the criterion being exceeded for the ith sea state on a year round basis is thus:

$$p_{a_i} = p_{s_i}\, p(h > H_L) \qquad (6.2)$$

where p_{s_i} is the annual probability of occurrance of the sea state. The performance index for all sea states for the given heading angle is thus given as:

$$P_{1_j} = \sum_{i=1}^{N} p_{a_i} \qquad (6.3)$$

and the performance index for all N sea states and all M heading angles is given as:

$$P_1 = \sum_{j=1}^{M} p_{ha_j} \sum_{i=1}^{N} p_{a_i} \qquad (6.4)$$

where p_{ha_j} is the probability of the jth heading angle. This approach is suitable for the calculation of a moonpool performance index based on the first indicator suggested in section 6.1. The index obtained, P_1 is essentially an estimate of the proportion of the time for which the moonpool limit criterion would be exceeded if the ship were to work continuously all year round in the chosen operational area.

Spectral Approach: Performance Indicator II

In order to obtain a performance index based on the second performance indicator a more precise definition of operability is required. A yes/no decision must be made as to whether or not the vessel is operable with respect to all limit criteria excepting the moonpool before the moonpool itself is assessed. Each contributory process (eg station keeping, roll motion etc.) must therefore be assessed and the decision made as to whether the operation could safely be carried out; the moonpool operability of interest only if all of these processes are operable.

If a given limit criterion is expressed in terms of the maximum value which can be sustained whilst still continuing the operation then there are two basic approaches to this decision. In the case of an operation of indeterminate duration, an exceedance probability p for the process must be calculated using (6.1) and compared with a probability regarded as 'safe' for that process; the value chosen for this 'safe' probability will in itself depend upon the perceived consequences of an exceedance of the limit

criterion. If the exceedance probability is greater than the 'safe' probability then the vessel is defined as inoperable for that sea state. Alternatively, if the operation is of a well defined duration, then the expected maximum value of the process can be calculated using the expression (Longuet Higgins [1952])

$$h_{max} = (8m_o)^{1/2}\left[(\ln C)^{1/2} + 0.2886(\ln C)^{-1/2}\right] \qquad (6.5)$$

where C is the number of cycles occurring during a typical operation. In many cases this will be equal to the number of waves occurring during the operation, which may be obtained from the mean zero crossing period for the sea state. If this value is less than the limit criterion then the vessel may be regarded as operable in that sea state.

If the limit criterion can be appropriately expressed in terms of the 'significant' value of the process rather then the maximum, the decision can be made directly for any length of operation simply by calculation of the significant value of the process and comparison with the limit criterion.

In either case a yes/no decision can be taken, and by considering all the relevant limit criteria a decision can be made as to whether or not the vessel is operable excepting the moonpool. This is not to say, however, that the moonpool operability should necessarily be treated as a yes/no decision for the purposes of a performance index. The expression of the moonpool operability in terms of a probability of exceedance of the limit criterion gives a more accurate indication of the moonpool performance than a simple statement that the moonpool is operable or inoperable. A peformance index based on the second indicator suggested could thus be expressed as:

$$P_2 = \sum_{J=1}^{M} P_{ha_j} \sum_{i=1}^{N} P_{a_i} \delta_i \qquad (6.6)$$

where δ_i = 1 if vessel is otherwise operable
δ_i = 0 if vessel is otherwise inoperable

The index obtained, P_t is essentially an estimate of the proportion of the time for which the moonpool limit criterion would be exceeded if the ship were to work all year round in all otherwise operable sea states in the chosen operational area.

It must be stressed that neither of the performance indices suggested actually give operabilities for the system under consideration. A strict operability calculation would require that all limit criteria, including the moonpool were evaluated on a yes/no basis. The operability would then be given as:

$$P_o = \sum_{j=1}^{M} P_{ha_j} \sum_{i=1}^{N} P_{s_i} \delta_i \qquad (6.7)$$

where δ_i = 1 if vessel as a whole is operable
δ_i = 0 if vessel as a whole is inoperable

Non Spectral Approach

If the process to which the limit criterion is applied cannot be modelled using a spectral technique, or the spectrum obtained is not of narrow bandwidth (such that a Rayleigh distibution of maxima is inappropriate) then, whilst the overall procedures remain as described, the method of calculation of the exceedance probability will differ. In such a case the exceedance may be caclculated by generating realisations of an appropriate length for the operation in question, and using these directly by fitting a suitable probability distribution to the data obtained. However, since the number of exceedances per realisation will in itself be distributed, it is necessary to carry out an initial study on a series of representative sea states in order to determine the number of realisations necessary to

achieve convergence, before embarking on the performance calculations proper. Having ascertained a suitable number of realisations to be calculated, the exceedance probability can be obtained by dividing the number of exceedances by the number of realisations (though it should, of course, be noted that the exceedance probability cannot be greater than unity). The probability is then used in exactly the same manner as if it were calculated from the process power spectrum.

Practical Application

A Computer program was written in order to carry out the performance index calculations described in this chapter. The long term wave statistics used were taken from Andrews et.al. [1984] for the sea area 1.1 (Northern North Sea). Whilst no real data is available to verify the results produced by the program, each element of the calculation has been verified in previous chapters. A series of worked examples is presented in Appendices 6.1 - 6.4 in order to illustrate the potential use of the method.

The performance of the moonpool is, however, only one of several criteria by which a moonpool design may be judged; other considerations such as the space required and the cost and complexity of fabrication must also be considered. In order to produce a design which best satisfies the requirements of a given client, a systematic procedure must be carried out. Such a procedure is described in the following chapter.

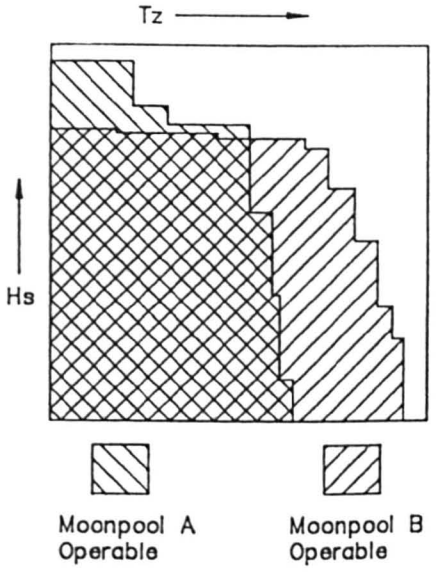

Figure 6.1

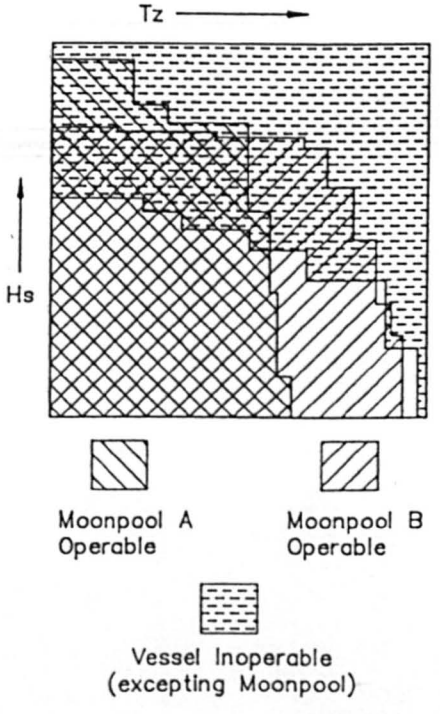

Figure 6.2

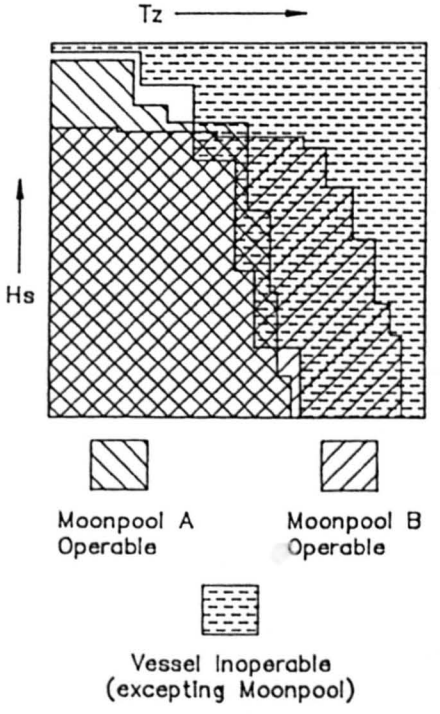

Figure 6.3

Figure 6.4

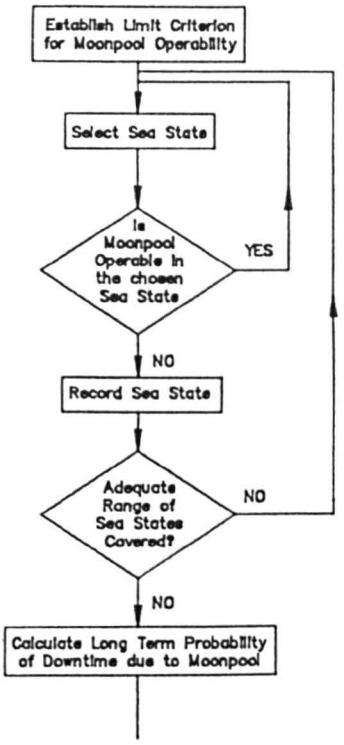

Figure 6.5

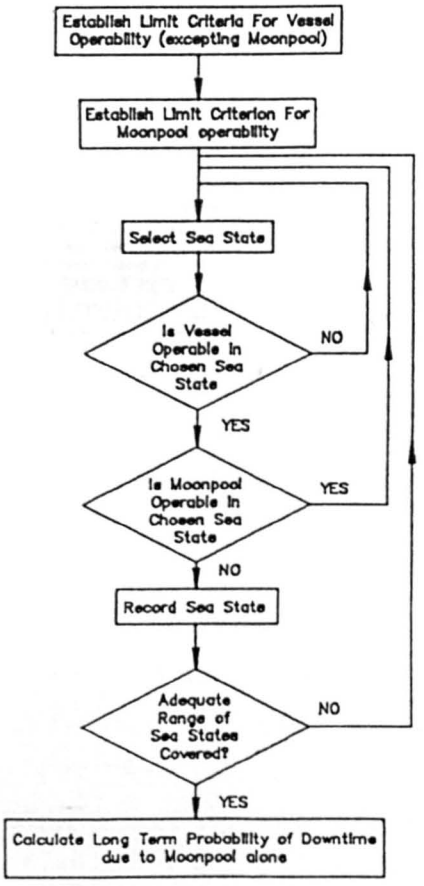

7. A PRACTICAL MOONPOOL DESIGN PROCEDURE

7.1 INTRODUCTION

The work set out in the previous chapters describes how an understanding has been acquired of the way in which changes in the exit geometry of a moonpool may affect the performance of a moonpool (see Chapters 4 - 5). In addition, a quantitative method for assessing that performance has been proposed (see Chapter 7). The next and final step to be taken in this study is to integrate the method and the understanding to produce a procedure which may be used to design a moonpool to handle any given subsea unit from any given vessel in any operational area. The steps involved in the procedure developed for this purpose are described in the following section.

7.2 DESIGN PROCEDURE

The moonpool design procedure may be broken down into five basic steps; these are illustrated in Figure 7.1.

STEP 1: Acquire Design Data

All data on the project in hand which is relevant to the specific problem of moonpool design must be obtained at this stage. If the data is not available, then estimates should be used. This information may be broadly split into three categories.

(i) Subsea Equipment:
Dimensions and weights of equipment to be handled
Clearances required between equipment and moonpool wall
Inertia and Drag coefficients for Subsea units (where moonpool is to be used for launch and retrieval)

(ii) Vessel:
Hull form data (eg lines plan or table of offsets)
General Arrangement
Operational limits for vessel (eg Station Keeping limits)

(iii) Operational Area(s):
Long term wave statistics for operational area(s) Wave Spectral Model(s) for operational area(s)

STEP 2: Establish Design Evaluation Criteria

In order to evaluate the designs produced, the criteria by which the designs are to be judged must be established. In all cases the performance of the moonpool (as described in Chapter 7) will be an important criterion; however there will also be other criteria to consider. The selection of these criteria will depend upon the purpose for which the vessel is intended. Typical criteria to be considered would include:

Moonpool Performance
Space required
Ease of Fabrication
Cost

or a suitably weighted combination of some or all of these.

STEP 3: Establish Design Constraints

The evaluation of the designs produced will be carried out on the basis of the criteria established in the previous step; however the range of designs which may be considered for evaluation will be limited by constraints upon some or all of these criteria. Typically the space available for the moonpool may be limited, or the vessel may be considered impractical if the performance does not meet a certain

target.

STEP 4: Select Configuration

The configuration to be adopted for the moonpool is selected on the basis of two factors:

(i) the frequency of peak response of a smooth moonpool satisfying the design data
(ii) the frequencies at which the majority of the wave energy is present on a long term basis

The first may be calculated simply using estimated hydrodynamic coefficients, whilst the second may be obtained from the data on the operational area(s). If the peak response frequency for the smooth moonpool is lower than the frequency of the predominant waves, then the correct strategy is to reduce the peak response frequency of the design moonpool by adopting the flow constriction configuration. Conversely, if the peak response frequency for the smooth moonpool is higher than the frequency of the predominant waves, then by a similar argument, the flow expansion configuration should be selected.

STEP 5: Select Detailed Moonpool Geometry

The selection of the detailed geometry of the moonpool is not a task which can be carried out in one stage. In order to produce the best design within the constraints imposed, an iterative procedure must be followed. The form of the iteration is illustrated in the form of a flow diagram in Figure 7.2. The tasks involved in the iteration are as follows:

(i) Propose detailed geometry

A detailed layout of the moonpool is produced. The design should set out the basic geometry of the chosen configuration (ie the depth and breadth of the constriction or expansion), and include any additional damping devices as appropriate.

(ii) Assess Performance of Design

The performance of the design thus produced is assessed using the technique described in Chapter 7. A decision making process is then carried out on the basis of this assessment.

(iii) Design satisfies Constraints?

If the design satisfies all the constraints imposed it may be retained for evaluation at a later stage; if not, then it may be discarded.

(iv) Examine Scope for Further Designs

If there is still scope for further geometries to be considered within the constraints imposed, then the next step would be to propose another geometry. If the scope for further geometries has been exhausted, then the evaluation should take place; however it is possible that none of the geometries proposed satisfy all of the constraints and the whole problem will need to be reassessed.

(v) Evaluate designs

The designs which satisfy all of the imposed constaints must be evaluated in terms of the criteria established earlier, and the geometry considered most suitable may be selected. The detailed structural design of the moonpool may then be considered. If it proves impossible to produce a design satisfying the constraints then the problem must be reassessed. This may involve the relaxation of one or more of the constraints, the modification of the design data (for example the size of the vessel), or, in an extreme case, the abandonment of the project as infeasible.

It may be the case that the client wishes to examine several scenarios with varying design constraints in order to establish, for example, the relationship between the available space and the performance for the particular set of design data under consideration. In such a case the iteration procedure may be carried out for each suggested set of constraints.

A worked example illustrating the use of the procedure in a practical design problem is given in Appendix 7.1.

Figure 7.1

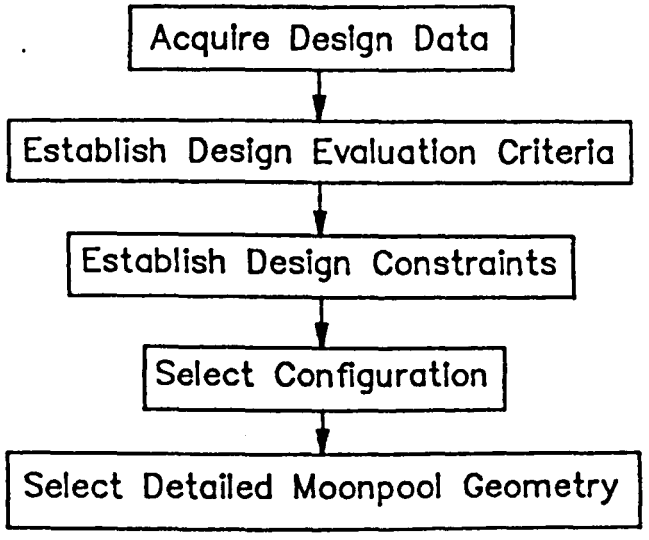

Figure 7.2

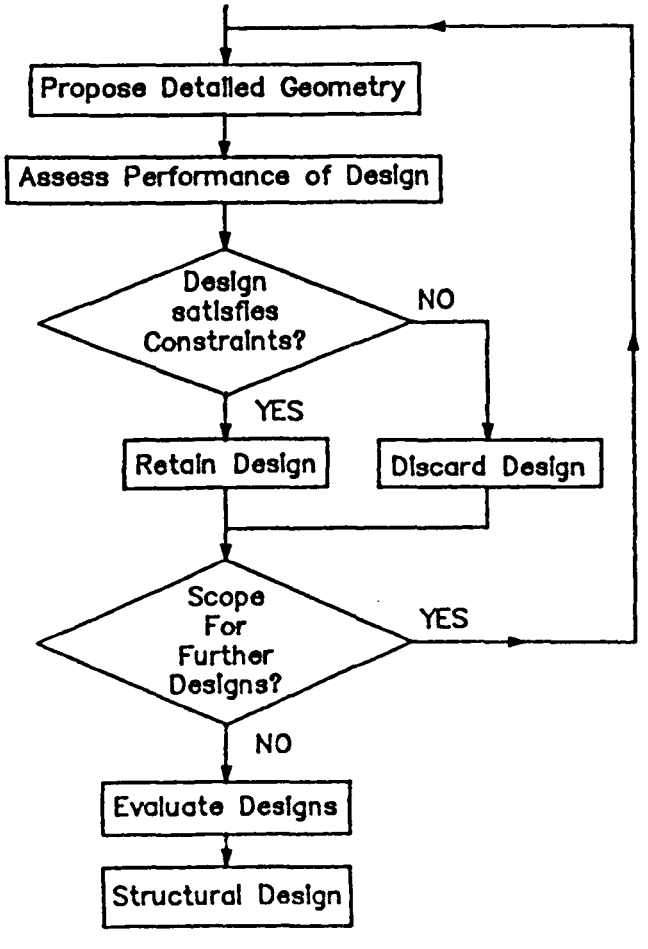

8. DISCUSSION

Achievement of Aims

The main aims of this study were outlined in section 1.2. These were stated as being:

(i) To acquire an understanding of the water column oscillation in the moonpool with or without the presence of a subsea unit.

(ii) To develop a technique to calculate the hydrodynamic loading on a subsea unit in the moonpool.

(iii) To model the ship/moonpool system mathematically, and examine the effects of variation of important geometric parameters on the system response.

(iv) To verify the conclusions reached and examine any deficiencies in the theoretical work by means of experimental studies.

(v) To devise a quantitative means of comparison of different moonpool designs, and to propose a practical procedure for the design of moonpools.

The extent to which these aims have been met by the work presented here will now be discussed.

A mathematical model has been proposed with which the moonpool water column oscillation response spectrum may be calculated. The method involves the experimental acquisition of three hydrodynamic coefficients for the moonpool. A procedure for obtaining these coefficients accurately has been devised. The model and the experimental procedure have been verified with a series of random wave tests in which a good agreement is demonstrated between the response spectrum calculated from the measured water column oscillation realisation and that predicted using the proposed technique. In nine tests carried out the mean absolute percentage error

between the predicted significant oscillation and the measured significant oscillation was of the order of 7.5%.

The model has also been demonstrated to give reasonably good predictions for the moonpool water column oscillation response spectrum for the case of a moonpool with a subsea unit present, even at high blockage ratios. Over the nine random wave tests carried out with a subsea unit in a moonpool the mean absolute percentage error between predicted significant and measured significant oscillation was of the order of 11%. Suggestions have been put forward as to how both the experimental procedure used to obtain the moonpool hydrodynamic coefficients and the mathematical model itself used to predict the response spectrum might be improved. An understanding of the of the water column oscillation in the moonpool can therefore be said to have been achieved.

Two mathematical models have been proposed with which the hydrodynamic force on a subsea unit fixed in a moonpool may be calculated. One model uses a time domain formulation of the problem, whilst the other uses a frequency domain approach. Both methods require the acquisition of inertia and drag coefficients for the subsea unit; a method with which these coefficients might be obtained at suitable Reynolds numbers and Keulegan Carpenter numbers has been suggested. The models have been verified with a series of random wave tests in which good agreement is demonstrated between the force spectrum measured and that predicted for both models. In the nine random wave tests carried out, the mean absolute percentage error between the predicted significant force and that measured was less than 6%. An understanding of the hydrodynamic loading on the subsea unit in the moonpool can therefore be said to have been gained.

A two dimensional mathematical model of the ship-moonpool system has been set up and solved for five exit configurations; a smooth moonpool, a moonpool with a thin baffle at the exit, a moonpool with a thin baffle on the interior wall, a moonpool with a flow expansion at the exit, and a moonpool with a flow constriction at the exit. A numerical parametric study has been carried out, showing that the most promising configurations, in terms of the shift in peak response frequency, would be the flow expansion and flow constriction configurations. The model did not, however, give any indication of the effects of the configurations on the system damping.

An experimental parametric study of the two most promising configurations has been carried out on the basis of the numerical study. The results confirmed the trends suggested by the two dimensional model, but the shifts in peak response frequency were shown to be much larger in the case of the three dimensional physical model than in the two dimensional mathematical model. The results also indicate that the configurations studied greatly increase the system damping. This increase has benefits in terms of magnitude of the peak response, but also affects the shift in peak response frequency. The effect of the configurations on the moonpool response has been established. The use of the mathematical model to suggest favourable exit configurations has thus been backed up by the experimental study to indicate the effect of the variation of the exit geometry parameters.

A quantitative definition of moonpool performance has been proposed in the form of a moonpool performance index. The performance index is obtained using long term sea state statistics for the operational area or areas of the vessel in question; the method allows for the moonpool performance to be defined in terms of either the water column oscillation or the force on a subsea unit in the moonpool. Information regarding the operational limits of the vessel excepting the

moonpool can be included in the calculation of the performance index. A series of worked examples is presented using moonpool configurations studied experimentally in order to demonstrate the application of the method to practical moonpool design problems.

The work described so far has been integrated in the form of a practical procedure for the design of moonpools. The use of this procedure is illustrated with a worked example taken from a real design problem.

In summary then, the majority of the aims set out have been achieved. There are, however, areas where future research would lead to greater understanding.

Future Research

There is much room for improvement in the force prediction models set out in Chapter 3 by way of including the effects of variations in the inertial and drag coefficients with Keulegan Carpenter Number, direction of flow, blockage coefficients, and proximity of the free surface. On a more fundamental level, it would be very useful to carry out studies with the aim of establishing trends showing how the coefficients vary with these parameters, in order that designers might have guidelines for the purposes of preliminary design.

9. CONCLUSIONS

A mathematical model of the Ship/Moonpool/Subsea Unit system has been developed, allowing the prediction of the water column oscillation in the moonpool (with or without the presence of a subsea unit) and the hydrodynamic force on a subsea unit in the moonpool. Experimental tests have shown the model to give results sufficiently accurate for the purposes of engineering design.

The effect of simple variations in the exit geometry of the moonpool on these dynamics has been studied mathematically using a two dimensional potential flow model. Two configurations were identified as yielding significant shifts in the frequency of peak response of the water column.

An experimental parametric study of the configurations identified was carried out. The study proved that large shifts in peak response frequency could be obtained in practice using modifications of the moonpool exit geometry, and showed how the magnitude of the frequency shift varied with the geometry of the moonpool exit.

A quantitative procedure for the assessment of moonpools has been devised using an approach based on the long term probability of vessel downtime due to the moonpool. The method allows for information on the vessel operability to be used to increase the reliability of the assessment. A series of worked examples has been presented in order to illustrate the application of the procedure to realistic cases.

A practical design procedure has been proposed based on the understanding and knowledge gained through the study. A worked example based on a real design problem is presented in order to show how the method may be used to carry out a moonpool design.

ACKNOWLEDGEMENTS

I am indebted to the following people, without whom this work would not have been possible:

Professor Chengi Kuo, who initiated research into moonpool design at the University of Strathclyde and who supervised this thesis.

Dr B.S.Lee for his advice on many aspects of moonpool design.

Dr P.Sayer of the Division of Ship and Marine Technology at Strathclyde, Dr D.McGhee of the Department of Mathematics at Strathclyde, and Dr J.Martin of the Department of Mathematics at the University of Edinburgh for their helpful suggestions in the field of complex analysis.

Mr D.Clelland for his invaluable help in the design of the computer control systems and instrumentation used in the experimental tests.

Mr I.Bellingham and Mr W.West who built the experimental models.

The Science and Engineering Research Council who funded much of the Moonpool Research at the University of Strathclyde.

REFERENCES

AALBERS,A.B. 1984 The Water Motions in a Moonpool. Ocean Engg., Vol 11, No 6, pp 557-579

ANDREWS,K.S., DACUNHA,N.M.C & HOGBEN,N. 1984 SAFESHIP: ENVIRONMENTAL ASPECTS Part I: Data for High Risk Areas. NMI report No.185 for Dept.of Transport 'SAFESHIP' programme

BISHOP,J.R. 1984 Wave Force Investigations at the Second Christchurch Bay Tower. NMI report No.R177 for Dept.of Energy Offshore Energy Technology Board

BISHOP,R.E.D. & PRICE,W.G. 1979 The Hydroelasticity of Ships. Cambridge University Press

BORGMAN,L.E. 1967a Spectral Analysis of Ocean Wave Forces on Piling. Proc.ASCE J.Waterways & Harbours Div., Vol 93 No WW2

BORGMAN,L.E. 1967b Random Hydrodynamic Forces on Objects. Annals of Math.Stats., pp 37-51

BORGMAN,L.E. 1969 Ocean Wave Simulation for Engineering Design. Proc.ASCE J.Waterways & Harbours Div., No WW4

CARTWRIGHT,D.E. & LONGUET-HIGGINS,M.S. 1956 The statistical distribution of the maxima of a random function. Proc.Roy.Soc.Lond. A Vol 237 pp 212-232

CLOUGH,R.W. & PENZIEN,J. 1975 Dynamics of Structures. McGraw-Hill Kogakusha, Ltd., Tokyo.

CUONG,H.T.,TROESCH.A.W. & BIRDSALL,T.G. 1982 The Generation of Digital Random Time Histories. Ocean Engg., Vol 9 No 6 pp 581-588

FIDLERIS,V. & WHITMORE,R.L. 1961 Experimental determination

of the wall effect for spheres falling axially in cylindrical vessels. Brit.J.App.Physics Vol 12 pp 490-494

FRANK,W. 1967 Oscillation of cylinders in or below the free surface of deep fluids. NSRDC Rep.2375

FUKUDA,K. 1977 Behaviour of Water in vertical well with bottom opening of ship and its effects on ship motions. J.Soc.Nav.Arch. of Japan, Vol 141

GOREN,Y., & SPRINGETT,C.N. 1974 Selection and Design of a Semisubmersible Drilling Vessel. RINA Symposium on Ocean Engineering, London

GRAN,S. 1983 Wave Induced Forces on a Diving Bell in a Moonpool. Det Norske Veritas Research Division Technical Rep.No.83-0324.

HUTCHISON,B.L. 1981 Risk and Operability Analysis in th Marine Environment. Trans.SNAME, Vol 89

JENKINS,G.M., & WATTS,D.G. 1968 Spectral Analysis and its applications. Holden-Day, San Francisco

KUO,C. 1978 A Controlled Handling Method for effective offshore support operations. Proc.10th OTC, Houston

LAMB,H. 1962 Hydrodynamics. 6th Ed., Camb.Univ.Press.

LEE,B.S. 1982 On the properties of vertical water oscillation in a moonpool. Ph.D Thesis, Department of Ship & Marine Tech., University of Strathclyde

LONGUET-HIGGINS,M.S. 1952 J.Mar.Res. Vol 11 p245

MADSEN,N.F. 1980 Prediction of Water level motion and forces acting on a Diving Bell during Launching through a Moonpool.

Danish Ship Res.Lab., Bulletin no. 45

MASSEY,B.S. 1975 Mechanics of Fluids. Van Nostran Reinhold Co.

MELLEM,T. 1979a Surface Handling of Diving Bells and Submersibles in Rough Seas. Paper No. 3530 Proc.11th OTC, Houston, Texas

MELLEM,T. 1979b Offshore Handling of a Diving Bell through a Centerwell. Det Norske Veritas Report No.79-0590

MORISON,J.R.,O'BRIEN,M.P.,JOHNSON,J.W. & SCHAAF,S.A. 1950 The forces exerted by surface waves on piles. Pet.Trans., AIME Vol 189

NEWMAN,J.N. 1974 Interaction of water waves with two closely spaced vertical obstacles. J.Fl.Mech., Vol 66, pp 97-106

PEARCEY,H.H. 1984 The Effects of Reynolds Number and Keulegan Carpenter Number on Wave Force Coefficients - A Review of Relevant Data

PRANDTL,L. 1965 Stromungslehre. Friederick Vieweg & Sohn, Braunschweig.

RAWSTRON,P.J.M. & BLIGHT,G.J. 1978 Prediction of Weather Downtime for Derrick Barges. Proc.10th OTC, Houston, Texas

SARPKAYA,T. 1986 In-line and Transverse Forces on Smooth and Rough Cylinders in Oscillatory flow at High Reynolds Numbers. Interim Report for National Science Foundation, Washington DC. No NPS69-86-003

SAYER.P. & BAKER,J.H.A. 1986 Experimental Scaling Effects on the Hydrodynamics of Remotely Operated Vehicles. Proc.5th Int.Offshore Mechanics and Arctic Engg. Symp., Tokyo p272

SCHWARTZ,M. & SHAW,L. 1975 Signal Processing Discrete Spectral Analysis Detection and Estimation. McGraw-Hill, New York.

SPANGEBERG,S. & JACOBSEN,B.K. 1983 Reduction of the Water Motion in the Moonpool. Proc.MARINTEC OFFSHORE CHINA Conf., Shanghai

SPANOS,P-T.D. 1983 ARMA Algorithms for Ocean Wave Modeling. Trans.ASME J.Energy Resources Tech., Vol 105 pp 300-309

SPANOS,P-T.D. & HANSEN,J.E. 1981 Linear Prediction Theory for Digital Simulation of Sea Waves. Trans.ASME J.Energy Resources Tech., Vol 103 pp 243-249

TUCK,E.O. 1974 Transmission of waves through small apertures. J.Fl.Mech., Vol 49, 1974.

TUCKER,M.J.,CHALLENOR,P.G. & CARTER,D.J.T. 1984 Numerical simulation of a random sea: a common error and its effect upon wave group statistics. App.Ocean Res., Vol 6 No 2 pp 118-122

VAN DYKE,M. 1975 Perturbation Methods in Fluid Mechanics. The Parabolic Press, California.

WEHAUSEN,J.V. & LAITONE,E.V. 1960 'Surface Waves' from Handbuch der Physik IX. Springer-Verlag, Berlin.

WOLFRAM,J. & THEOPHANATOS,A. Division of Ship & Marine Technology, Dept of Mechanical and Offshore Engg., Univ.of Strathclyde. Personal Communication

A P P E N D I C E S

APPENDIX 2.1

MEASUREMENT OF THE MOONPOOL HYDRODYNAMIC COEFFICIENTS

In order to utilise the moonpool water column oscillation response model proposed in section 2.3, it is necessary to have numerical values for three hydrodynamic coefficients for the moonpool: the added mass coefficient a , and two damping coefficients ξ_2 and ξ_c. For moonpools with small damping values, these coefficients can be obtained from free oscillation tests; however for moonpools with large damping values this approach becomes impractical, as the oscillation dies to zero within a few cycles. A forced oscillation test must therefore be used.

The characteristic of the system which is most suitable for measurement using the forced oscillation test is the dynamic magnification factor (DMF), denoted D. This is defined as the ratio of the dynamic system response amplitude to the equivalent static response (ie the displacement which the system would undergo if a force of the same amplitude as the dynamic excitation were applied statically). This is given as:

$$D = H_m r_m / |F_m| \qquad \text{(A2.1.1)}$$

where H_m is the water column oscillation response amplitude. A forced oscillation test over a range of frequencies will yield the system response amplitude; the excitation may be calculated from the waveheights used using the source distribution method due to Frank as described in section 2.4.

The DMF may also be calculated directly, using the hydrodynamic coefficients for the moonpool. The equation of motion for the water column oscillation is given in equation (2.5) as:

$$m_m \ddot{Z}_m + C_m \dot{Z}_m + r_m Z_m = Re\left[F_m e^{-i\omega t}\right]$$

This leads to an expression for the DMF of the system (see for example Clough & Penzien [1975]) as:

$$D = \left[(1-\beta)^2 + (2\xi\beta)^2\right]^{-1/2} \qquad \text{(A2.1.2)}$$

where β is the ratio of the forcing frequency, ω to the undamped natural frequency ω_n, and ξ is the ratio of the system damping c_m to the critical damping c_c. The undamped natural frequency ω_n is given by equation (2.8) as:

$$\omega_n = \left[g/T(1+a_m)\right]$$

and thus:

$$\beta = \omega\left[g/T(1+a_m)\right]^{-1/2} \qquad \text{(A2.1.3)}$$

The critical damping for the system is given as:

$$c_c = 2m_m\omega_n$$

where m_m, the virtual mass of the system is given in equation (2.6) as:

$$m_m = \rho A_m T(1+a_m)$$

and thus:

$$\xi = \frac{c_m}{2\rho A_m}\left[gT(1+a_m)\right]^{-1/2} \qquad \text{(A2.1.4)}$$

Thus if a_m and c_m are known, substitution of (A2.1.2) and (A2.1.3) into (A2.1.1) yields a solution for the DMF at any given forcing frequency ω.

The hydrodynamic coefficients a_m and c_m can thus be obtained by an iterative procedure; a guess is made as to their values, and the corresponding DMF calculated. This is then compared with the actual dynamic magnification factor

measured in the forced oscillation test and the comparison used to improve the estimate. This comparison relies on the assumption that the damping is linear. In order to conform to this assumption, the test should be carried out in such a way that the damping is constant with frequency; ie the waveheight at each frequency should be chosen such that the system response remains constant.

The result of this test then is the value of the added mass coefficient a_m, and a value for the equivalent linear damping c_m at whatever constant oscillation amplitude was chosen. In order to obtain the values of the two damping coefficients describing the non-linearity of the damping, a further test is required. If the ratio β in (A2.1.2) is set to unity, then the expression reduces to:

$$D = 1/2\xi \qquad \text{(A2.1.5)}$$

Knowing a_m, (from the first test) the undamped natural frequency ω_n can be calculated, and a series of tests carried out at this frequency with varying wave amplitude. The damping ratio can then be calculated for each test using (A2.1.5), and the two damping coefficients obtained by regression of these damping ratio values against the non-dimensional response amplitude H_m / T.

The tests were carried out with the moonpools mounted in a ship model, for three reasons. Firstly, it was felt that similarity between the model and the full scale would be obtained more closely if the moonpools were mounted in a ship raither than simply fixed in the tank on their own. The flow at the moonpool exit is found to have a pronounced effect on the moonpool performance (see chapter 7), and the fluid flow around a 90° corner (for a ship mounted moonpool) will be quite different from the flow around a 180° corner (for an isolated moonpool). Secondly, the waves in the tank were found to behave better with regard to stray reflections with

a ship model in the tank, rather than an isolated moonpool. Finally, the excitation on the moonpool, Fm, can reasonably be calculated using a 2D model if the moonpool is ship mounted; for the case of an isolated moonpool, a full 3D solution would be required in order to include the effects of wave diffraction. The pressures at the moonpool base were measured in order to test the accuracy of the calculations; Figure A2.1.1 shows the comparison of theoretical and experimental results. The discrepancy between the two in the frequency band around 0.6 - 0.64 Hz was due to the poor quality of the waves at these frequencies; other tests also showed erratic results in this range. It can be seen that apart from this small frequency band the agreement between experimental and theoretical results is excellent.

The main assumption made about the moonpool is thus that the flow in and out of the moonpool is similar between the ship used in the lab tests, and the full scale ship. It was not possible to test this assumption experimentally, since only one ship was available for use. However, for flat bottomed ships there are no obvious physical reasons why the assumption should not be valid. In the case of a full scale ship where the moonpool is sited in a part of the hull with distinct curvature, it may become necessary to build a model of the ship as well as the moonpool.

It did not prove practical to hold the water column oscillation constant during the first test, as the range of wave amplitudes available at a given frequency was not always large enough to accomodate the range of RAO values found. A compromise was reached where the wave height was kept constant over the frequency range; this had the advantage that the same values for voltage amplitude could be sent to the wavemakers for every test. The error induced by this approximation is not quantifiable; if a test could be carried out at a constant response amplitude in order to assess the effect of the error, then the approximation would not be

needed in the first place.

The tests were carried out in the wave tank at the Department of Ship and Marine Technology at the University of Strathclyde. The wavemakers were driven by a programmable Frequency Response Analyser which was addressed by a Sirius Microcomputer. The response of the water column oscillation and the waves outside the moonpool were measured with resistance type wave probes; the analogue signals produced were sampled using a Rexagen analogue to digital (a/d) converter, and the digital values obtained written to the memory of the computer. A schematic diagram showing the equipment used is given in figure A2.1.2.

A program was written which allowed the measurement of the DMF for all frequencies of interest with no intervention required. For each frequency, the voltage appropriate to the chosen constant waveheight was read from a 'look-up' table. The computer then instructed the Frequency response analyser to drive the wavemakers at the chosen frequency with the voltage amplitude read. A delay period then ensued whilst the waves and the water column oscillation 'settled down' to a steady state. Time histories for the water surface elevation inside and outside the moonpool were then measured and the results stored in memory. The waves were switched off, and the results processed to give wave and water column response amplitudes; these were written to the disc. The wave probes were then sampled until the water in the tank and in the moonpool was calm; the next frequency would then be run. The results could then be analysed to find the added mass coefficient a_m and the undamped natural frequency ω_n ; this was achieved by estimating the added mass and equivalent linear damping, and plotting the theoretical DMF given by (A2.1.2) against the experimental procedure, then iterating to find the best fit. It was found that a visual method gave better agreement than an attempt to fit the results using a regression type approach for two reasons: firstly because

the regression procedure had to be carried out iteratively due to the form of (A2.1.2) and it proved to hard to establish an error criterion which was appropriate to the whole range of added mass and damping values found in the tests; secondly because any data points which were obviously incorrect due to experimental problems could be ignored by eye. An example of the quality of fit obtained is given in Figure A2.1.3. Having obtained the added mass for the moonpool, a similar procedure was carried out with a second program, running waves at the natural frequency with varying amplitudes. Regression of the damping ratio values thus obtained against the non-dimensional response amplitude H_m/T yielded the two coefficients required. An example of the fit of the two coefficient model to the data obtained is shown is Figure A2.1.4.

In practice the method described worked well, giving RAOs (and hence DMFs) which closely fitted the theoretical model; however results at certain frequencies were less reliable than the rest; as mentioned before, the waves appeared badly shaped (ie not sinusoidal) between 0.6 and 0.64Hz. It was concluded that this represented a resonance of the tank itself, at which standing waves were dominant. A further problem was associated with waves above 1.1 Hz, in that significant transverse waves were generated by the diffraction about the ship model; these took a considerable time to die down, as the tank possessed no damping for such waves.

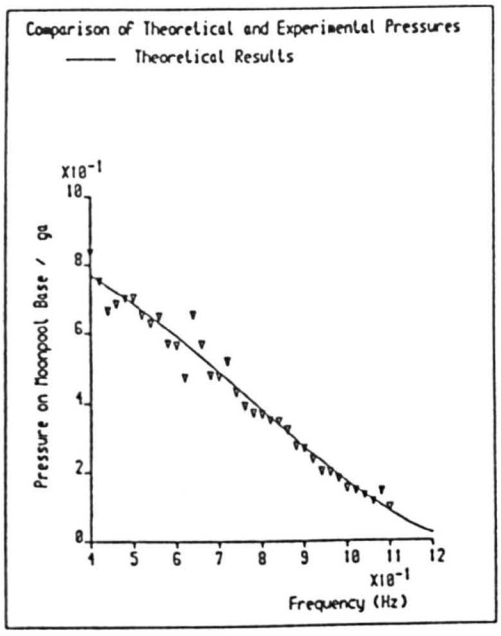

Figure A2.1.1

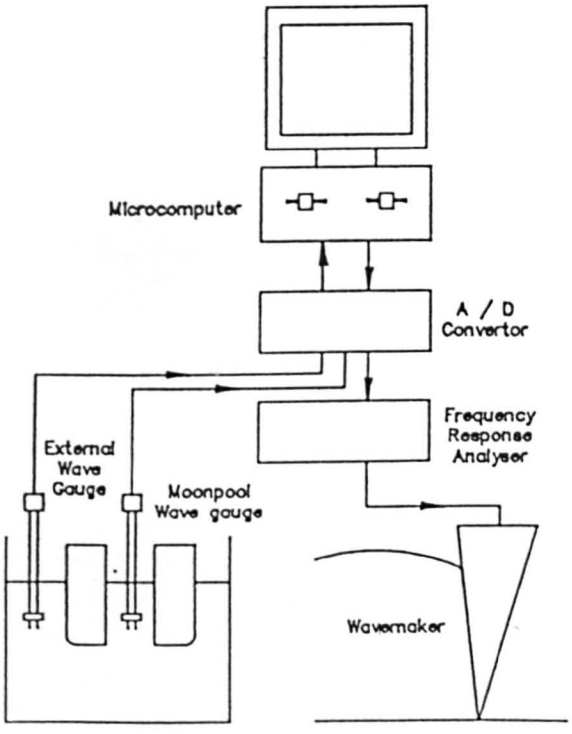

Figure A2.1.2

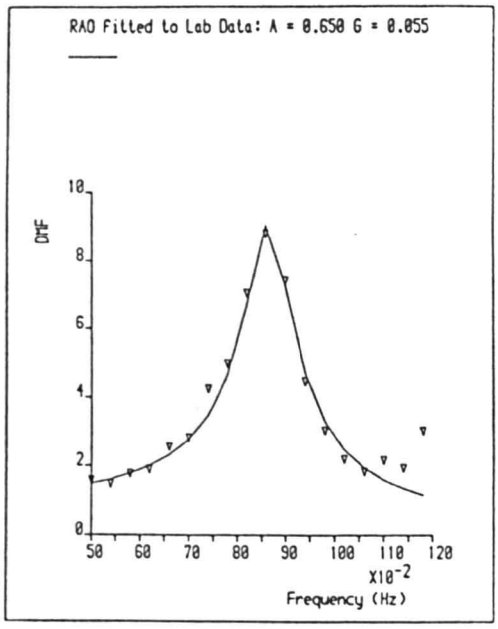

Figure A2.1.3

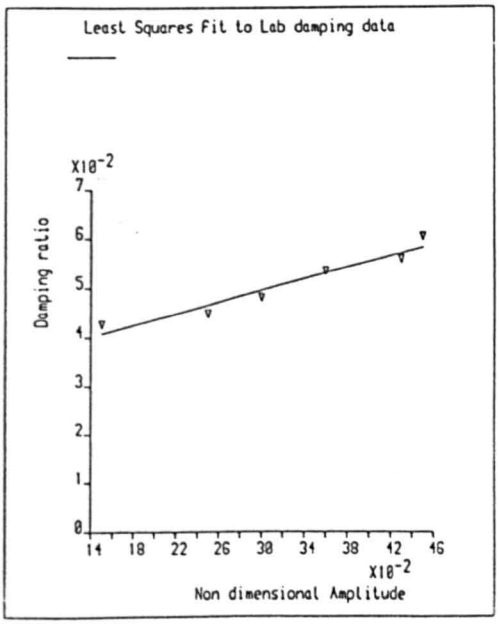

Figure A2.1.4

APPENDIX 2.2

HYDRODYNAMIC COEFFICIENTS FOR THE MOONPOOLS TESTED

Moonpool	1	2	3
	$a_m = 0.27$	$a_m = 0.22$	$a_m = 0.40$
	$\xi_1 = 0.0113$	$\xi_1 = 0.0101$	$\xi_1 = 0.0007$
	$\xi_c = 0.1846$	$\xi_c = 0.2163$	$\xi_c = 0.1897$

APPENDIX 2.3

SIGNIFICANT MOONPOOL OSCILLATIONS: PREDICTED AND MEASURED

Realisation	1	2	3
Moonpool			
	2.03	3.86	5.14
1	2.50	4.68	5.70
	2.18	4.34	5.57
	14.7%	7.8%	2.3%
	2.25	3.73	4.84
2	2.58	4.11	5.04
	2.28	3.72	4.92
	13.2%	10.5%	2.4%
	1.89	3.49	4.50
3	2.75	5.62	6.24
	2.63	5.97	6.67
	4.6%	-5.9%	-6.4%

In each case the first number is the measured significant waveheight (cm), the second and third are the predicted and measured significant water column oscillations, and the fourth is the absolute percentage error between the predicted and measured values.

APPENDIX 3.1

THE FORCE COEFFICIENTS FOR A SUBSEA UNIT IN A MOONPOOL

In order to use either of the methods proposed for the calculation of the random process statistics for the force on the subsea unit inside the moonpool, it is necessary to have numerical values for the force coefficients (inertial and drag) for the unit inside the moonpool. Before these may be measured it is necessary to determine what factors will affect the coefficients, in order that appropriate steps may be taken in the experimental method.

The values will depend very strongly on the blockage coefficient (defined as the ratio of the projected area of the subsea unit to the cross sectional area of the moonpool); the nominal flow velocity will be calculated on the basis of the velocity of the free surface, whilst local velocities may be much higher. Some measurements have been made for small smooth spheres falling in cylindrical vessels (eg Fidleris and Whitmore [1961]), but it is felt that the differences in the flow regime around a smooth sphere and a subsea unit are too great for any direct comparison to be made. Madsen [op.cit.] and Gran [op.cit.] attempted to derive empirical relationaships between force coefficients and blockage ratios, but Gran's comparison of their results with full scale measurements show serious discrepancies. This is perhaps not surprising, as there is a great variation in the shape of both subsea units and moonpools which cannot be accounted for using this approach. In addition problems arise as to how the precise definition of projected areas may be achieved (eg in the case of a diving bell whether the projected area is defined in terms of the pressure hull or whether the appendages on the outside such as emergency gas bottles and protective cages should be included). In order to sidestep these difficulties, the measurements of the force coefficients may be carried out using a model of the unit

inside a model of the moonpool, thus eliminating any doubt about the effects of unit or moonpool shape at the extra cost of the construction of one (or more) moonpool models at the same scale as the subsea unit model required anyway.

The values of the force coefficients will also depend upon the Reynolds Number attained during the tests, defined as:

$$R_e = V_{max} D / \nu \qquad \text{(A3.1.1)}$$

where

Vmax is the maximum flow velocity attained

D is the characteristic dimension of the subsea unit (in this case the vertical dimension of the unit)

ν is the kinematic viscosity of sea water (~ 0.000011)

In the case of simple harmonic motion, the equation can be written as:

$$R_e = \frac{2\pi a D}{\nu T} \qquad \text{(A3.1.2)}$$

where

a is the amplitude of the motion (in this case the water column oscillation amplitude)

T is the period of the motion

In order to represent accurately the full scale case, the Reynolds Number should be in the same range for the model testing as for the full scale system. It is known, however, that the coefficients do not vary significantly with Reynolds number once the values are sufficiently high, and supercritical, or fully turbulent, flow is established; this value of Re is sometimes denoted Rp. The values of Rp have not been studied to any great extent for subsea units; Sayer and Baker [1986] conducted steady velocity measurements for the RCV225 ROV which show that the drag coefficient does not vary significantly for Re > 200000; however many subsea units

will have significantly larger appendages than the RCV225 (eg protection frames, lighting, gas bottles etc.) leading to supercritical flow at lower Reynolds Numbers. Bishop [1984] using results from Pearcey [1984] concludes that, in the case of wave forces on cylinders, Rp reduces significantly in oscillatory flow conditions; the value dropping from Rp = 1000000 for a slightly roughened cylinder in steady flow to Rp = 35000 for the same cylinder at Kc = 6. Considering both of these factors, it is quite likely that for subsea units with large appendages in oscillatory flow the force coefficients would not vary significantly for quite small Reynolds numbers; possibly as low as 20000.

The range of Reynolds numbers occurring at full scale can be illustrated by considering two examples; one for a small oscillation at a high frequency, and one for a large oscillation at a lower frequency. If the full scale subsea unit were 2.5m deep, and the water column oscillation in the moonpool had an amplitude of 1m with a period of 4s, then the Reynolds Number would be of the order of 350000. If the oscillation had an amplitude of 4m with a period of 7s then the Reynolds Number would be of the order of 800000. In general, then, the flow regime around the unit would thus be supercritical in all cases, and the force coefficients for the subsea unit would not be greatly affected by the Reynolds Number. This suggests that the experimental technique required to obtain the force coefficients must attain a Reynolds Number of at least 20000 to simulate accurately the flow around the unit; as long as this value is obtained, then the Reynolds Number can be safely disregarded.

The values calculated for the hypothetical full scale case given here are based on the nominal maximum velocity (ie the maximum velocity of the free surface inside the moonpool); the maximum local velocity will be greater than this by a factor:

$$V_L = V_n / [1 - A_B/A_M] \qquad \text{(A3.1.4)}$$

where V_L is the nominal maximum flow velocity
V_n is the maximum local flow velocity
A_M is the cross sectional area of the moonpool
A_B is the cross sectional area of the subsea unit

This will have the effect of increasing the Reynolds Numbers locally. The maximum increase due to this effect is likely to be of the order of five, corresponding to a blockage coefficient of 0.8. This increase will not affect the conclusions drawn in either case; as previously stated, a further increase in Reynolds Number beyond Rp will provide no significant variation in force coefficients.

Since the flow around the subsea unit is oscillatory, the force coefficients will also depend upon the Keulegan-Carpenter Number (Kc), where Kc is defined as:

$$K_c = V_{max} T / D \qquad \text{(A3.1.4)}$$

For simple harmonic motion this may be rewritten as:

$$K_c = 2\pi a / D \qquad \text{(A3.1.5)}$$

There appears to be no published work showing the dependancy of force coefficients for subsea units; results published by Sarpkaya [1986] for cylinders with surface roughness of 1/50 and Wolfram and Theophanatos [1986] for cylinders of roughness 1/20 suggest that there is a strong dependancy between the force coefficients and the Keulegan-Carpenter Number for Kc < 30. The hypothetical cases discussed earlier for the subsea unit in a moonpool would yield 2.5 < Kc < 10 on the basis of the nominal flow velocity. Since the Keulegan-Carpenter number effects relate to the way the turbulent wake oscillates back and forwards over the body, the argument for increasing the velocity value used to

calculate Kc from the nominal value to the local value becomes much more suspect in the case of Kc (as compared to Re), as the main oscillation of the wake will probably take place at a similar frequency to the frequency of oscillation of the water column.

The experimental technique must, therefore, measure the coefficients at a Keulegan-Carpenter Number appropriate to the water column oscillation which will occur in the full scale case. Since it is likely that the force random process statistics will be required for a range of sea states, a range of tests should be performed at varying Keulegan-Carpenter Numbers. The force coefficients used to calculate the force random process statistics should be chosen on the basis of a value of Kc typical in some way of the water column oscillation spectrum concerned. The exact procedure of choosing a typical value of Kc for such a calculation is not immediately obvious, and further study of the problem would be of great use.

In order to measure the inertial and drag coefficients at the appropriate values of Re and Kc, it is necessary to use a sinusoidal distribution of fluid velocity (and hence acceleration) past the subsea unit. The inertial coefficients can then be obtained by examining points where the flow velocity is zero, and the drag coefficient by examining the points where the flow acceleration is zero. A regression technique may alternatively be used to fit the data at all points in the record.

The experimental procedure adopted for the measurement of the inertial and drag coefficients of the subsea unit in the moonpool was based quite heavily on the procedure established for the measurement of the moonpool hydrodynamic coefficients described in Appendix 2.1. The moonpool was mounted in a ship model and the subsea unit fixed in position in the moonpool using a specially designed force measurement rig.

The measurement of the force on the bell was carried out using a tension/compression force transducer with a maximum rating of 10lb. The transducer was driven with a bridge amplifier with variable gain; due to the high output of the transducer, the gain could be kept to less than 100x, virtually eliminating electrical noise. The transducer was, however, very delicate with regard to out of plane loading; in order to protect it from any side forces on the unit (due for example to slight asymmetry of the unit in the moonpool) the force was transmitted to the transducer using a slide running through four roller bearings.

The initial intention was to force oscillate the bell inside the moonpool, thus giving known velocities and accelerations from which the coefficients could be calculated. When this was tried, however, it was found that the bell motion excited a substantial water column oscillation. This meant that the water surface elevation would have to be recorded in addition to the bell position in order to determine the flow velocity relative to the unit. It was therefore decided to use the water column oscillation excited by external waves to provide the force excitation. The water surface elevation was recorded using a wave probe in the moonpool, and the force on the bell recorded using the force transducer mentioned above. This approach has the additional advantage of representing the actual flow conditions more accurately than would be the case if the unit were to be oscillated. For tests which are intended to model real subsea units, however, the forced oscillation approach would probably have to be adopted, as the oscillation of the water column due to the wave excitation using the second approach would be too small to allow realistic Reynolds Numbers (ie Re > 20000) to be attained at the appropriate Keulegan-Carpenter Numbers without building very large scale models. The subsea units could then be oscillated inside a long tube (representing the moonpool), positioned such that free surface oscillations were minmised. This might be achieved be positioning the

tube horizontally in the test tank, so that the tube did not break the free surface.

Since the factor to be varied between tests was the Keulegan-Carpenter Number, a series of frequencies were chosen for which the water column oscillation response of the moonpool varied substantially. The control system for the tests was exactly as in the moonpool coefficient measurements described in Appendix 2.1; the results were stored in the form of realisations of force and water column elevation. The velocity and acceleration of the fluid flow were calculated from the water column elevation data; however, due to the noise on the data and the relatively small number of samples in each full cycle of oscillation (less than fifteen samples/cycle in most cases) the simple difference equations given in equation (3.1) could not be used with any reliability. An eight point moving average differentiator was found to give sufficient smoothing to allow accurate calculation of the values; this can be expressed in the form:

$$\left(\frac{dx}{dt}\right)_i = \frac{1}{\Delta t}\left[\frac{(x_{i+3}-x_{i-4})}{28} + \frac{(x_{i+2}-x_{i-3})}{20} + \frac{(x_{i+1}-x_{i-2})}{12} + \frac{(x_i-x_{i-1})}{4}\right] \quad \text{(A3.1.6)}$$

Knowing the velocity and the acceleration time history, the coefficients were obtained by an iterative curve fitting procedure.

A schematic diagram and photographs showing the force measurement rig with the subsea unit in the moonpool are shown in Figures A3.1.1-A3.1.2. An example of the fit obtained to the force realisation is given in Figures A3.1.3(a-d). It can be seen that the fitted force suffers from significant noise in some cases, whilst the measured force is fairly smooth. This noise is due to irregularities in the measured water surface elevation, which, despite smoothing, leads to substantial fluctuations in the calculated flow velocity and acceleration. If the tests were carried out using the forced oscillation approach then these

fluctuations could be largely removed, and a better fit obtained. Some of the discrepancies between fitted and measured force do, however, undoubtedly arise as a result of the inertial and drag coefficients varying with the direction of flow and the proximity of the free surface; these effects would repay further study.

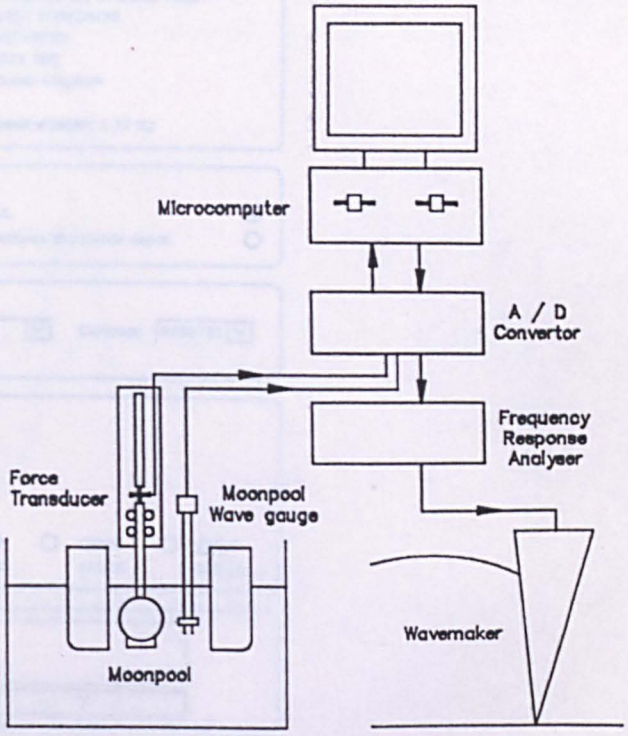

Figure A3.1.1

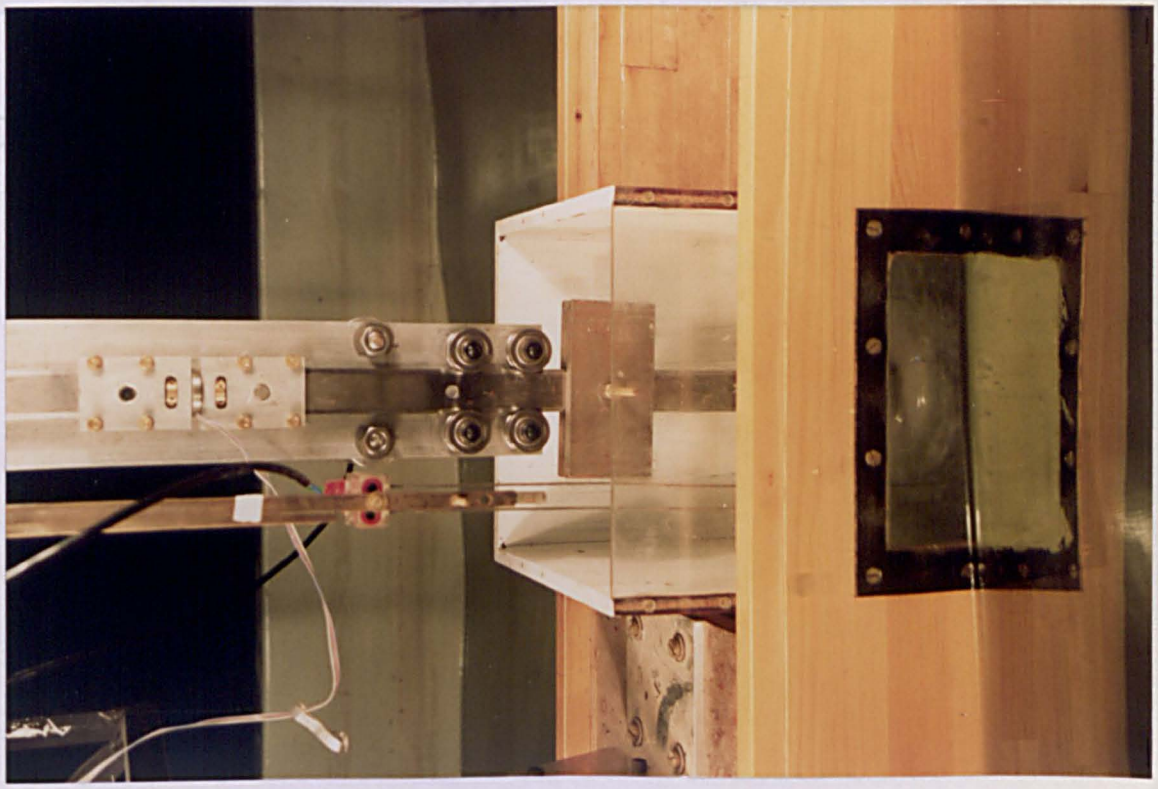

Figure A3.1.2

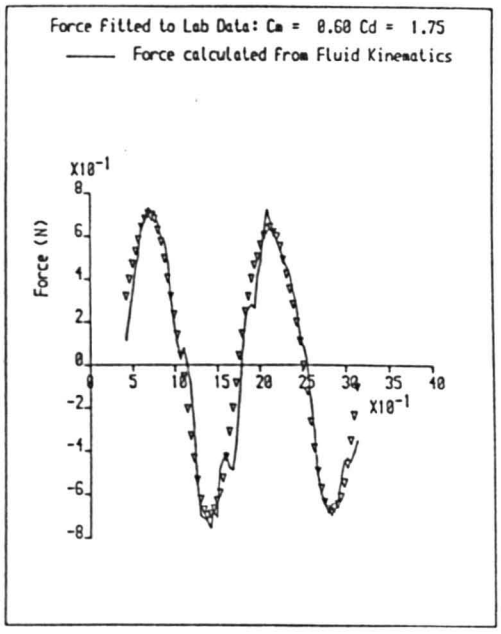

Figure A3.1.3a

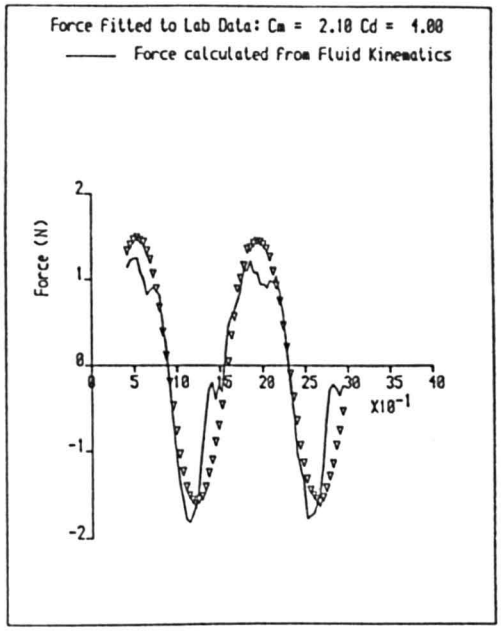

Figure A3.1.3b

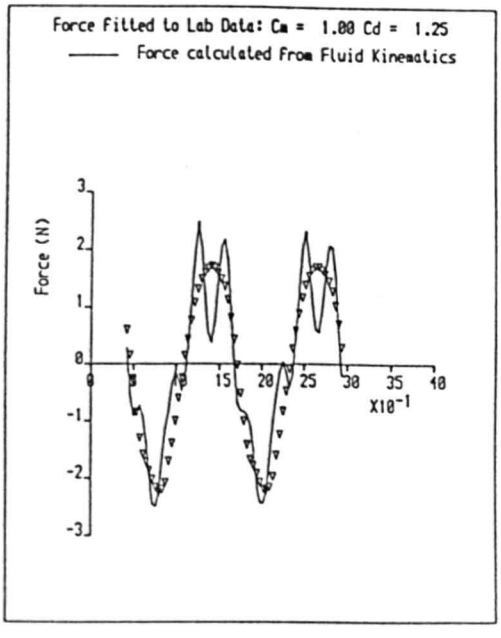

Figure A3.1.3c

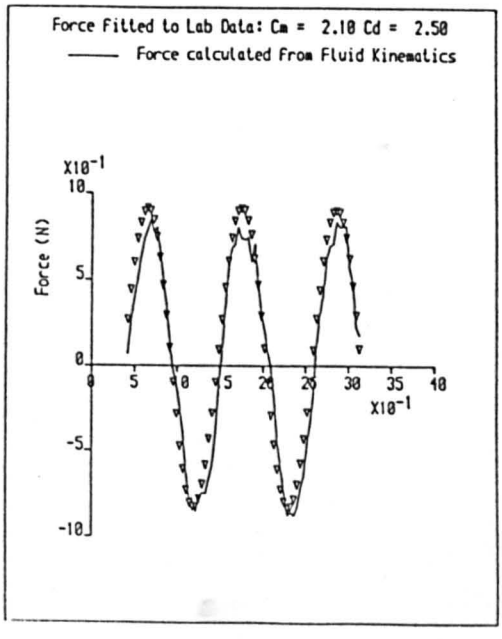

Figure A3.1.3d

APPENDIX 3.2

CALCULATION OF WATER SURFACE TIME HISTORY

The calculation of water surface elevation realisations z (t) from the power spectrum of the random process S (f) is generally based on the assumption that the elevation follows a zero mean Gaussian distribution, and can be calculated from the summation of a series of Fourier components:

$$z(t) = \sum_{n=1}^{N} C_n \cos(2\pi f_n t + \Phi_n) \qquad \text{(A3.2.1)}$$

where N is the number of components used

f_n are fixed frequencies

c_n are fixed amplitudes obtained from the assumed power spectrum

Φ_n are phases with a uniform random distribution between 0 -> 2π

This may be written alternatively in terms of cosine and sine components as:

$$z(t) = \sum_{n=1}^{N} a_n \cos 2\pi f_n t + b_n \sin 2\pi f_n t \qquad \text{(A3.2.2)}$$

where $a_n^2 + b_n^2 = c_n^2$

and $\tan (b_n / a_n) = \Phi_n$

or in complex form as:

$$z(t) = \sum_{i}^{N} Z_n e^{i 2\pi f_n t} \qquad \text{(A3.2.3)}$$

where $Z_n = a_n - ib_n$. This formulation is, however, only valid as N -> ∞ (see Cartwright & Longuet-Higgins [1956]). If N is finite, then the use of deterministic amplitudes c_n will lead to reduced values of the variance, and a non-Gaussian representation of the elevation (Tucker et al [1984]). An alternative formulation is thus proposed wherein

the elevation does follow a Gaussian distribution despite the finite number of components.

If the number of components N is finite, then the length of record z (t) which can be created without repetition is also finite. If z (t) consists of N values sampled discretely at sampling interval Δt, and the frequencies f_n are equally spaced from $1 / N\Delta t \rightarrow 1 / \Delta t$, then:

$$f_n = n/N\Delta t$$
$$\Delta f_n = 1/N\Delta t$$
$$t_r = r\Delta t$$

and (A3.2.3) becomes:

$$z_r = \sum_{n=1}^{N} Z_n e^{i2\pi rn/N} \qquad \text{(A3.2.4)}$$

where Z_n is given by the expression:

$$Z_n = a_n - ib_n \qquad \text{(A3.2.5)}$$

Here a_n and b_n are Gaussian random variables with variance $\sigma_n = S_{zz}(f)\ df$.

This may alternatively be expressed in the form:

$$Z_n = c_n \cos\phi_n - i c_n \sin\phi_n \qquad \text{(A3.2.6)}$$

where
c_n is a Rayleigh random variable with an RMS value of $\sqrt{2\sigma_n}$
ϕ_n is uniformly randomly distributed between $0 \rightarrow 2\pi$.

The amount of computer time required to find a solution of (A3.2.4) depends heavily on the method used to find the solution. It would be possible to calculate all the values of Z_n and simply sum all the components at each time step r.

This would be an extremely inefficient means of arriving at a solution; it is much more efficient to use an inverse discrete Fourier transform (IDFT), particularly if the most efficient form of algorithm, the inverse fast Fourier transform (IFFT) is employed. This approach is suggested by Cuong et al [1982]; however Cuong's formulation uses the second formulation for Z_n (A3.2.6); in practice, the first formulation (A3.2.5) will be more efficient as the calculation of two gaussian distributed random numbers can be achieved more quickly than the calculation of one uniformly distributed and one Rayleigh distributed random number.

The series of Fourier Coefficients Z_n is thus taken as a series of N complex numbers $(a_n - ib_n)$, where N will usually be chosen as a power of two in order to optimise the IFFT algorithm used. However, if the realisation is obtained simply by choosing Δt such that $1 / \Delta t$ is equal to the maximum frequency present in the spectrum $S_{zz}(f)$, (denoted here as f_m) calculating the N terms, and taking an IFFT of this series, then the phenomenon of aliasing will cause the the realisation to be unrepresentative of the spectrum, since, according to the Shannon criterion, the maximum frequency f_s for which (A3.2.4) is valid is:

$$f_s = 1/2\Delta t$$

If S_{zz} is considered non-zero over the frequency range $0 \rightarrow f_m$ then, in order to satisfy the Shannon criterion, f_m must be set equal to f_s, corresponding to the $N / 2$ th component. In order to ensure a smooth realisation where no frequency components higher than f_m are present, then the remaining $N / 2$ terms are padded with zeros up to the frequency $2f_m$, such that N points are actually considered.

Further smoothing may be achieved by padding the series with an additional N zeros, increasing f_{max} to $4f_m$, and reducing the time increment to $\Delta t / 2$. The process of smoothing by adding zeros could be continued, but at a significant cost in computer time.

APPENDIX 3.3

HYDRODYNAMIC COEFFICIENTS FOR THE MOONPOOLS TESTED WITH A BELL

Moonpool	1	2	3
	$A_s / A_M = 0.695$	$A_s / A_M = 0.545$	$A_s / A_M = 0.283$
	$a_m = 1.2$	$a_m = 0.80$	$a_m = 0.55$
	$\xi_{r_1} = 0.0369$	$\xi_{r_1} = 0.0202$	$\xi_{r_1} = 0.0238$
	$\xi_{r_c} = 0.8643$	$\xi_{r_c} = 0.4415$	$\xi_{r_c} = 0.1114$

APPENDIX 3.4

SIGNIFICANT OSCILLATIONS FOR MOONPOOLS WITH BELL: PREDICTED AND MEASURED

Realisation	1	2	3
Moonpool			
	3.13	4.40	6.03
1	1.12	4.08	6.00
	0.88	3.72	5.25
	27.3%	9.7%	14.3%
	1.86	3.17	4.54
2	1.19	4.61	5.27
	1.27	5.18	5.62
	6.3%	11.0%	6.6%
	3.20	4.44	5.61
3	2.26	6.70	7.08
	2.45	7.42	7.38
	8.4%	9.7%	4.1%

In each case the first number is the measured significant waveheight (cm), the second and third are the predicted and measured significant water column oscillations, and the fourth is the absolute percentage error between the predicted and measured values.

APPENDIX 3.5

FORCE COEFFICIENTS FOR THE BELL IN THE MOONPOOLS TESTED

Moonpool	1	2	3
	$A_B/A_M = 0.695$	$A_B/A_M = 0.545$	$A_B/A_M = 0.283$
	Cm = 2.1	Cm = 1.25	Cm = 0.60
	Cd = 4.0	Cd = 1.00	Cd = 1.75
	Re = 1700	Re = 570	Re = 1460
	Kc = 0.92	Kc = 0.22	Kc = 0.79

APPENDIX 3.6

SIGNIFICANT FORCE ON THE BELL IN THE MOONPOOL: PREDICTED AND MEASURED

Realisation	1		2		3	
Moonpool						
1	0.759		2.576		2.829	
	0.852	10.4%	2.582	0.2%	2.776	1.8%
	0.827	12.2%	2.557	0.7%	2.759	2.5%
2	1.253		4.089		3.113	
	1.370	9.4%	4.076	0.3%	3.201	2.8%
	1.355	8.1%	4.035	1.3%	3.174	1.9%
3	1.299		3.517		3.064	
	1.474	13.4%	3.666	4.7%	3.341	9.0%
	1.462	12.5%	3.641	3.5%	3.320	8.4%

In each case the number on the first row is the measured significant force (N), the numbers on the second row are the significant force (N) predicted using the frequency domain approach and the error in the prediction, whilst the numbers on the third row are the significant force (N) predicted using the time domain method, and the error in the prediction.

APPENDIX 4.1

SOLUTION OF THE INNER REGION FOR A SMOOTH DUCT

Consider the flow-field bounded by the rigid walls as shown in Figure A4.1.1a. The flow field is transformed into the upper half of the ζ-plane, with the boundaries of the z-plane on the real axis of the ζ-plane, as shown in Figure A4.1.1b. The appropriate Schwarz-Christoffel transform is given in (4.1) as:

$$z = \mathbb{K} \int_0^{\zeta} t^{1/2}(t-1)^{-1}\, dt + \mathbb{L} \qquad (4.1.1)$$

subject to the boundary conditions

$$z = b \quad @ \quad \zeta = 0 \qquad (4.1.2)$$

$$Re[z] = 0 \quad @ \quad \zeta > 1 \qquad (4.1.3)$$

The evaluation of the integral yields an expression for z:

$$z = \mathbb{K}\left[2\zeta^{1/2} + \ln \frac{\zeta^{1/2}-1}{\zeta^{1/2}+1} - i\pi\right] + \mathbb{L} \qquad (4.1.4)$$

Substitution of (4.1.2) into this expression yields:

$$\mathbb{L} = b \qquad (4.1.5)$$

Substitution of (4.1.3) into (4.1.4) yields:

$$Re\left[\mathbb{K}\left(2\zeta^{1/2} + \ln \frac{\zeta^{1/2}-1}{\zeta^{1/2}+1} - i\pi\right] + b\right] = 0$$

and hence

$$-i\mathbb{K}\pi + b = 0$$

thus

$$K = \frac{-ib}{\pi} \qquad (4.1.6)$$

The potential in the ζ-plane is given by Equation (4.6) as

$$\zeta = 1 + e^{\alpha w + \beta} \qquad (4.1.7)$$

Substitution of this expression into (4.1.6) gives the complete solution for the inner region:

$$z = \frac{-ib}{\pi}\left[2(1+e^{\alpha w+\beta})^{1/2} + \ln\frac{(1+e^{\alpha w+\beta})^{1/2}-1}{(1+e^{\alpha w+\beta})^{1/2}+1}\right] \qquad (4.1.8)$$

This expression may be used to obtain a streamline / potential line plot for the smooth duct. Figure A4.1.2 shows such a plot for a duct with $\varepsilon = 0.1$.

The constants α and β must now be found. The asymptote of this expression in the overlap domain is found by taking the leading term

$$z = \frac{-ib}{\pi}\, 2(1+e^{\alpha w+\beta})^{1/2}$$

yielding:

$$\alpha w + \beta = -i\pi + 2\ln\frac{\pi}{2b} + \ln\left(z^2 + \frac{4b^2}{\pi^2}\right)$$

Writing $z = re^{i\theta}$ gives:

$$\alpha w + \beta = -i\pi + 2\ln\frac{\pi}{2b} + \ln\left[r^2\cos 2\theta + \frac{4b^2}{\pi^2} + ir^2\sin 2\theta\right]$$

and writing $r^2\cos 2\theta + 4b^2/\pi^2 + i\, r^2 \sin 2\theta$ as $R\, e^{i\tau}$:

$$\alpha w + \beta = -i\pi + 2\ln\frac{\pi}{2b} + \tfrac{1}{2}\ln R^2 + i\tau$$

where

$$R^2 = r^4\left[1 + \frac{8}{\pi^2}\cos 2\theta\left(\frac{b}{r}\right)^2 + \frac{16}{\pi^4}\left(\frac{b}{r}\right)^4\right]$$

Hence if (b / r) << 1 :

$$\alpha w + \beta = -i\pi + 2\ln\frac{\pi}{2b} + 2\ln r + i\tau$$

and

$$\phi = \frac{2}{\alpha}\ln\frac{\pi r}{2b} - \frac{\beta}{\alpha} \qquad (4.1.9)$$

The asymptote high up in the duct is found by rearranging (4.1.8) as

$$z = \frac{-ib}{\pi}\left[2\zeta^{1/2} + \ln(\zeta-1) - 2\ln(1+\zeta^{1/2})\right] \qquad (4.1.10)$$

and letting $\zeta \to 1$:

$$z = \frac{-ib}{\pi}\left[2 + \alpha w + \beta - 2\ln 2\right]$$

thus

$$\frac{\pi y'}{b} = \alpha\phi + \beta + 2(1-\ln 2)$$

Substituting y' = (a - y) yields the potential:

$$\phi = \frac{1}{\alpha}\left[\frac{\pi}{b}(a-y) - \beta - 2(1-\ln 2)\right]$$

This expression is substituted into the free surface boundary condition

$$K\phi + \frac{\partial\phi}{\partial y} = 0\Big|_{y=0}$$

to yield β :

$$\beta = \frac{\pi}{b}\left[\frac{1}{K} - a\right] - 2(1-\ln 2) \qquad (4.1.11)$$

NB This expression differs from that given in Lee [1982].

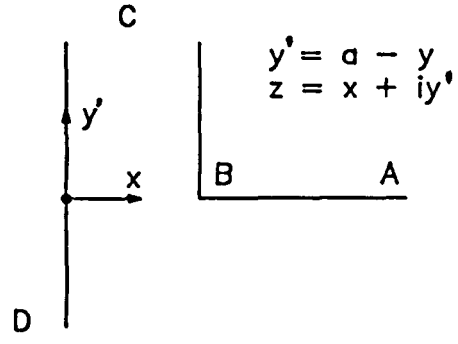

Figure A4.1.1a

Figure A4.1.1b

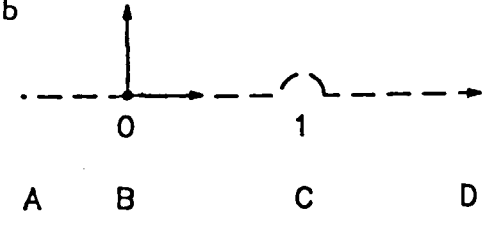

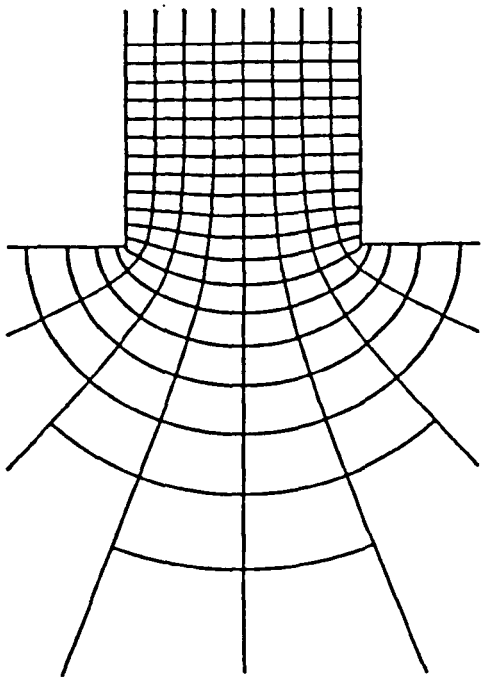

Figure A4.1.2

APPENDIX 4.2

SOLUTION OF THE INNER REGION FOR A DUCT WITH A THIN BAFFLE AT THE EXIT

Consider the flow-field bounded by by the rigid walls as shown in Figure 4.5a. The flow field is transformed into the upper half of the ζ -plane, with the boundaries of the z-plane on the real axis of the ζ -plane, as shown in Figure 4.5b. The appropriate Schwarz-Christoffel transform is given in the form

$$z = K \int_0^{\zeta} F(t)\,dt + L \tag{4.2.1}$$

where $F(t) = t\,(t - k)^{-1/2}(t - 1)^{-1}$ subject to the boundary conditions

$$z = b - p \quad @ \quad \zeta = 0 \tag{4.2.2}$$

$$z = b \quad @ \quad \zeta = k \tag{4.2.3}$$

$$Re[z] = 0 \quad @ \quad \zeta > 1 \tag{4.2.4}$$

Substitution of (4.2.2) into (4.2.1) yields:

$$L = b - p \tag{4.2.5}$$

whilst substitution of (4.2.3) into (4.2.1) yields:

$$K = P \Big/ \int_0^k F(t)\,dt \tag{4.2.6}$$

Finally, substituting of (4.2.4) into (4.2.1) and taking the real part of the expression yields:

$$b - p + P \Big/ \int_0^k F(t)\,dt \cdot i\,Im\left[\int_0^{\zeta} F(t)\,dt\right] = 0 \Big|_{\zeta > 1} \tag{4.2.7}$$

There are two contributions to the imaginary part of

$\int_0^\zeta F(t)\,dt$: the integral from $\zeta = 0$ to $\zeta = k$ and the contour integral around the simple pole at $\zeta = 1$ in the upper half plane (see Figure (4.5b)). This integral is now evaluated.

Considering the integral all the way around the singularity ($\oint F(t)\,dt$) it is seen that

$$\oint F(t)dt = \int_0^k F(t)dt + \int F(t)dt$$

and hence

$$\oint F(t)dt = \int_0^k F(t)dt + \int \overline{F(t)}\,\overline{dt}$$
$$= 2i\,\mathrm{Im}\left[\int_0^k F(t)dt\right] \qquad (4.2.8)$$

where the overbar denotes the complex conjugate. Using a theorem due to Cauchy the integral around the singularity is evaluated :

$$\oint F(t)dt = -2\pi i\,(1-k)^{-1/2} \qquad (4.2.9)$$

Equating (4.2.8) and (4.2.9) it is seen that

$$2i\,\mathrm{Im}\left[\int_0^k F(t)dt\right] = -2\pi i\,(1-k)^{-1/2}$$

and thus

$$\mathrm{Im}\left[\int_0^k F(t)dt\right] = -i\,(1-k)^{-1/2} \qquad (4.2.10)$$

Returning to equation (4.2.7) it is seen that substitution of (4.2.10) yields:

$$p-b = \frac{P}{\int_0^k F(t)dt}\cdot\left[\int_0^k F(t)dt - i\pi(1-k)^{-1/2}\right]$$

and thus

$$P/_b = -i \int_0^k F(t)dt \,/\, \pi(1-k)^{-1/2} \qquad (4.2.11)$$

Using (4.2.11) in conjunction with (4.2.6) the constant K is found:

$$K = \frac{-ib}{\pi(1-k)^{-1/2}} \qquad (4.2.12)$$

and thus

$$Z = \frac{-ib}{\pi(1-k)^{-1/2}} \int_0^{\zeta} F(t)dt + b - p \qquad (4.2.13)$$

Carrying out the integration yields the result:

$$\int F(t)\,dt = 2\sqrt{t-k} + \frac{1}{\sqrt{1-k}} \ln \frac{\sqrt{t-k} - \sqrt{1-k}}{\sqrt{t-k} + \sqrt{1-k}} \qquad (4.2.14)$$

thus

$$\int_0^k F(t)dt = 2i\left[\frac{1}{\sqrt{1-k}} \tan^{-1}\sqrt{\frac{k}{1-k}} - \sqrt{k}\right]$$

and

$$P/_b = 2\tan^{-1}\sqrt{\frac{k}{1-k}} - \sqrt{k(1-k)} \qquad (4.2.15)$$

and, after some manipulation,

$$Z = \frac{-ib\sqrt{1-k}}{\pi}\left[2\sqrt{\zeta-k} + \frac{1}{\sqrt{1-k}} \ln \frac{\sqrt{\zeta-k} - \sqrt{1-k}}{\sqrt{\zeta-k} + \sqrt{1-k}}\right] \qquad (4.2.16)$$

As in the case of the smooth duct, the flow in the transform plane is represented by a source / sink singularity placed at $\zeta = 1$, leading to the expression

$$\zeta = 1 + e^{\alpha w + \beta}$$

The complete solution for the inner region is thus obtained as:

$$Z = \frac{-ib\sqrt{1-k}}{\pi}\left[2\sqrt{(1-k)+e^{\alpha w+\beta}} + \frac{1}{\sqrt{1-k}} \ln \frac{\sqrt{(1-k)+e^{\alpha w+\beta}} - \sqrt{1-k}}{\sqrt{(1-k)+e^{\alpha w+\beta}} + \sqrt{1-k}}\right] \qquad (4.2.17)$$

The asymptote of the solution in the overlap domain is found by taking the leading term of this expression:

$$Z = \frac{-ib\sqrt{1-k}}{\pi} \cdot 2\sqrt{(1-k) + e^{\alpha w+\beta}} \qquad (4.2.18)$$

yielding

$$\alpha w+\beta = -i\pi + 2\ln\frac{\pi}{2b\sqrt{1-k}} + \ln\left(z^2 + \frac{4b^2(1-k)}{\pi^2}\right)$$

and, using a procedure similar to that of Appendix 4.1 :

$$\phi = \frac{2}{\alpha}\ln\frac{\pi r}{2b\sqrt{1-k}} - \frac{\beta}{\alpha} \qquad (4.2.19)$$

The aymptote of the potential high up in the duct is found by rearranging (4.2.17) as:

$$Z = \frac{-ib}{\pi}\sqrt{1-k}\left[2\sqrt{(1-k)+e^{\alpha w+\beta}} + \frac{1}{\sqrt{1-k}}\ln(\zeta-1) - \frac{2}{\sqrt{1-k}}\ln\left(\sqrt{\zeta-k}+\sqrt{1-k}\right)\right] \qquad (4.2.20)$$

and letting $\zeta \to 1$:

$$Z = \frac{-ib\sqrt{1-k}}{\pi}\left[2\sqrt{1-k} + \frac{1}{\sqrt{1-k}}\ln(\zeta-1) - \frac{2}{\sqrt{1-k}}\ln 2\sqrt{1-k}\right]$$

thus

$$\frac{\pi y'}{b} = -\sqrt{1-k}\left[2\sqrt{1-k} + \frac{1}{\sqrt{1-k}}(\alpha\phi+\beta) - \frac{2}{\sqrt{1-k}}\ln 2\sqrt{1-k}\right]$$

Substitution of y' = (a - y) yields the potential:

$$\phi = \frac{1}{\alpha}\left[\frac{\pi(y-a)}{b} - \beta - 2(1-k) + 2\ln 2\sqrt{1-k}\right]$$

Substitution of this expression into the free surface boundary condition gives the constant β :

$$\beta = \frac{\pi}{b}\left[\frac{1}{K} - a\right] - 2\left[(1-k) - \ln 2\sqrt{1-k}\right] \qquad (4.2.21)$$

APPENDIX 4.3

SOLUTION OF THE INNER REGION FOR A DUCT WITH AN INTERNAL BAFFLE

Consider the flow-field bounded by by the rigid walls as shown in Figure 4.8a. The flow field is transformed into the upper half of the ζ -plane, with the boundaries of the z-plane on the real axis of the ζ -plane, as shown in Figure 4.8b. The appropriate Schwarz-Christoffel transform is given in the form shown in equation (4.11):

$$z = \mathbb{K}\int_0^{\zeta} F(t)dt + \mathbb{L} \qquad \text{(A4.3.1)}$$

where $F(t) = t^{1/2}(t-k)^{-1/2}(t-\lambda)\,(t-\mu)^{-1/2}(t-1)^{-1}$. The geometrical constraints on the problem allow the solution of this integral subject to the following boundary conditions:

(i)
$$z = b \quad @ \quad \zeta = 0 \qquad \text{(A4.3.2)}$$

which yields $\mathbb{L} = b$

(ii)
$$z = b + iq \quad @ \quad \zeta = k \qquad \text{(A4.3.3)}$$

and hence:

$$\mathbb{K} = iq \Big/ \int_0^k F(t)\,dt \qquad \text{(A4.3.4)}$$

where $\int_0^k F(t)\,dt$ is real negative.

(iii)
$$z = b - p + iq \quad @ \quad \zeta = \lambda \qquad \text{(A4.3.5)}$$

thus

$$-p + iq = iq \int_k^{\lambda} F(t)dt \Big/ \int_0^k F(t)\,dt$$

and

$$P/q = -i\int_k^{\lambda} F(t)dt \Big/ \int_0^k F(t)dt \qquad \text{(A4.3.6)}$$

where $\int_k^{\lambda} F(t)\,dt$ is imaginary negative, giving p / q real positive as would be expected.

(iv)

$$z = b + iq \quad @ \quad \zeta = \mu \qquad \text{(A4.3.7)}$$

thus

$$\int_k^{\mu} F(t) = 0$$

and

$$\int_k^{\lambda} F(t)dt + \int_{\lambda}^{\mu} F(t)\,dt = 0 \qquad \text{(A4.3.8)}$$

where $\int_{\lambda}^{\mu} F(t)\,dt$ is imaginary positive.

(v)

$$Re[z] = 0 \quad @ \quad \zeta > 1 \qquad \text{(A4.3.9)}$$

thus

$$iy' = iq\int_0^{\zeta} F(t)dt \Big/ \int_0^k F(t)dt + b\Big|_{\zeta>1}$$

where $\int_0^{\zeta} F(t)\,dt$ is calculated along the contour shown in Figure 4.8b. The integral $\int_0^{\zeta} F(t)\,dt$ is positive real along the ζ-axis for $\zeta > 1$; the imaginary part is due to the contribution of the pole at $\zeta = 1$. The relevant condition is, then:

$$-q\,Im\left[\int_0^{\zeta} F(t)dt\right] \Big/ \int_0^k F(t)dt + b = 0 \qquad \text{(A4.3.10)}$$

The contour integral around the pole is given by Cauchy's Residue Theorem as:

$$\oint = -2\pi i\,(1-k)^{-1/2}(1-\lambda)(1-\mu)^{-1/2} \qquad \text{(A4.3.11)}$$

The integral around the semi-circle indented into the upper half plane (as shown in Figure 4.8b) is related to this integral by the expression:

$$\oint = 2i\,\mathrm{Im}\left[f_t\right] \qquad \text{(A4.3.12)}$$

(see Appendix 4.2). Equating (A4.3.11) and (A4.3.12) yields the expression:

$$\mathrm{Im}\left[f_t\right] = -\pi(1-k)^{-1/2}(1-\lambda)(1-\mu)^{-1/2} \qquad \text{(A4.3.13)}$$

and substitution of this expression into (A4.3.10) gives q / b:

$$q/b = \int_0^k F(t)\,dt \Big/ \pi(1-k)^{-1/2}(1-\lambda)(1-\mu)^{-1/2} \qquad \text{(A4.3.14)}$$

Using (A4.3.6) and (A4.3.14) an expression for p / b is obtained:

$$p/b = i\int_k^\lambda F(t)\,dt \Big/ \pi(1-k)^{-1/2}(1-\lambda)(1-\mu)^{-1/2} \qquad \text{(A4.3.15)}$$

and finally, using (A4.3.4) and (A4.3.14) K is obtained as:

$$K = \frac{-ib}{\pi(1-k)^{-1/2}(1-\lambda)(1-\mu)^{-1/2}} \qquad \text{(A4.3.16)}$$

The flow in the transform plane is represented by a source / sink type singularity placed at $\zeta = 1$, yielding an expression for ζ :

$$\zeta = 1 + e^{\alpha w + \beta} \qquad \text{(A4.3.17)}$$

This is used as the upper limit of the integral in (A4.3.1) to give the complete inner solution:

$$Z = \frac{-ib}{\pi C_m}\int_0^{1+e^{\alpha w+\beta}} F(t)\,dt + b \qquad \text{(A4.3.18)}$$

where $C_m = (1-k)^{-1/2}(1-\lambda)(1-\mu)^{-1/2}$, subject to the

geometrical constraints given in (A4.3.8), (A4.3.14) and (A4.3.15).

The aaymptote of this solution high up in the duct is found by rewriting (A4.3.18) in the form:

$$Z = \frac{-ib}{\pi C_m} \int_0^{\zeta} F(t) - C_m (t-1)^{-1} dt \; \frac{-ib}{\pi C_m} \int_0^{\zeta} C_m (t-1)^{-1} dt + b \qquad \text{(A4.3.19)}$$

and hence

$$Z = \frac{-ib}{\pi} \int_0^{\zeta} (t-1)^{-1} dt - \frac{ib}{\pi C_m} \int_0^{1} F(t) - C_m (t-1)^{-1} dt - \frac{ib}{\pi C_m} \int_1^{\zeta} F(t) - C_m (t-1) dt + b \qquad \text{(A4.3.20)}$$

Writing:

$$N = \int_0^{1} F(t) - C_m (t-1)^{-1} dt \qquad \text{(A4.3.21)}$$

the expression becomes:

$$Z = \frac{-ib}{\pi} \int_0^{\zeta} (t-1)^{-1} dt - \frac{ib}{\pi} \frac{N}{C_m} - \frac{ib}{\pi C_m} \int_1^{\zeta} F(t) - C_m (t-1)^{-1} dt + b \qquad \text{(A4.3.22)}$$

The third term is of order ($\zeta - 1$). Letting $\zeta \to 1$, neglecting the order term and using (A4.3.17) gives:

$$\lim_{\zeta \to 1} Z = \frac{-ib}{\pi} [\alpha W + \beta + i\pi] - \frac{ib}{\pi C_m} N + b$$

and hence:

$$y' = (a-y) = \frac{-b}{\pi} [\alpha \phi + \beta] - \frac{b}{\pi} \frac{N}{C_m}$$

yielding an expression for the potential:

$$\phi = \frac{\pi}{\alpha b}[y-a] - \frac{\beta}{\alpha} - \frac{N}{\alpha C_m} \qquad \text{(A4.3.23)}$$

Using the free surface boundary condition:

$$K\phi + \frac{\partial \phi}{\partial y} = 0 \Big|_{y=0}$$

The constant β is obtained:

$$\beta = \frac{\pi}{b}\left[\frac{1}{K} - a\right] - \frac{N}{C_m} \qquad \text{(A4.3.24)}$$

The asymptote of the solution in the overlap domain is obtained by rewriting (A4.3.18) in the form

$$z = \frac{-ib}{\pi C_m}\left[\int_0^\zeta t^{-1/2}\,dt + \int_0^\zeta F(t) - t^{1/2}\,dt\right] + b \qquad \text{(A4.3.25)}$$

The second integral is bounded as $|\zeta| \to \infty$; hence:

$$\lim_{|\zeta|\to\infty} z = \frac{-ib}{\pi C_m}\int_0^\zeta t^{1/2}\,dt$$

$$\lim_{|\zeta|\to\infty} z = -\frac{2ib}{\pi C_m}\left(1+e^{\alpha\omega+\beta}\right)^{1/2} \qquad \text{(A4.3.26)}$$

Using a procedure similar to that of Appendix 4.1, the asymptote of the potential is obtained:

$$\phi = \frac{z}{\alpha}\ln\frac{r}{2a} + \frac{z}{\alpha}\frac{\pi a C_m}{b} - \frac{\beta}{\alpha} \qquad \text{(A4.3.27)}$$

APPENDIX 4.4

SOLUTION OF THE INNER REGION FOR A DUCT WITH A FLOW EXPANSION

Consider the flow-field bounded by by the rigid walls as shown in Figure A4.4.1a. The flow field is transformed into the upper half of the ζ-plane, with the boundaries of the z-plane on the real axis of the ζ-plane, as shown in Figure A4.4.1b. The appropriate Schwarz-Christoffel transform is given in the form:

$$z = \mathbb{K} \int_0^{\zeta} F(t)dt + \mathbb{L} \qquad \text{(A4.4.1)}$$

where $F(t) = t^{1/2}(t-k)^{-1/2}(t-\lambda)^{1/2}(t-1)^{-1}$ The geometrical constraints on the problem allow the solution of this integral subject to the following boundary conditions:

(i) $$z = b+p \quad @ \quad \zeta = 0 \qquad \text{(A4.4.2)}$$

which yields $\mathbb{L} = b + p$

(ii) $$z = b+p+iq \quad @ \quad \zeta = k \qquad \text{(A4.4.3)}$$

and hence:

$$\mathbb{K} = iq / \int_0^k F(t)dt \qquad \text{(A4.4.4)}$$

where $\int_0^k F(t)\,dt$ is real negative.

(iii)

$$z = b+iq \quad @ \quad \zeta = \lambda \qquad \text{(A4.4.5)}$$

thus

$$b + iq = iq / \int_0^k F(t)dt \cdot \int_0^{\lambda} F(t)dt + b + p$$

and

$$p/q = -i \int_k^\lambda F(t)dt \Big/ \int_0^k F(t)dt \qquad \text{(A4.4.6)}$$

where $\int_k^\lambda F(t)\,dt$ is imaginary negative, giving p / q real positive as would be expected.

(iv)

$$Re[z] = 0 \quad @ \quad \zeta > 1 \qquad \text{(A4.4.7)}$$

thus

$$-\left[q/\int_0^k F(t)dt\right] Im\left[\int_0^\zeta F(t)dt\right] + b + p = 0 \qquad \text{(A4.4.8)}$$

where $\int_0^\zeta F(t)\,dt$ is calculated along the contour shown in Figure A4.4.1b. The integral $\int_0^\zeta F(t)\,dt$ is positive real along the ζ-axis for $\zeta > 1$; the imaginary part is due to the integration between $\zeta = k$ and $\zeta = \lambda$ and the contribution of the pole at $\zeta = 1$. The contour integral around the pole is given by Cauchy's Residue Theorem as:

$$\oint = -2\pi i\,(1-k)^{-1/2}(1-\lambda)^{1/2} \qquad \text{(A4.4.9)}$$

The integral around the semi-circle indented into the upper half plane (as shown in Figure A4.4.1b) is related to this integral by the expression:

$$\oint = 2i\,Im[f] \qquad \text{(A4.4.10)}$$

(see Appendix 4.2). Equating (A4.4.10) and (A4.4.9) yields the expression:

$$Im[f] = -\pi\,(1-k)^{-1/2}(1-\lambda)^{1/2} \qquad \text{(A4.4.11)}$$

and thus

$$Im\left[\int_0^\zeta\right] = -\pi(1-k)^{-1/2}(1-\lambda)^{1/2} - i\int_k^\lambda F(t)dt \qquad \text{(A4.4.12)}$$

Substitution of this expression into (A4.4.8) gives q / (b + p):

$$q/_{b+p} = -\int_0^k F(t)dt \Big/ \left[\pi(1-k)^{-1/2}(1-\lambda)^{1/2} + i\int_k^\lambda F(t)dt\right] \quad \text{(A4.4.13)}$$

Using (A4.4.6) and (A4.4.13) an expression for p / (b + p) is obtained:

$$P/_{b+p} = i\int_k^\lambda F(t)dt \Big/ \left[\pi(1-k)^{-1/2}(1-\lambda)^{1/2} + i\int_k^\lambda F(t)dt\right] \quad \text{(A4.4.14)}$$

and finally, using (A4.4.4) and (A4.4.13) K is obtained as:

$$K = -ib \Big/ \pi(1-k)^{-1/2}(1-\lambda)^{1/2} \quad \text{(A4.4.15)}$$

The flow in the transform plane is represented by a source / sink type singularity placed at $\zeta = 1$, yielding an expression for ζ :

$$\zeta = 1 + e^{\alpha w + \beta} \quad \text{(A4.4.16)}$$

This is used as the upper limit of the integral in (A4.4.1) to give the complete inner solution:

$$z = \frac{-ib}{\pi C_m} \int_0^{1+e^{\alpha w+\beta}} F(t)dt + b + p \quad \text{(A4.4.17)}$$

where $C_m = (1 - k)^{-1/2} (1 - \lambda)^{1/2}$, subject to the geometrical constraints given in (A4.4.13) and (A4.4.14). If F (t) is decomposed into real and imaginary parts, a plot of the streamlines and potential lines may be obtained. Figure 4.4.2 shows such a plot for $\varepsilon = 0.1$, p/b = 0.5, and q/b = 1.0.

The procedure for obtaining the asymptotes is exactly as shown in Appendix 4.3.

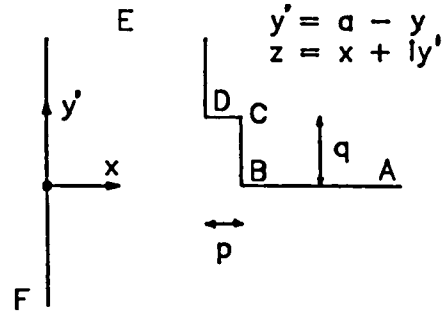

Figure A4.4.1a

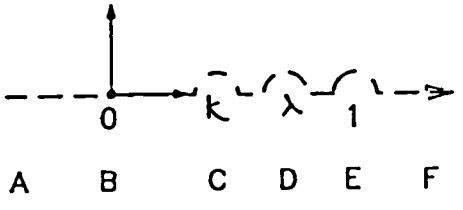

Figure A4.4.1b

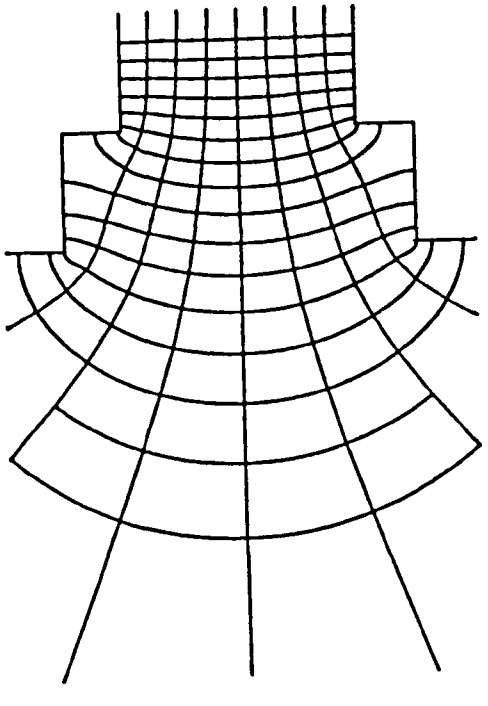

Figure A4.4.2

APPENDIX 4.5

SOLUTION OF THE INNER REGION FOR A DUCT WITH A FLOW CONSTRICTION

Consider the flow-field bounded by by the rigid walls as shown in Figure A4.5.1a. The flow field is transformed into the upper half of the ζ-plane, with the boundaries of the z-plane on the real axis of the ζ-plane, as shown in Figure A4.5.1b. The appropriate Schwarz-Christoffel transform is given in the form shown:

$$z = \mathbb{K} \int_0^{\zeta} F(t)dt + \mathbb{L} \qquad \text{(A4.5.1)}$$

where $F(t) = t^{1/2}(t-k)^{1/2}(t-\lambda)^{-1/2}(t-1)^{-1}$ The geometrical constraints on the problem allow the solution of this integral subject to the following boundary conditions:

(i)

$$z = b-p \quad @ \quad \zeta = 0 \qquad \text{(A4.5.2)}$$

which yields $\zeta = b-p$

(ii)

$$z = b-p+iq \quad @ \quad \zeta = k \qquad \text{(A4.5.3)}$$

and hence:

$$\mathbb{K} = iq / \int_0^k F(t)dt \qquad \text{(A4.5.4)}$$

where $\int_0^k F(t)\,dt$ is real negative.

(iii)

$$z = b+iq \quad @ \quad \zeta = \lambda \qquad \text{(A4.5.5)}$$

thus

$$b+iq = iq \int_0^{\lambda} F(t)dt \Big/ \int_0^k F(t)dt + b - p$$

and

$$p/q = i\int_k^\lambda F(t)\,dt \Big/ \int_0^k F(t)\,dt \qquad \text{(A4.5.6)}$$

where $\int_k^\lambda F(t)\,dt$ is imaginary positive, giving p / q real positive as would be expected.

(iv)

$$\mathrm{Re}\,[z] = 0 \quad @ \quad \zeta > 1 \qquad \text{(A4.5.7)}$$

thus

$$-q\,\mathrm{Im}\left[\int_0^\zeta F(t)\,dt\right] \Big/ \int_0^k F(t)\,dt + b + p = 0 \qquad \text{(A4.5.8)}$$

where $\int_0^\zeta F(t)\,dt$ is calculated along the contour shown in Figure A4.5.1b. The integral $\int_0^\zeta F(t)\,dt$ is positive real along the ζ-axis for $\zeta > 1$; the imaginary part is due to the integration between $\zeta = k$ and $\zeta = \lambda$ and the contribution of the pole at $\zeta = 1$. The contour integral around the pole is given by Cauchy's Residue Theorem as:

$$\oint = -2\pi i\,(1-k)^{1/2}(1-\lambda)^{-1/2} \qquad \text{(A4.5.9)}$$

The integral around the semi-circle indented into the upper half plane (as shown in Figure A4.5.1b) is related to this integral by the expression:

$$\oint = 2i\,\mathrm{Im}[f_\infty] \qquad \text{(A4.5.10)}$$

(see Appendix 4.2). Equating (A4.5.10) and (A4.5.9) yields the expression:

$$\mathrm{Im}[f_\infty] = -\pi(1-k)^{1/2}(1-\lambda)^{-1/2} \qquad \text{(A4.5.11)}$$

and thus

$$\mathrm{Im}\left[\int_0^\zeta F(t)\,dt\right] = -\pi(1-k)^{-1/2}(1-\lambda)^{1/2} + i\int_k^\lambda F(t)\,dt \qquad \text{(A4.5.12)}$$

Substitution of this expression into (A4.5.8) gives q / (b - p) :

$$q/(b-p) = -\int_0^k F(t)\,dt \Big/ \left[\pi(1-k)^{1/2}(1-\lambda)^{-1/2} + i\int_k^\lambda F(t)dt\right] \quad \text{(A4.5.13)}$$

Using (A4.5.6) and (A4.5.13) an expression for p / (b - p) is obtained:

$$p/(b-p) = -i\int_k^\lambda F(t)\,dt \Big/ \left[\pi(1-k)^{1/2}(1-\lambda)^{1/2} + i\int_k^\lambda F(t)dt\right] \quad \text{(A4.5.14)}$$

and finally, using (A4.5.4) and (A4.5.13) K is obtained as:

$$K = -ib/\pi(1-k)^{+1/2}(1-\lambda)^{-1/2} \quad \text{(A4.5.15)}$$

The flow in the transform plane is again represented by a source / sink type singularity placed at $\zeta = 1$, yielding an expression for ζ :

$$\zeta = 1 + e^{\alpha w + \beta} \quad \text{(A4.5.16)}$$

This is used as the upper limit of the integral in (A4.5.1) to give the complete inner solution:

$$z = \frac{-ib}{\pi C_m}\int_0^{1+e^{\alpha w+\beta}} F(t)\,dt + b - p \quad \text{(A4.5.17)}$$

where $C = (1-k)^{1/2}(1-\lambda)^{-1/2}$ subject to the geometrical constraints given in (A4.5.12) and (A4.5.13). This expression may be used to obtain a plot of the streamlines and potential lines by decomposition of F (t) into real and imaginary parts. Figure 4.5.2 shows such a plot for $\varepsilon = 0.1$, p/b = 0.5, and q/b = 1.0.

The asymptotes of this solution are found using exactly the same procedure as shown in Appendix 4.3.

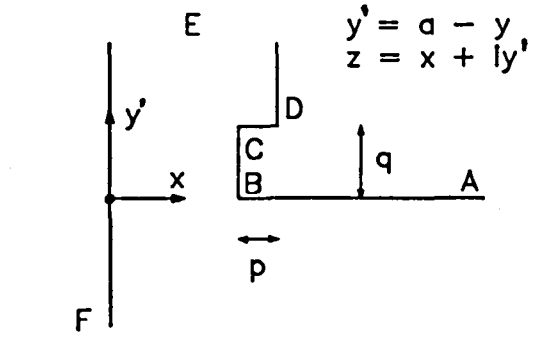

Figure A4.5.1a

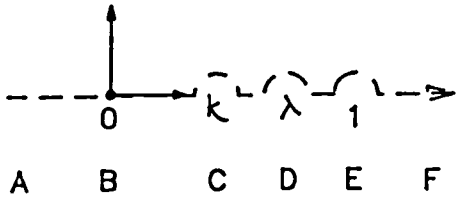

Figure A4.5.1b

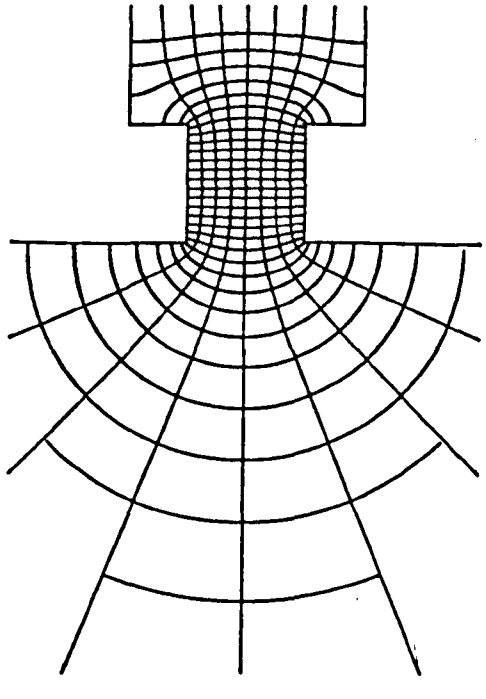

Figure A4.5.2

APPENDIX 5.1

HYDRODYNAMIC COEFFICIENTS FOR FLOW CONSTRICTION

q/b	0.00	0.40	0.80	1.20	1.60
p/b					
	0.3900				
0.00	0.0049				
	0.1652				
	0.4600	0.5300	0.6200	0.7000	0.6500
0.12	0.0494	0.0183	0.0167	0.0102	0.0321
	0.3344	0.2494	0.2698	0.3282	0.1164
	0.5600	0.8000	0.9200	1.0500	1.3000
0.24	0.0849	0.0097	0.0313	0.0436	0.0592
	0.5064	0.5362	0.5890	0.4058	0.2430
	0.7500	1.2000	1.4500	1.7500	2.1500
0.36	0.1072	0.0066	0.0194	0.0226	0.0578
	1.0700	1.2884	0.9854	0.9224	0.5878
	1.1000	1.7500	2.4000	2.9000	3.9000
0.48	0.1667	0.0422	0.1291	0.0913	0.0842
	1.2272	2.3608	1.0272	0.8958	0.6454

For each configuration the first number is the added mass a_m, the second is the damping ratio intercept ξ_I, and the third is the damping ratio gradient ξ_G.

APPENDIX 5.2

HYDRODYNAMIC COEFFICIENTS FOR FLOW EXPANSION

q/b p/b	0.00	0.40	0.80	1.20	1.60
	0.3900				
0.00	0.0049				
	0.1652				
		0.2700	0.2200	0.1750	0.1500
0.12		0.0412	0.0163	0.0274	0.0849
		0.0140	0.1572	0.1038	0.5064
		0.1800	0.0800	0.0000	-0.0600
0.24		0.0196	0.0073	0.0223	0.0213
		0.0758	0.2000	0.0610	0.0116
		0.1000	-0.0500		
0.36		0.0162	0.0112		
		0.1644	0.0814		
		0.0300	-0.0800		
0.48		0.0082	0.0002		
		0.2054	0.1690		

For each configuration the first number is the added mass a_{ww} the second is the damping ratio intercept ξ_I, and the third is the damping ratio gradient ξ_G.

APPENDIX 6.1

PERFORMANCE INDEX WORKED EXAMPLE I

The first worked example shows the simplest application of the procedure proposed. It is assumed that no information about the operability of the ship is available, and, as such, a calculation of the first type must be performed. It is further assumed that the ship concerned is a floating production vessel with a working draft of 10.0m, and the only concern about the moonpool is the magnitude of the water column oscillation. In order to demonstrate the effect of the choice of the criterion used for the exceedance calculation, a series of three water column oscillation criteria are used. The water column oscillation amplitudes for which the performance indices are calculated are 2.0m, 3.0m, and 4.0m (ie 4.0m, 6.0m, and 8.0m peak-to-peak oscillation). These might correspond to oscillations for which different precautions must be taken. It is assumed that the maximum cross sectional area available for the moonpool is 10m x 10m, while the working area of the moonpool must be no less than 5m x 5m. The moonpool thus fits within the bounds of the model tests described in the previous chapter. Five moonpools are chosen for comparison; these are:

(i) A Smooth moonpool
(used here to provide a datum for comparison)

(ii) A Moonpool with a thin baffle at the exit with p/b = 0.48
(selected as having the highest damping ratio intercept)

(iii) A Moonpool with a flow constriction at the exit with p/b = 0.48 and q/b = 0.40
(selected as having the highest damping ratio gradient)

(iv) A Moonpool with a flow constriction at the exit with p/b = 0.48 and q/b = 1.60
(selected as having the highest added mass)

(v) A Moonpool with a flow expansion at the exit with p/b = 0.48 and q/b = 0.80
(selected as having the lowest added mass)

The calculations are carried out in each case for heading angles of 0°, 22.5° and 45°. These represent a best case, a worst case, and an intermediate case. It is unlikely that a floating production vessel would ever be forced to work beam on to the predominant waves, but with a wind direction (and hence the local wind waves) in a different direction to a swell, it is quite possible that the vessel would be forced to take up a heading between the two. The heading angles are assumed to have probabilities of 0.7 (0°), 0.2 (22.5°), and 0.1 (45°).

The results of the calculation are presented in Table A6.1.1. For the case of the 2.0m criterion, the vessel is quite sensitive to the moonpool performance, with the worst performance coming from the smooth moonpool, at 19.8 days of downtime in typical years operation. The best moonpool is the first of the two flow constrictions considered, with only 2.4 days of downtime in a typical year, closely followed by the thin baffle at 3.5 days downtime per year. The difference between the best and the worst moonpools is thus quite significant, at 17.4 days per year.

The performance indices improve radically as the criterion becomes less stringent. The rankings of the moonpools do not, however, alter. For the case of the 3.0m criterion the worst performance is again that of the smooth moonpool at 5.3 days per year, whilst the best performance is again the first of the flow constrictions at 0.2 days per year. In the case of the 4.0m criterion, the smooth moonpool gives 1.5 days per year, whilst the first flow constriction virtually eliminates downtime due to the moonpool at 0.01 days per year. Thus, even with the least stringent criterion, an extra 1.5 days operation per year would be achieved by the selection of the

most appropriate moonpool if the vessel were to work continuously.

Whilst the rankings do not change as the criterion changes in this case, it is quite possible that in other cases a large change in the criterion value would lead to a change in the rankings, especially in a case where one moonpool has a large damping ratio intercept, but a small damping ratio gradient, whilst another has a small intercept and a large gradient.

TABLE A6.1.1 PERFORMANCE INDICES FOR 2.0m OSCILLATION AMPLITUDE CRITERION

Moonpool	P (0°)	P (22.5°)	P (45°)
(i)	4.180%	5.445%	13.994%
(ii)	0.945%	1.029%	0.805%
(iii)	0.632%	0.686%	0.677%
(iv)	2.033%	2.315%	3.346%
(v)	4.519%	3.620%	2.811%

The performance indices over all heading angles are thus calculated as:

$$P_1 = 0.7 \times P\,(0^\circ) + 0.2 \times P\,(22.5^\circ) + 0.1 \times P\,(45^\circ)$$

(i)	$P_1 = 5.41\%$	or	19.8 days/year
(ii)	$P_1 = 0.95\%$	or	3.5 days/year
(iii)	$P_1 = 0.65\%$	or	2.4 days/year
(iv)	$P_1 = 2.22\%$	or	8.1 days/year
(v)	$P_1 = 4.17\%$	or	15.2 days/year

TABLE A6.1.2 PERFORMANCE INDICES FOR 3.0m OSCILLATION AMPLITUDE CRITERION

Moonpool	P (0°)	P (22.5°)	P (45°)
(i)	0.997%	1.497%	4.515%
(ii)	0.105%	0.116%	0.075%
(iii)	0.045%	0.051%	0.063%
(iv)	0.375%	0.447%	0.772%
(v)	0.777%	0.607%	0.484%

The performance indices over all heading angles are thus calculated as:

$$P_1 = 0.7 \times P\,(0^\circ) + 0.2 \times P\,(22.5^\circ) + 0.1 \times P\,(45^\circ)$$

(i)	P_1 = 1.45%	or	5.3 days/year
(ii)	P_1 = 0.10%	or	0.4 days/year
(iii)	P_1 = 0.05%	or	0.2 days/year
(iv)	P_1 = 0.43%	or	1.6 days/year
(v)	P_1 = 0.71%	or	2.6 days/year

TABLE A6.1.3 PERFORMANCE INDICES FOR 4.0m OSCILLATION AMPLITUDE CRITERION

Moonpool	P (0°)	P (22.5°)	P (45°)
(i)	0.257%	0.439%	1.529%
(ii)	0.010%	0.012%	0.006%
(iii)	0.003%	0.003%	0.007%
(iv)	0.074%	0.093%	0.196%
(v)	0.142%	0.109%	0.092%

The performance indices over all heading angles are thus calculated as:

$$P_I = 0.7 \times P\,(0^\circ) + 0.2 \times P\,(22.5^\circ) + 0.1 \times P\,(45^\circ)$$

(i)	P_I = 0.42%	or	1.53 days/year
(ii)	P_I = 0.01%	or	0.04 days/year
(iii)	P_I = 0.00%	or	0.01 days/year
(iv)	P_I = 0.09%	or	0.33 days/year
(v)	P_I = 0.13%	or	0.48 days/year

APPENDIX 6.2

PERFORMANCE INDEX WORKED EXAMPLE II

The second calculation presented illustrates how the choice of the vessel influences the choice of the moonpool. It is assumed this time that the vessel concerned is a diving / ROV support vessel with a working draft of 4.0m, and that no knowledge of the subsea units to be launched or the vessel operability is available in the initial stages of the design. The only criterion available for evaluating the moonpool performance is thus the water column oscillation; a value of 2.0m amplitude (ie 4.0m peak-to-peak) is chosen as the maximum working condition. It is assumed that the maximum cross sectional area of the moonpool is 4.0m x 4.0m, and that the working area must be no less than 2.0m x 2.0m. The moonpool thus has the same geometry as the previous example; accordingly the same five moonpools are examined.

In this case, however, the heading angles examined are different; a diving support vessel may, in some circumstances, be forced to work alongside a fixed structure; in so doing the vessel may have to work beam on to the predominant sea. The three angles used for the calculation are thus taken as 0°, 45°, and 90°, with assigned probabilities of 0.6 (0°), 0.25 (45°), and 0.15 (90°). The results of the calculation are set out in Table A6.2.1.

It can be seen that there is a dramatic change in the ranking of the five moonpools examined for this vessel, as compared to those obtained for the floating production system. The best moonpool in this case is the moonpool with the flow expansion at the exit at 0.5 days downtime in a typical year of continuous operation; this moonpool was the second worst performer in the previous example. The worst performance does not come from the smooth moonpool, (as might be expected) but from the moonpool with the large flow

constriction at 14.7 days per year; this moonpool was in the middle of the rankings in the previous example. The best performer from the previous example, the moonpool with the smaller flow constriction, is the second worst in this case, giving more downtime per year than the smooth moonpool.

This serves to reemphasise the point that the design of a moonpool cannot be successfully carried out without consideration of the ship for which it is intended.

TABLE A6.2.1

Moonpool	P (0°)	P (45°)	P (90°)
(i)	0.930%	0.683%	5.771%
(ii)	0.370%	0.930%	4.576%
(iii)	1.278%	2.226%	5.774%
(iv)	2.554%	4.132%	9.761%
(v)	0.126%	0.057%	0.320%

The performance indices over all heading angles are thus calculated as:

$$P_1 = 0.6 \times P\ (0^\circ) + 0.25 \times P\ (45^\circ) + 0.15 \times P\ (90^\circ)$$

(i)	$P_1 = 1.59\%$	or	5.8 days/year
(ii)	$P_1 = 1.14\%$	or	4.2 days/year
(iii)	$P_1 = 2.19\%$	or	8.0 days/year
(iv)	$P_1 = 4.03\%$	or	14.7 days/year
(v)	$P_1 = 0.14\%$	or	0.5 days/year

APPENDIX 6.3

PERFORMANCE INDEX WORKED EXAMPLE III

The third worked example presented illustrates how the rankings produced by the moonpool performance index calculations can be affected by prior knowledge of the vessel operating characteristics. The calculation takes the same ship, the same heading angles and the same five moonpools as in the previous example, but this time it is assumed that the vessel cannot operate in sea states for which the significant vessel heave is greater than 4.0m. This type of restriction may well apply in practice, as divers cannot enter and leave the bell in safety if the oscillation of the bell is too great. The sea states for which the previous calculations were carried out are shown in Figure A6.3.1; these are simply all sea-states with a non-zero occurrance probability. Figures A6.3.2-4 show the reduced number of sea-states to be considered when the heave constraint is applied. It can be seen that the greatest effect of the heave constraint is at the 90 heading angle, when the number of sea states for which the vessel can work (excepting the moonpool) is dramatically reduced.

The results of the calculation are set out in Table A6.3.1. It can be seen that the sensitivity of the vessel operation to the moonpool performance is reduced by this constraint; however the downtime lost to the moonpool is still as high as 6.6 days/year in the worst example. The ranking of the five moonpools remains the same, but the relative performance of the moonpools within the ranking varies noticeably. Table A6.3.2 shows the ratio of the downtime of each moonpool to the downtime of the best moonpool (v). The ratio for the worst moonpool increases by over 50% from 28.8 in the first calculation to 45 in the second; in contrast, the second best moonpool improves relative to the best as a result of this constraint, from a ratio of 8.1 in the first calculation to

only 2.0 in the second. In absolute terms, the extra downtime incurred by choice of the second best moonpool would reduce from 3.7 days per year down to 0.1 days per year as a result of the vessel operability criterion; as such the difference between the two on the basis of the criteria applied (both for moonpool and vessel operability) in the second example becomes negligable. The vessel performance is thus shown to have a significant effect on the moonpool performance in this case.

TABLE A6.3.1

Moonpool	P (0°)	P (45°)	P (90°)
(i)	0.510%	0.287%	2.534%
(ii)	0.001%	0.005%	0.540%
(iii)	0.035%	0.115%	0.863%
(iv)	0.838%	1.166%	6.717%
(v)	0.049%	0.012%	0.032%

The performance indices over all heading angles are thus calculated as:

$$P_t = 0.6 \times P\ (0°) + 0.25 \times P\ (45°) + 0.15 \times P\ (90°)$$

(i)	P_t = 0.76%	or	2.8 days/year
(ii)	P_t = 0.08%	or	0.3 days/year
(iii)	P_t = 0.26%	or	1.0 days/year
(iv)	P_t = 1.80%	or	6.6 days/year
(v)	P_t = 0.04%	or	0.1 days/year

TABLE A6.3.2

Moonpool	Downtime / Best Moonpool Downtime (Worked example II)	Downtime / Best Moonpool Downtime (Worked example III)
(i)	11.4	19.0
(ii)	8.1	2.0
(iii)	15.6	6.5
(iv)	28.8	45.0
(v)	1.0	1.0

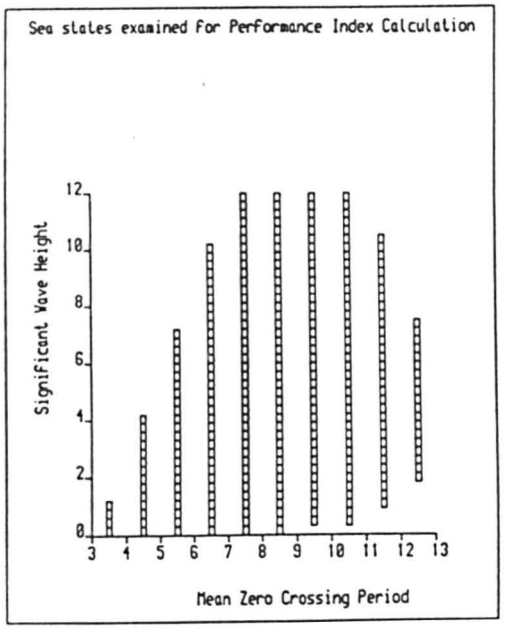

Figure A6.3.1

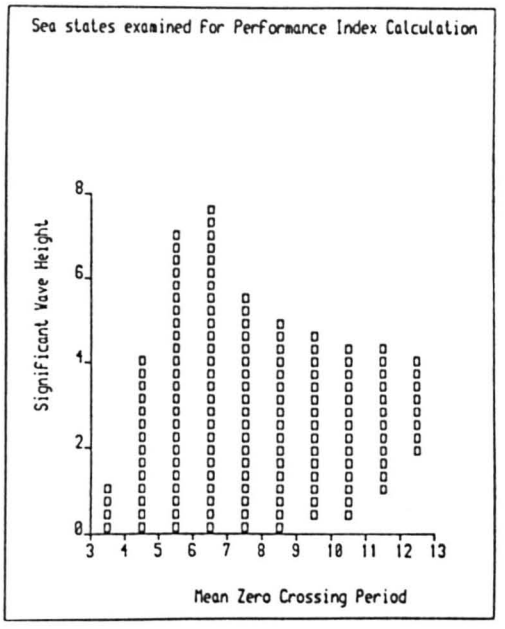

Figure A6.3.2

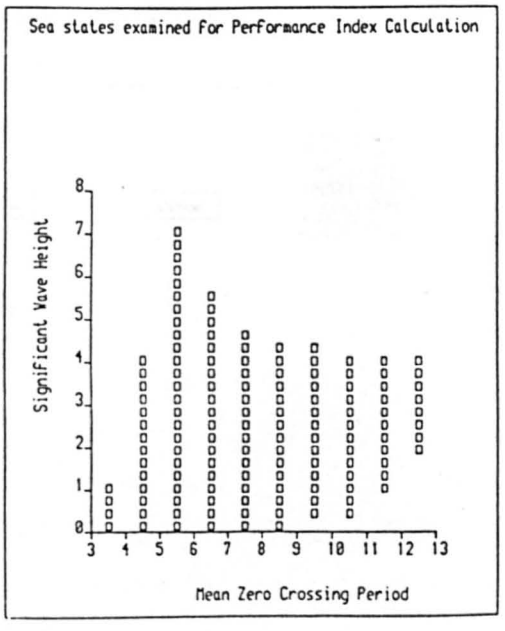

Figure A6.3.3

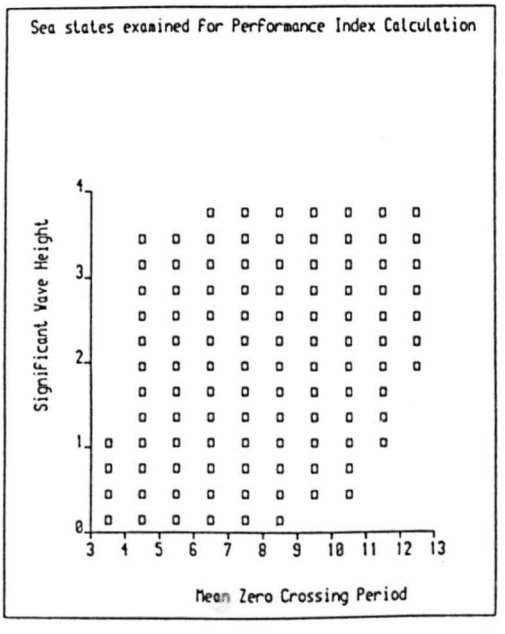

Figure A6.3.4

APPENDIX 6.4

PERFORMANCE INDEX WORKED EXAMPLE IV

The final worked example illustrates the use of the hoist wire tension criterion instead of the flooding criterion. The vessel chosen and the heading angles examined are exactly as in the previous two examples. It is again assumed that the vessel cannot work when the significant heave is greater than 4.0m. The calculation illustrates how the method might be used at an early stage of the design of a diving system.

The diving bell is assumed to have a projected area of 4.52m , a volume of 7.92m , and a wet weight of 2.5 tonnes. No laboratory tests have been carried out to determine the force coefficients of the bell in the moonpools to be exaxmined, and, in particular, the dependence of these coefficients on the Keulegan Carpenter Number of the flow regime inside the moonpool (see Appendix 3.1), but measurements on similar bells in 'open' water have yielded Cm = 0.9, and Cd = 1.9.

Three smooth moonpools are to be compared for the study: a circular moonpool of diameter 2.88m, a moonpool 2.88m square, and a moonpool 4.0m square. These correspond to the moonpools tested experimentally in Chapter 3. The blockage coefficients for the three moonpools are thus 0.695, 0.545, and 0.283 respectively. Since no information is available on the force coefficients for the bell inside the moonpool, an approximation must be employed. Madsen [op.cit.] suggests that the inertial coefficient for a bell in a moonpool may be calculated as:

$$\frac{C_m}{C_{m_o}} = 1 + 1.9\,B^{2.25} \qquad \text{(A6.4.1)}$$

where B is the blockage coefficient. Gran [op.cit.] suggests that the drag coefficient may be calculated as:

$$\frac{C_D}{C_{D0}} = \frac{1 - 0.5B}{(1-B)^2} \qquad \text{(A6.4.2)}$$

These equations lead to Cm and Cd values of 1.65 and 13.3 for moonpool 1, 1.34 and 6.68 for moonpool 2, and 1.00 and 3.17 for moonpool 3.

It is to be stressed that this approximation is far from ideal, taking no account of the shape of the moonpool or the oscillatory nature of the flow regime around the bell; however, if no other data were available, this would be the only method of comparing the moonpools in terms of the hoist wire tension criterion and thus examining the performance of the ship/moonpool/bell system as a whole.

The results of the calculation are presented in Table A6.4.1. It can be seen that moonpool 1 provides the best performance, with 22.4 days downtime due to the moonpool alone in a years continuous operations. This contrasts sharply with the performance of the moonpools in terms of the flooding criterion in the previous examples, suggesting that the tension criterion will be the more important in a diving support vessel. The complexity of the physical system is underlined by the performance of moonpool 1, since the high blockage for this moonpool leads to high values of Cm and Cd; however, this is more than offset by the effect of the bell on the moonpool water column oscillation properties. The other moonpools follow this trend, with moonpool 2 giving 31.6 days of downtime per year, and moonpool 3 giving 55.3 days downtime per year.

It should be stressed, however, that the empirical equations used here to estimate the effect of the blockage, coupled with the effects due to the variation of Keulegan Carpenter number over the sea states used to calculate the performance indices could lead to serious underestimation of the coefficients in many of the sea states considered. This might lead to very different conclusions being drawn.

The calculation of performance indices based on the tension criterion are thus shown to be of use in the moonpool design process. However, the technique would also be useful in a case where the moonpool is already in existence, but a new diving bell or other subsea equipment is being designed. This information could then be used to give designers a feel for the relationship between the wet weight of the units and the force coefficients required to give the operators a reasonable probability (in terms of the importance of the operation) of being able to launch and recover the unit safely.

TABLE A6.4.1

Moonpool	P (0°)	P (45°)	P (90°)
(i)	4.54%	1.84%	27.97%
(ii)	7.04%	2.60%	25.27%
(iii)	13.26%	8.44%	33.87%

The performance indices over all heading angles are thus calculated as:

$$P_t = 0.6 \times P(0^\circ) + 0.25 \times P(45^\circ) + 0.15 \times P(90^\circ)$$

(i)	P_t = 6.14%	or	22.4 days/year
(ii)	P_t = 8.66%	or	31.6 days/year
(iii)	P_t = 15.14%	or	55.3 days/year

APPENDIX 7.1

MOONPOOL DESIGN PROCEDURE: A WORKED EXAMPLE

The worked example presented here shows how the procedure proposed in chapter 7 may be used in practice. The vessel concerned formed part of a Floating Production System; the particular problem illustrated here is the design of a moonpool for the launch and recovery of ROVs.

STEP 1: Acquire Design Data

(i) Equipment:
The minimum working area required for the moonpool was specified as being 3.95m (longitudinally) X 5.00m (transversely). No information was available at the time on the type of ROVs to be launched; it was thus agreed that the design procedure be carried out on the basis of the risk of flooding of the handling area.

(ii) Vessel:
Information on the vessel was obtained in the form of a Body Plan, a set of Motion RAOs obtained from Model tests and computer calculations, and a General Arrangement plan. The ROV handling deck was found to be 3.5m above the still water level at a typical working draft; however in view of the serious consequences of the flooding of this deck, an oscillation amplitude of 3m was taken as the flooding criterion.

(iii) Operational Area:
The intended operational area was the North Sea. Long term wave statistics for this area are given in Andrews et al [1984], and the JONSWAP spectral model was assumed.

STEP 2: Establish Design Evaluation Criteria

The criteria established as being of prime importance to the client were the moonpool performance and the space required. The ease of fabrication and cost were of lesser importance.

STEP 3: Establish Design Constraints

The only specific constraint was placed upon the space available for the moonpool. The amount of space available longitudinally for the moonpool was restricted by the process area forward of the moonpool and a coffer dam aft of the moonpool. The distance between these was only 5m. In the transverse direction a total breadth of 10m was available. Due to the very tight restriction thus imposed, it was agreed to examine designs with fore and aft dimensions of up to 8m. The trade off between performance and space could thus be quantified. The desired performance was not stated explicitly; however the client did state that three specific sea states were of interest in addition to the long term assessment; these were significant wave height / mean zero crossing period sea state pairs of (4.5,7.2), (4.5,8.3), and (5.0,8.6).

STEP 4: Select Configuration

The typical working draft of the vessel was stated as being 11.00m; the natural frequency of a smooth moonpool in the vessel was therefore estimated as being 0.11Hz - corresponding to a natural period of about 9s. The long term wave statistics suggest that the predominant sea states in this area have mean zero crossing periods of the order of 5.5s - 8.5s. The strategy for the moonpool design must therefore be to attempt to reduce the natural frequency of the water column oscillation using the flow constriction configuration.

STEP 5: Select Detailed Moonpool Geometry

Iteration 1:

In order to illustrate the performance advantage gained through the moonpool design procedure, it was decided that a test of a smooth moonpool of the same dimensions as the minimum working area be carried out, and a performance index calculated. The performance of the designs carried out could therefore be assessed against the smooth moonpool.

The results for the Smooth Moonpool were found to be:

Design	H_s, T_z 4.5,7.2	H_s, T_z 4.5,8.3	H_s, T_z 5.0,8.6	Performance Index
Smooth Moonpool	42.1	33.0	39.1	11.1

N.B. All performance figures are % exceedance of the 3.0m oscillation amplitude criterion.

Iteration 2:

The initial geometry selected was a flow constriction in the transverse direction with a depth of one third of the vessel draft. Two large baffles were added above the flow constriction, and three small baffles added to the inner side of the flow constriction. Five small baffles were placed on the transverse walls at the same height. The overall dimensions of the design were 5m (longitudinally) X 10m (transversely). The configuration is illustrated schematically in Figure A7.1.1. It was felt that the baffles would be needed since the frequency shift induced by the flow constriction would not be very large because the fluid was only constricted in the transverse direction.

The results of the performance assessment are shown below:

Design	H_s, T_z 4.5,7.2	H_s, T_z 4.5,8.3	H_s, T_z 5.0,8.6	Performance Index
No 2	1.1	9.3	12.9	4.2

Whilst the results were encouraging, it was felt that the response in the 5.0m significant sea state was poor, and that the design could be improved.

Iteration 3:

A modification considered was the addition of a perforated tube to the initial design. This is shown in Figure A7.1.2.

Unfortunately the performance of the moonpool deteriorated slightly, as the results show:

Design	H_s, T_z 4.5,7.2	H_s, T_z 4.5,8.3	H_s, T_z 5.0,8.6	Performance Index
No 3	0.9	10.3	13.4	4.6

Whilst the addition of the tube increased both the added mass and the damping gradient, the damping intercept was reduced.

Iteration 4:
The next design considered involved the use of the maximimum amount of space allowed by the constraint; ie 8m (longitudinally) X 10m (transversely). The configuration was similar to design No.3, but incorporated flow constrictions in both longitudinally and transverse directions (see Figure A7.1.3).

The results obtained were:

Design	H_s, T_z 4.5,7.2	H_s, T_z 4.5,8.3	H_s, T_z 5.0,8.6	Performance Index
No 4	0.0	0.1	0.3	2.3

The design thus showed a significant increase in performance over the other designs considered.

Iteration 5:
A compromise between Designs No.3 and No.4 was examined, where the longitudinally dimension was reduced to 6.5m, and flow constrictions were present on three sides (Figure A7.1.4).

The results obtained were:

Design	H_s, T_z 4.5,7.2	H_s, T_z 4.5,8.3	H_s, T_z 5.0,8.6	Performance Index
No 5	0.0	0.6	0.9	2.4

The performance was thus only slightly reduced compared to the previous design.

Iteration 6:
The final design examined the possibility of using the minimum amount of space in the longitudinally direction (ie 4m) The design consisted of a modification of design No.3, with the small baffles on the transverse walls removed, and the perforated tube constructed in an octagonal shape (Figure A7.1.5).

The performances obtained were:

Design	H_s, T_z 4.5,7.2	H_s, T_z 4.5,8.3	H_s, T_z 5.0,8.6	Performance Index
No 6	3.4		14.4	4.7

At this stage it was considered that no scope for further designs remained.

The results as shown were presented to the client for evaluation. The space criterion was deemed to be dominant, and Design No.6 was selected. Subsequent model tests showed that the heave response of the vessel was substantially reduced by later changes in the hull form, and the performance of the moonpool improved as a result.

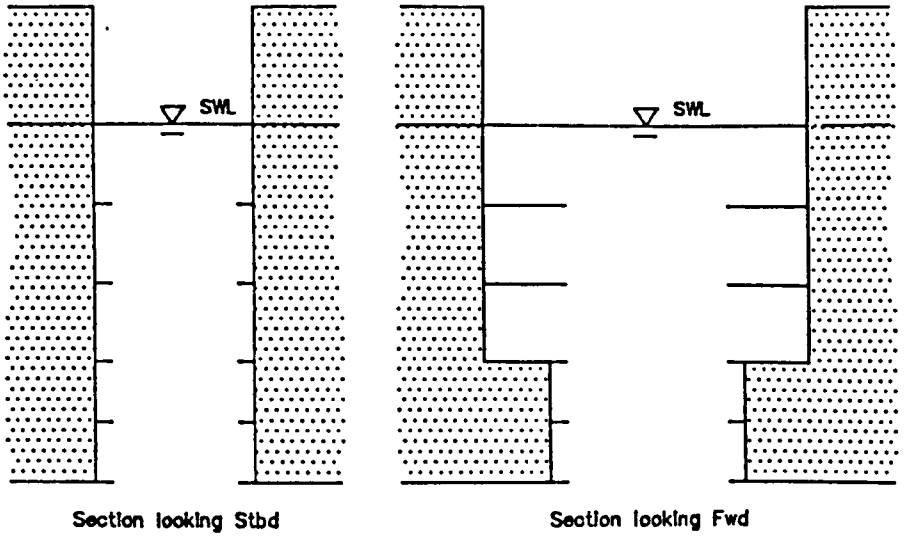

Figure A7.1.1

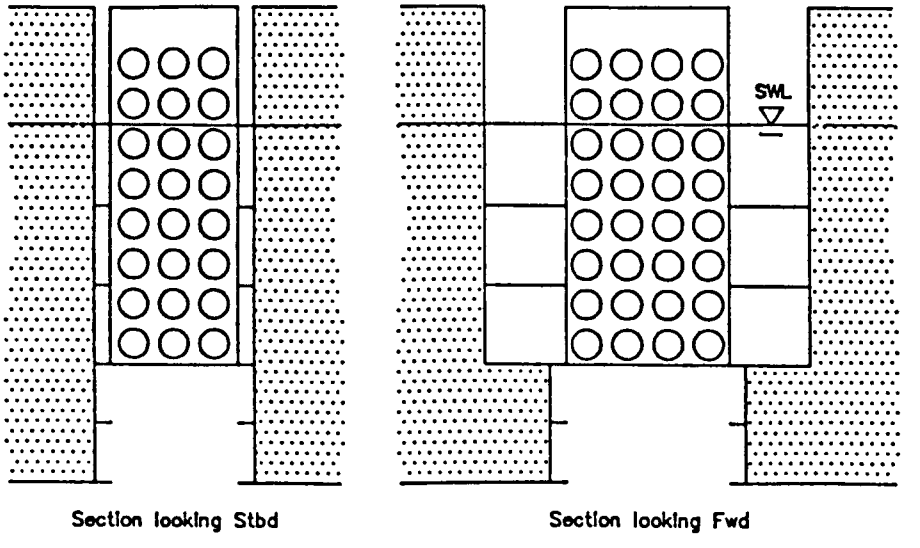

Figure A7.1.2

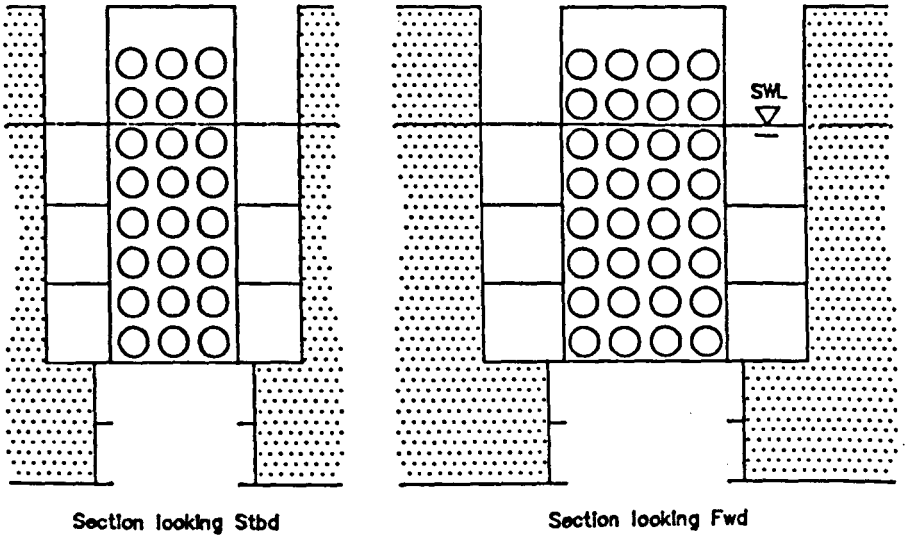

Figure A7.1.3

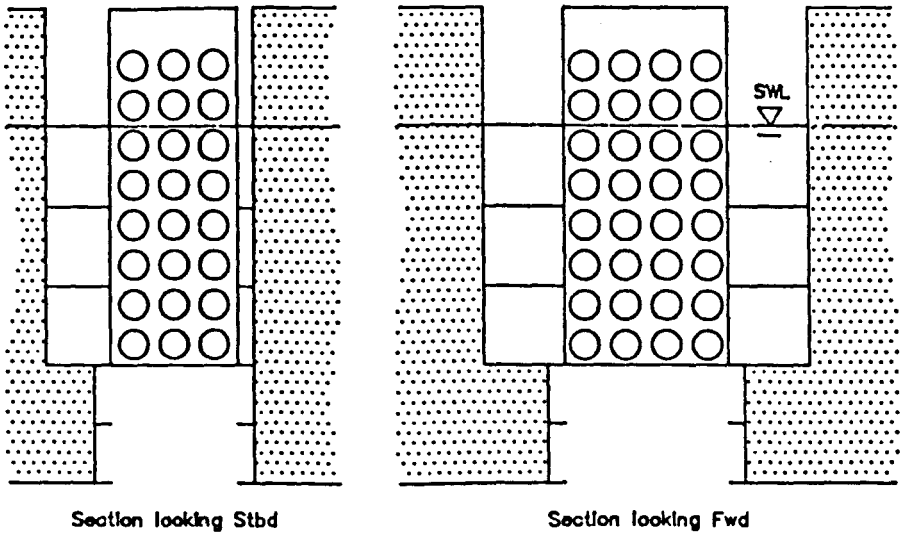

Figure A7.1.4

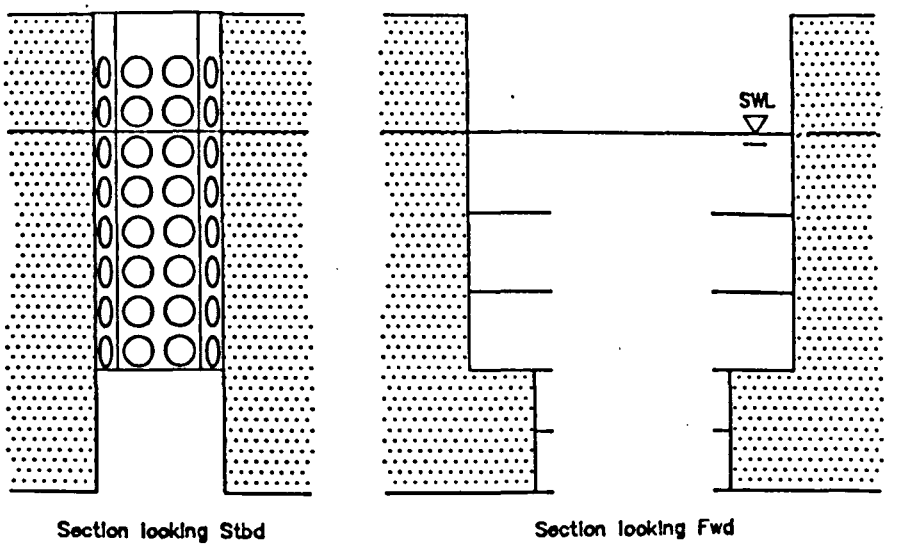

Figure A7.1.5